UNIVERSITEIT VAN PRETORIA
UNIVERSITY OF PRETORIA
YUNIBESITHI YA PRETORIA

THEORETICAL ANALYSES AND DESIGN, CONSTRUCTION AND TESTING OF A FLOW LOOP FOR THE STUDY OF GENERALISED FORCED AND NATURAL CONVECTION BOILING HEAT TRANSFER PHENOMENA ON TYPICAL LIGHT-WATER NUCLEAR REACTOR FUEL PIN CONFIGURATIONS

By

KUVENDRAN GOVINDER

Submitted in partial fulfilment of the requirements for the degree

MASTER OF SCIENCE (APPLIED SCIENCE - MECHANICS)

Department of Mechanical and Aeronautical Engineering,

Faculty of Engineering, the Built Environment and Information Technology (EBIT)

University of Pretoria

2019

Supervisors: Prof J.F.M. Slabber and Prof J.P. Meyer

Abstract

Title: Theoretical analyses and design, construction and testing of a flow loop for the study of generalised forced and natural convection boiling heat transfer phenomena on typical light-water nuclear reactor fuel pin configurations

Student: Kuvendran Govinder

Supervisors: Prof J.F.M. Slabber, Prof J.P. Meyer

In a worldwide quest to improve light-water-type nuclear power reactor safety, a more accident-tolerant fuel is required. In partial fulfilment of this initiative, an alternative fuel cladding to the currently used zirconium alloy-based materials had to be investigated and qualified. Silicon carbide was proposed as a probable replacement material. Accordingly, an experimental program was established at the University of Pretoria to conduct comparative boiling heat transfer studies of silicon carbide cladding tubes versus typical zirconium alloy-based nuclear fuel cladding (Zircaloy-4® was used for comparisons in this study). For the study, a purpose-built flow loop test facility, the University of Pretoria – Thermal-Hydraulic Flow loop Cell (UP-THFC), was subsequently designed, built and commissioned.

The test rig used water as the coolant and had capabilities for forced convection to be selected either vertically up or down, or horizontally through the test section. The test-clad tubes were internally heated with electrical resistance-type cartridge heaters, which were located and sealed within the clad tube bores to form heated pins. The arrangement of the pins in the test section allowed for external coolant flow over the clad tube surfaces. Operating test conditions in the test section were configured according to subcooled or saturated regimes, forced or natural convection, with the test section pressure being adjusted from ambient to around 200 kPa, and mass flux spanning from around 450 to 1 800 kg/m^2.s. Observation windows in the heated test section provided for visual inspection and digital camera recording of the boiling processes.

This dissertation reports on the evaluation and design criteria used for the building of the flow rig and the findings of the initial heat transfer tests on both tube materials. The set-up criteria used for the tests included the mean test section pressure maintained at around 200 kPa, four flow rate settings, three different bulk coolant inlet temperatures, and six heater power settings. The combination of these variables provided 192 test data points. Preliminary results indicated that although the silicon carbide had a higher thermal conductivity rating than Zircaloy-4®, it, however, produced marginally lower heat transfer capacity than Zircaloy-4®. The conducted heat transfer tests verified that the theoretical design analysis of the UP-THFC was satisfactory.

Acknowledgements

No project of this magnitude would have succeeded without the support and assistance of a team of people with their varied and many diverse skill sets and knowledge bases. I would thus like to acknowledge the following persons and/or organisations for their contributions made towards the successful outcome of the project:

- Prof J.F.M. Slabber (Project Supervisor), for his expertise, support and mentorship throughout the entire project;
- Prof J.P. Meyer (HOD: Department of Mechanical and Aeronautical Engineering, University of Pretoria), for supporting the project by providing additional funding and for availing the necessary technical resources and expertise of the Department towards the construction of the test facility;
- S.B. Leith, for his valuable time and contribution towards helping with the construction and installation of the system, thermocouple and RTD calibrations, assistance with setting up of the Labview graphical user interface (GUI), pipe network insulation, and testing of the system;
- W. Roberts, for assisting with the preparation of the manufacturing drawings of the various test section components and piping and instrumentation diagrams (P&ID), sight glass evaluation, and general support. He also needs to be thanked for arranging the donation of two water tank reservoirs from Hydrax SA;
- J. Maartens, for CFD evaluation of the plenum box components and overall general support;
- M. Alfama, for the test section and sight glass bolt spacing evaluation and thermocouple and pressure transducer validations;
- a special thanks to J. Clarke, for his advice on pipe fabrication methods and especially his invaluable expertise and skills in TIG welding of all the necessary stainless steel components;
- S. Roux, for his valuable assistance and advice with the Labview programming;
- D.M. Keetse and K.J. Mtombeni, for their support and assistance during the fabrication and installation of the system;
- J. Madileng, for the arc welding of various mild steel brackets and stands;
- N. Smit, B. Kent, E. Mohale and P. Kruger, for their skills and expertise in the CNC and/or conventional lathe and milling machining of various components;
- Endress+Hauser SA, for the donation of a high accuracy differential pressure transducer and calibration of the flow measuring device;
- H. Kampman CC, for the donation of two auxiliary pumps;
- Hydrax SA, for the donation of two water reservoir tanks;
- L. Wabeke, for assistance with the electrical wiring of various equipment;
- E. Schade-Weskott, for general assistance during the start-up and commissioning tests;
- T. Masilela and G. Magson, for assistance with the final ‘as-built’ CAD drawings of the system, and T. Mashego, for an independent Flownex simulation and CFD analysis of components;
- A special token of appreciation to Mrs R. Govinder, for her valuable moral support and encouragement throughout this project.

Table of Contents

List of Figures

List of Tables

Nomenclature

A_c	Cross-sectional area	m^2
A_s	Surface area	m^2
Bo	Boiling number, $\dot{q}/Gh_{fg}$	
C_f	Friction coefficient	
Co	Convection coefficient, $(x/(1-x))^{0.8}\ (\rho_v/\rho_l)^{0.5}$	
C_p	Specific heat	J/kg.°C
D	Diameter	m
D_H	Hydraulic diameter	m
D_e	Effective diameter	m
$ID;\ OD$	Inner diameter; outer diameter	m
E	Enhancement factor in Eqs. (2-13, 2-39, and 2-45)	
F	Enhancement factor in Eq. (2-34)	
F_{fl}	Fluid dependent parameter	
Fr	Froude number, $G^2/(\rho_l^2\ gD)$	
f	Friction factor	
f_T	Turbulent friction factor	
G	Mass flux, $\rho \cdot V/A_s$	$kg/m^2.s$
g	Gravitational acceleration	m/s^2
h	Heat transfer coefficient	$W/m^2.°C$
h_{fg}, h_{lv}	Enthalpy of vaporisation	J/kg
I	Input current	A
k	Thermal conductivity	W/m.°C
L	Length	m
L_e	Equivalent length	m
M	Molar mass	kg/mol
$\dot{m}$	Mass flow rate, $\rho V A_s$	kg/s
Nu	Nusselt number	
P	Pressure	Pa

Pr	Prandtl number	
p_r	Reduced pressure, P_{abs}/P_{crit}	
$\dot{Q}$	Heat transfer rate	W
$\dot{q}$	Heat flux	W/m^2
Re	Reynolds number, $\rho v D_H/\mu$	
Re_L	Liquid Reynolds number, $GD_o(1-x)/\mu_l$	
S	Suppression factor	
T	Temperature	°C
ΔT	Temperature difference	°C
V	Input voltage	V
$\dot{V}$	Volumetric flow rate	m^3/s
v	Velocity	m/s
X_{tt}	Lockhart-Martinelli parameter	
x	Axial position relative to a datum point	m
x	Vapour quality, $(h_l - h_{l,sat})/h_{lv} = C_p \Delta T_{sub}/h_{lv}$	%

Greek Symbols

ε	Surface roughness	m
ψ	Heat transfer enhancement factor in Eq. (2-24)	
σ	Surface tension	N/m
ρ	Density	kg/m^3
μ	Dynamic viscosity	kg/m.s
γ	Specific weight	N/m^3
δ_v	Velocity boundary layer thickness	m
δ_t	Thermal boundary layer thickness	m

Subscripts

1; 2	Reference points 1 or 2, respectively
∞	Far from surface
abs	Absolute
avg	The average or mean value
b	Bulk coolant
c	Condensation of water
c	Cross-sectional
$crit$	Critical
ent	Entrance side
ev	Evaporation of water
ext	Exit side
f	Film or interface
fc	Single-phase forced convection
h	hydrodynamic
$heated$	Heated length

i	Inside
in	Input or inlet
L	Total length
$l\ ;\ lo$	Liquid; liquid only condition
lam	Laminar
max	Maximum
min	Minimum
nb	Nucleate boiling
o	Outer
op	Operational value
out	Output or outlet
$pool$	Pool boiling condition
s	Surface
$sat\ ;\ s$	Saturated
SP	Single-phase condition
sub	Subcooled
sys	System
t	Thermal
tc	Transient condition
TP	Two-phase condition
t	thermal
tt	Turbulent liquid – turbulent vapour
$turb$	Turbulent
v	Vapour
v	Velocity
w	Wall or clad tube surface
x	Axial position relative to a datum point

Abbreviations

AC	Alternating current
ATF	Accident tolerant fuel
AWG	American wire gauge
BWR	Boiling water reactor
CANDU	CANadian Deuterium Uranium
CHF	Critical heat flux
DAQ	Data acquisition unit
DNB	Departure from nucleate boiling
EMF	Electromagnetic force
FBG	Fibre Bragg grating
FDNB	Fully developed nucleate boiling
GUI	Graphical user interface
HTC	Heat transfer coefficient
HTR	High-temperature reactor
LOCA	Loss of coolant accident
LWR	Light water reactor
MAD	Mean absolute deviation
NPP	Nuclear power plant
NTU	Number of transfer units

ONB	Onset of nucleate boiling
OSV	Onset of significant void
PNB	Partial nucleate boiling
RFI	Radio frequency interference
RPV	Reactor pressure vessel
SiC	Silicon carbide
SSR	Solid state relay
TRISO	Tristructural-isotropic
UP	University of Pretoria, South Africa
UP-THFC	University of Pretoria – Thermal-Hydraulic Flow loop Cell
UO_2	Uranium-oxide
VAC	Voltage- alternating current
VDC	Voltage- direct current
VDF	Vertical downflow
VFD	Variable frequency drive
VUF	Vertical upflow
Zr-4	Zircaloy-4®

1 Introduction

In typical light-water reactors (LWRs) of civilian nuclear power plants (NPPs), the heat generated by fission reactions and fission product decay in the nuclear fuel needs to be removed as effectively as possible. Uncontrolled heat build-up in nuclear fuel is undesirable and could lead to the rupture of the fuel rods [1]. Consequently, this could result in the release of radioactive material to the environment if the reactor containment structure is breached. It is thus the function of the re-circulating bulk coolant flow in the primary loop of the NPP to remove as effectively as practically possible the heat generated in the fuel and consequently maintain the nuclear fuel at safe operating temperatures [2].

In an unfortunate incident at the Fukushima-Daichii NPP in 2011, a loss of cooling accident (LOCA) occurred stemming from an earthquake event that automatically triggered the shutdown of the reactors. A sequence of events thereafter prevented the coolant pumps from recirculating the water coolant through the reactor vessels and the spent fuel cooling pools to remove heat produced by fission product decay. The stationary water inventory subsequently boiled off. The investigations revealed that an exothermic chemical reaction between the exposed hot metallic fuel clad tube outer surfaces in contact with the surrounding steam produced large amounts of hydrogen [3]. This resulted in substantially reduced heat transfer from the fuel leading to the rapid fuel heat-up, which subsequently contributed to the meltdown of some of the reactor cores and spent fuel in the pools. To mitigate such a reoccurrence in the future and to facilitate improved NPP safety, a more accident tolerant fuel (ATF) is currently being investigated worldwide [3].

1.1 Project Background

The nuclear fuel for most light-water reactor power plants is typically in the form of compressed and sintered uranium oxide (UO_2) pellets. The uranium (mainly the uranium-235 isotope) fissions and produces in the process fission products, which are very radioactive. The fission products must be kept as closely as possible to the point where they were created. For this reason, the fuel is protected from releasing fission products by insertion into long cylindrical tubes (fuel-clad tubes) to form a fuel rod or fuel pin. Helium gas is filled inside the fuel rod to serve as an inert heat transfer medium between the tube wall and the fuel material and thereafter the fuel pins are hermetically sealed at each end. A number of fuel pins are then arranged into an array to suit the reactor core requirements. The fuel pin array, together with the inlet- and outlet-flow nozzles, support guides, and spacer grids with flow mixers form a fuel assembly. Certain spaces are allocated in or around the fuel pin array for reactivity control rods and neutron monitoring instrumentation. A number of fuel assemblies are positioned

inside the reactor pressure vessel (RPV), within which the fission process occurs [2] [4]. This assembly of fuel within the reactor pressure vessel is referred to as a reactor core.

The nuclear fuel clad tubes serve as the main heat transfer medium to conduct the heat generated by the fuel to the bulk coolant water flowing through the reactor and around the fuel rods. As stated above, these also act as the primary fission product retention barrier in the NPP. The material from which the fuel-clad tube is constructed must have particular properties such as low neutron absorption cross-section and high corrosion resistance [2] [4]. The fuel-clad tubes must also be able to withstand large internal and external pressures including thermal and structural stresses.

Relatively few materials are adequately suited for use as nuclear fuel tube clad structures for LWR requirements. Unfortunately, the zirconium-based materials have certain operational limitations in nuclear reactors as explained above hence the quest to qualify suitable alternative materials [5] [6]. Some of these issues are discussed in the following sections.

1.1.1 Zirconium Alloy

For over 50 years, metallic zirconium-based alloys (typically trademarked as Zircaloy®) in the form of cylindrical cladding has been the material of choice for providing the primary barrier to contain the fission products in LWRs. The material is an alloy of zirconium (Zr), tin (Sn), iron (Fe) and chrome (Cr) as used in pressurised water reactors (PWRs) and CANadian Deuterium Uranium (CANDU) nuclear reactors and commercially marketed as Zircaloy-4® (Zr-4) [1]. The alloy with added nickel (Ni) is used for fuel cladding in boiling water-type reactors (BWR). Zircaloy-2® (Zr-2) is used for calandria tubing in CANDU reactors. There are few other suitable materials available that can perform the variety of functions that the Zircaloy® material provides such as good heat transfer properties, small neutron capture affinity, a structural component with reasonably long-term stability while exposed to neutron irradiation when subjected to high temperature and pressure conditions [4] [2].

Under neutron irradiation in a typical core environment, the total lifespan of Zircaloy® is limited to about five years on average due to hydration effects that lead to the swelling of the metallic structure [6]. Currently, most Zircaloy® clad fuel is replaced in around 18-month cycles due to the consumption of the fissile material, build-up of fission products and also to guard against potential structural failure of the cladding [5]. Zirconium-based materials also are potentially capable of generating explosive hydrogen gas when exposed to steam [5] [7], the consequences of which were discussed earlier. Extended exposure of Zircaloy® to extreme heat sources, such as decay heat produced by fission products, could also lead to embrittlement of the metallic structure. This may result in the degradation of the cladding, which could potentially cause the uncontrolled release of

fission products [1]. In an extreme case, the radioactivity could be released into the environment if the pressure boundary and the reactor containment structure are both also breached.

The Fukushima incident has emphasised the relevance of seeking and validating a more accident tolerant fuel (ATF) that uses a better fuel-clad material that would have a higher resistance to degradation under LOCA conditions. One of the possible materials that have been proposed to replace Zircaloy® is silicon carbide (SiC), also known as Carborundum [8]. The merits thereof are discussed next.

1.1.2 Silicon Carbide (Carborundum)

Even before the Fukushima incident, an international collaborative effort had been started to evaluate the feasibility of silicon carbide (SiC) as a suitable replacement material for the zirconium-based nuclear fuel clad tubes [8] [9].

SiC-based compounds were previously used in tristructural-isotropic (TRISO) fuel particles in high-temperature reactors (HTR) and demonstrated excellent performance [9]. In other research facilities, researchers conducted extensive tests on un-irradiated and irradiated SiC samples [7] [10] [11]. Some of these tests involved temperature versus tensile strength threshold tests conducted on propriety composite SiC samples. The test results indicated superior temperature threshold levels of the SiC compounds as compared with other current nuclear reactor core materials. The results also revealed larger strength retention levels for the SiC compounds at elevated temperatures.

The higher temperature potential of the SiC could possibly also provide an increase of the burnout margin, which is the margin between the heat flux during operation and the critical heat flux where the heat cannot be sufficiently removed by convective heat transfer. Fuel cladding material that provides a higher burnout margin is therefore important to designers. The positive characteristics of the SiC would then also promote power uprates of LWRs due to the higher heat flux potential that could be generated by the nuclear fuel elements and consequently enabling a more complete burn-up potential of the nuclear fuel [11]. Additionally, the higher neutron exposure capability revealed in the HTR fuel performance testing has demonstrated the potential for the proposed SiC-based nuclear fuel clad tubes for utilisation in longer fuel reload cycles. Potentially, this could lead to increased availability of the NPP with the obvious economic benefits.

1.2 Project Configuration

In contributing to the validation of SiC as a suitable replacement for the zirconium alloy fuel clad tubes in LWRs, studies in the Department of Mechanical and Aeronautical Engineering at the University of

Pretoria (UP) were initiated to conduct the heat transfer investigations of typical Zircaloy® versus SiC materials. The heat transfer performance from the zirconium-based materials was used as the baseline comparator to gauge the heat transfer performance of the SiC-based materials.

1.2.1 Problem Statement

A purpose-built thermal hydraulic test rig had to be designed, built, and commissioned before the required experimental heat transfer-orientated testing could commence. The bulk of the testing focused on forced convection boiling heat transfer in both subcooled and saturated flow regimes. The test rig thus had to incorporate the necessary instrumentation for the collection of the correct sets of data for further post-processing.

This dissertation discusses the theoretical evaluation and development of the UP – Thermal-Hydraulic Flow loop Cell (UP-THFC) for the study of the heat transfer characteristics of existing and proposed nuclear fuel clad tube materials.

1.2.2 Project Aims and Objectives

One of the main outcomes of the project was to establish the heat transfer coefficients (HTC) from the external surfaces of the various nuclear fuel clad tube materials when the tubes were subjected to internally generated heat flux with specified external forced convection flow conditions. The results were to be generated for the vertical- up flow and down flow as well as for horizontal flow regimes. The test rig had to cater for heat transfer studies from the onset of nucleate boiling (ONB), the fully developed nucleate boiling (DNB), and critical heat flux (CHF) regions. Testing in both the subcooled and saturated flow boiling regimes also had to be accommodated.

1.2.3 Test Rig Design Directives

The generic requirements for the UP-THFC were as follows:

- The physical simulation of the flow conditions had to be demonstrated around a specific reactor fuel pin geometry typical of a new-generation LWR fuel assembly for the study of both forced and natural convection heat transfer phenomena. As such, a suitable test chamber had to be designed and configured for the effective study of the above.

- The fuel pin under investigation had to be internally heated and the boiling heat transfer characteristics assessed individually as well as in the local vicinity of neighbouring heated or unheated pins.
- Coolant flow rate adjacent to the heated pin(s) in the test chamber had to be adjustable according to the test specification.
- The test chamber had to be equipped with viewing ports for both video camera recording and ordinary visual inspection/observation of the boiling phenomena.
- The test chamber had to be fitted with access points for the instrumentation and other electrical leads.
- The system had to be capable of maintaining a mean internal hydrostatic pressure in the test section of at least 200 kPa (absolute).
- If required, external heating had to be available to preheat the water in the flow loop.
- Sufficient safety devices had to be employed, such as pressure relief and venting valves in order to ensure the safety of workers as well as that of the equipment.
- The working coolant had to be demineralised water or other high purity water.
- A heat exchanger located in the flow circuit had to be included to remove any excess heat generated by the heated test specimens and the pump in order to control the coolant inlet temperature to the test section for each experiment.
- The necessary data recording, measuring instrumentation and control systems had to be included (typically, this instrumentation would include temperature, pressure, and flow measurement devices). Facilities for the establishment of effective Nusselt number, $Nu\ f(Re, Pr)$, per respective flow regime had to be catered for. A graphical user interface (GUI) had to be included as part of the electronics control suite.
- The refilling and draining of the water from the test rig required the installation of appropriate facilities.

2 Literature Study

2.1 Introduction

Information pertaining to the heat transfer performances of nuclear grade materials is propriety information and access to it is to a high degree restricted. Accordingly, little information regarding this subject matter is available in the general literature. Independent experimentation was thus required to establish some of these performance characteristics for the SiC clad material. For parity of experimental results, test specimens consisting of individual zirconium alloy (specifically Zr-4) and SiC cladding tubes required standardised test conditions. The heat transfer characteristics and/or performance analysis of the Zr-4 tubes formed the baseline comparator for the SiC tubes. This experimental comparative analysis thus required an appropriate testing facility to conduct the experimental tests. This chapter thus highlights the theoretical considerations for the design of the UP-THFC.

Studies of the heat transfer characteristics of the test-clad tubes subjected to subcooled and saturated forced convection flow conditions were of particular interest. Studies focusing on the clad heat transfer performance during critical heat flux (CHF) conditions were scheduled for future considerations in the extended study program.

A survey of the literature that focused primarily on forced convection boiling theory allowed for the identification of the relevant measurands and test parameters as required in the specific design analysis of the experimental test rig. These and some pertaining fundamentals frame the discussion in the following sections.

2.2 Boiling Heat Transfer Fundamentals

Boiling heat transfer phenomena comprise mechanisms that are complex and have been a subject of research and investigations. Simply defined, boiling is a process in which the addition of heat to a liquid leads to the generation of vapour [12]. Boiling becomes possible when a heated surface exceeds the saturation temperature of the surrounding coolant. This holds true whether the bulk fluid temperature is at or below the local saturation temperature. When the bulk fluid temperature is equal to its saturation temperature then the phenomenon is referred to as saturated- or bulk- boiling [13]. In the case when the bulk fluid temperature is lower than its saturation temperature, then the boiling condition is designated subcooled boiling. These boiling conditions are typical in high heat flux

applications such as nuclear reactor cores, accelerator targets and advanced microelectronic cooling modules.

Pioneering work by Nukiyama (1934) [14] identified the different phases of the boiling regime, as well as the effects of the superheat on the wall (ΔT_w) with respect to the wall heat flux generated ($\dot{q}_w$). Other researchers identified heat and mass transfer and associated energy transport properties together with parameters such as the fluid and the heated surface conditions as some of the other major mechanisms that influence the boiling processes [15] [16] [17].

Generally, pool boiling and forced convection boiling are the two main boiling types. Pool boiling heat transfer consists mainly of natural convection mechanisms and is devoid of any mechanically induced circulation. This type of boiling occurs by vapour generation from a heated surface immersed in a pool of liquid [12] [13].

In forced convection boiling (also referred to as flow boiling), depending on the local saturation pressure and temperature, the evaporation of the liquid occurs in a heated flow channel in which the generated vapour and the remaining liquid form a two-phase flow that contributes significantly to the heat transfer to the bulk liquid [18].

The information pertaining to the heat transfer characteristics of the flow boiling and pool boiling phenomena are typically plotted in boiling curve graphs [14]. In these boiling curves, the heated wall superheat temperatures (ΔT_W) is compared with the heat flux ($\dot{q}$) on the heated surface. ΔT_W is the difference between the heated wall surface temperature (T_W) and the saturated temperature of the liquid medium (T_{sat}). Typically, the inclusion of the forced convection processes (flow boiling) allows for higher heat flux as compared with the pool boiling curve for the same ΔT_W [19].

Of prime importance in the current study are the partial nucleate boiling and the fully developed nucleate boiling phase regions of the flow boiling regime. These regions identify the nucleate boiling regimes under which most LWR-type power reactors operate. The start of the formation of vapour bubbles on the heated surface typically indicates the start or onset of the nucleate boiling phase (ONB). Upstream of the ONB is the region where the single-phase forced convection is the dominant heat transfer mechanism. Downstream of the ONB, and dependent on the flow velocity and the wall temperature, the vapour bubbles on the heated surface would begin to slide along the heated surface and lift off. The onset of significant void (OSV) designates the point when the fully developed nucleate boiling phase contains flow that has significant vapour void content in the bulk flow.

The critical heat flux (CHF) condition occurs at the first instance when there is a significant net decrease in the heat flux ($\dot{q}$) for increasing power input [20]. For subcooled flow, the CHF is an

occurrence in which a small increase in heat flux leads to abrupt wall overheating. The transition or departure from nucleate boiling (DNB) to film boiling causes this phenomenon to occur. The CHF point can increase substantially with the addition of convective flow over the heated surface as compared with the pool boiling scenario. The design of typical subcooled flow boiling systems requires the operating conditions to maintain heat fluxes lower than the CHF for the prevention of potential failure by overheating or burnout. The boiling phenomena downstream of the CHF are thus of no further interest in this dissertation. Studies involving CHF experiments would form the focus of future research to determine the safe generation of the maximum heat flux by the proposed SiC fuel clad material. To cater for the envisaged CHF studies, the necessary functional requirements had to be included in the initial design configuration of the UP-THFC.

2.2.1 Vapour Bubble Dynamics

As mentioned earlier, the nucleate boiling phases involve vapour bubble generation that contributes immensely to the heat transfer to the subcooled liquid. A flow boiling model presented by Basu *et al*. (2003) details various heat transfer mechanisms [21] [22] [23]. As described in this model, for the areas on the heated surface between the ONB and OSV regions that are not occupied by vapour bubbles, all the heat energy from the heated wall is directly transferred to the subcooled liquid by the single-phase forced convection ($\dot{Q}_{fc}$) component. A fraction of the heat from the superheated liquid layer adjacent to the heated wall contributes to the evaporation of the liquid ($\dot{Q}_{ev}$). Heat transfer via condensation ($\dot{Q}_{c}$) occurs from the top of the attached vapour bubbles that, in turn, are exposed to the subcooled liquid. Whenever the thermal boundary layer is disturbed by either bubble growth, bubble sliding or bubble departure, a period of transient conduction ($\dot{Q}_{tc}$) occurs followed by a $\dot{Q}_{fc}$ period.

The partitioning and analysis of the wall heat flux into its constituent components form part of a future study programme for the heat transfer characterisation of the SiC fuel clad. The design of the UP-THFC thus incorporated the required system capability to allow for these studies.

2.2.2 Void Fraction

Vapour bubbles that steadily lift off the surface downstream of the OSV and become entrained in the bulk liquid flow, creates a vapour void fraction in the ensuing flow [13] [21] [22]. The prediction of the location of the OSV and void fraction along the flow direction during subcooled flow boiling is very

important for LWRs. Depending on the specific reactor design; the void fraction can have a positive or negative impact on the reactivity of the reactor and is normally included in the design of the control algorithm of reactors.

The nuclear industry uses thermal-hydraulic codes (e.g. RELAP-5) to compute the void fraction value based on the interaction of three constitutive models [24]. The results from these constitutive models enable the following:

i. The determination of the fraction of wall heat flux for vapour generation (source term for void fraction) which is derived from wall nucleation or wall heat flux partitioning modelling techniques.
ii. The establishment of a sink term value derived from the modelling of the interfacial heat and mass transfer occurring during vapour bubbles lifting off and subsequent condensation of the vapour inside the bubbles in the subcooled fluid.
iii. Quantifying of the interfacial friction component.

Several studies for the determination of the void fraction and contributing mechanisms were conducted in the past. Most of these studies used a wall heat flux partitioning technique to determine the void fraction and the overall heat flux. The research paper by Basu *et al*. (2002) [21] reviewed the details of these studies.

Due to the specialised content and the nature of the void fraction analysis, this portion of the work will be conducted as part of a future research project. In order to cater to these studies, the design of the UP-THFC thus had to include observation windows in the test section for ordinary visual observations and digital camera recording of the ensuing boiling processes.

2.2.3 Other Influences on Boiling Behaviour

Some other factors that play important roles in the boiling processes are as follows [22]:

- heated fluid composition and properties;
- pH level, dissolved gases and other impurities in the water;
- heated surface effects such as surface roughness, wettability, thermal conductivity and geometry;
- surface tension effects.

Any changes to these parameters or combinations thereof significantly affect the boiling processes. These complex parameters have been extensively investigated and reported in the literature [18] [25] [26] [27] and for brevity are not discussed in this dissertation.

The following pertinent aspects, although highly relevant, are also not included in the current discussion:

- the heat source and dissipation thereof;
- effects of varying thermal properties;
- porous wall surface effects;
- effects due to unsteady-state conditions;
- metastable phase stability of the water;
- combined radiation and convection conditions.

Further details regarding the above topics are available in the literature [26] [27].

2.3 Design Requirements for the UP-THFC

It is clear from the previous discussions that the evaluation of the UP-THFC configuration revolved around the need for experimental studies focused mainly on the partial and fully developed nucleate boiling phases with both subcooled and saturated inlet flow considerations using demineralised or other high purity water specified as the flow medium. The specimen tube configurations had to be fully submerged in the water within the test section duct, which was flowing full with the regulated forced convection water and flowing axially (parallel) to the heated (fuel cladding) surface(s).

For the comparative testing parameters, the inlet flow condition was required to be steady and uniform with respect to pressure, temperature, and mass flow – all of which was to be adjustable within the designed operating range of the system.

With all of the required operational aspects considered, the specific design of the test section entailed a compound flow problem consisting of an internal flow condition for the flow medium through the test section duct and an external flow condition for the flow over the fully submerged test clad specimens.

The internal flow condition consisted of the evaluation of the flow channel cross-sectional parameters and the thermal hydraulic entrance and exit lengths of the test section. These analyses, which included the flow aspects of the entire thermal hydraulic pipe network and the system pumping requirements, are included in the discussion in Chapter 3. The analysis of the external flow condition consisted mainly of the heat transfer aspects related to the current study requirements and included the heat transfer performance and characteristics of the test specimens. The following sections discuss the pertinent factors.

2.4 External Flow Boiling Analysis

The design of the experimental set-up (heated portion of the test section)was based on heated pin geometries with flow parallel to the length of the heated surface. This established the basis from which the experimental heat transfer performances of the test clad-tubes could be compared against predicted results from other established heat transfer correlations as obtained from the literature. The following sections review the underlying evaluation criteria of the relevant heat transfer characteristics on the heated clad-tube pins.

2.4.1 Flow Over Surfaces with Unheated Starting Length

For the heat transfer experiments, the test specimen clad tubes with internally located electrical heaters had to be fully submerged and supported within a channel that was flowing full. The available heaters had cold sections at each end. The location of these heater(s) within the test specimen clad tube(s) created an unheated starting length for the external coolant flow over the tube surfaces. As a first approximation, equations for external flow over surfaces with unheated starting length provided a basis for the analytical evaluation (prediction) of the heat transfer characteristics of the test specimen clad tubes in terms of the experimental arrangement as described previously. Only the test specimen clad surfaces that were directly heated by the heater were considered as the heated surface area (A_s) for the heat transfer evaluations. The unheated sections of the clad tubes were considered for the thermal velocity boundary layer and friction coefficient determinations and were evaluated according to the respective laminar, turbulent, and/or combined criteria. The heat produced by the heater was assumed as transmitted in a unidirectional manner with the heat conducted radially from the heater through the wall of the test specimen clad tubes and thereafter into the water flow medium. This assumption agrees with the findings of Ribatski and Jabardo (2003), who found experimentally that heat conducted axially was negligibly small [16]. Another test criterion assumed a uniform heat flux along the heated section of the test-clad tubes. The following subsections highlight the relevant equations for the heat transfer evaluations and analysis.

2.4.1.1 Velocity Boundary Layer Thickness

For a clad tube located within a free stream and with the external coolant bulk flow assumed as being turbulence free, the local velocity boundary layer thickness ($\delta_{v,x}$) in the flow direction at a local Reynolds number (Re_x) and axial position (x) with respect to a reference point, is determined from:

Laminar, $$\delta_{v,x} = \frac{4.91\ x}{Re_x^{1/5}} \qquad \{Re_x < 5 \times 10^5\} \qquad (2\text{-}1)$$

Turbulent, $$\delta_{v,x} = \frac{0.38\ x}{Re_x^{1/5}} \qquad \{5 \times 10^5 < Re_x < 10^7\} \qquad (2\text{-}2)$$

2.4.1.2 Local Reynolds Number

The local Reynolds number for external flow is determined from the following equation:

$$Re_x = \frac{\rho\ v\ x}{\mu} = \frac{v\ x}{\nu} \qquad (2\text{-}3)$$

Depending on the surface roughness and the variation of the pressure along the surface, the consideration laminar flow conditions require Reynolds number larger or equal to 1×10^5 for the external flow over the clad tube(s). The critical Reynolds numbers were assumed at approximately $Re_{crit} = 5 \times 10^5$ and the fully turbulent values accepted as being around 3×10^6 [20].

2.4.1.3 Local Thermal Boundary Layer

The local thermal boundary layer thickness is determined using the following equation:

Laminar: $$\delta_{t,lam} = \frac{4.91\ x}{Pr^{1/3}\sqrt{Re}} \qquad \{0.6 \leq Pr \leq 50\} \qquad (2\text{-}4)$$

Turbulent: $$\delta_{t,turb} = \delta_v \qquad \{Independent\ of Pr\} \qquad (2\text{-}5)$$

2.4.1.4 Friction Coefficient

The average friction coefficient over the entire surface is determined using:

Laminar: $$C_{f,lam} = \frac{1.33}{Re_{x=L}^{0.5}} \qquad \{Re \leq 5 \times 10^5\} \qquad (2\text{-}6)$$

Turbulent: $$C_{f,turb} = \frac{0.074}{Re_{x=L}^{0.2}} \qquad \{5 \times 10^5 < Re_x < 10^7\} \qquad (2\text{-}7)$$

In the case for which the specific heated surface assessed as sufficiently long for the flow to become turbulent but not long enough to disregard the laminar flow region, the following equation computes the combined average friction coefficient over the surface:

Combined: $$C_{f,turb} = \frac{0.074}{Re_{x=L}^{0.2}} - \frac{1\,742}{Re_{x=L}} \qquad \{5 \times 10^5 < Re_x < 10^7\} \qquad (2\text{-}8)$$

For the heated surfaces considered as being rough, the Schlichting correlation [28] provides the coefficient of friction:

Turbulent (*Rough)*: $$C_f = \left(1.89 - 1.62\ \log\frac{\varepsilon}{L}\right)^{-2.5} \qquad \{5 \times 10^5 < Re_x < 10^7\}\ \{\varepsilon/L > 10^{-4}\} \qquad (2\text{-}9)$$

ε represents the surface roughness and L the clad tube length.

2.4.1.5 Heat Flux

For a given rate of heat transfer ($\dot{Q}$) and the surface temperature (T_s) at a distance (x), the local heat flux is determined by:

$$\dot{q}_s = \frac{\dot{Q}}{A_s} \qquad (2\text{-}10)$$

and $$\dot{q}_s = h_x[T_s(x) - T_\infty] \qquad (2\text{-}11)$$

2.4.2 Flow Boiling Correlations from Literature

The heat transfer evaluations of the experimental rig adopted generalised correlations for forced convection boiling. Most of these correlations relate flow conditions within heated tubes in the

vertical and horizontal orientations for various fluid types. These correlations typically describe a combination of the macro-convective mechanisms associated with the flowing fluids (convection boiling subscript fc) and the micro-convective mechanisms associated with vapour bubble nucleation and growth (nucleate boiling subscript nb). Rohsenow (1952) first suggested this hypothesis [29] which he expressed as follows:

$$h = h_{fc} + h_{nb} \tag{2-12}$$

As many other researchers have discovered, Eq. (2-12) does not fully define the varied complexities of flow boiling since factors to cater for the large variation of boiling effects and aspects have to be included. The correlations used in the analytical heat transfer assessments in this study include those for which general applicability has been claimed and which are widely recognised. These are briefly detailed next.

2.4.2.1 Chen Correlation

Chen (1966) proposed the first widely recognised flow boiling heat transfer correlation for studies in vertical tubes. The correlation included an additive mechanism to account for the micro- and macro-convective heat transfer to predict saturated flow boiling initially and later on included subcooled flow boiling aspects [30]. These mechanisms were accounted for by means of a forced convection enhancement function (F) and a pool boiling suppression function (S). The following equation defines the Chen two-phase flow boiling heat transfer correlation:

$$h_{TP} = Fh_l + Sh_{pool} \tag{2-13}$$

For the micro- and macro-convective boiling heat transfer coefficients, the Forster and Zuber correlation [31] yields the pool boiling result and the modified Dittus-Boelter correlation [32] the forced convection boiling result; the respective equations expressed as:

$$h_{pool} = 0.00122 \frac{k_l^{0.79} C_{p,l}^{0.45} \rho_l^{0.49} (T_w - T_s)^{0.24} (P_w - P_s)^{0.75}}{\sigma^{0.5} \mu_l^{0.29} h_{fg}^{0.24} \rho_v^{0.24}} \tag{2-14}$$

$$h_l = 0.023\, Re_l^{0.8}\, Pr_l^{0.4} \left(\frac{k_l}{D_H}\right) \tag{2-15}$$

In the above equations, the subscripts w and s indicate the external wall (surface) temperature of the clad tube and the saturated bulk coolant water temperature respectively. The subscript l indicates the liquid only phase condition of the bulk coolant water and D_H is the hydraulic diameter.

The F function multiplier in the Chen correlation, originally presented in graphical format, but subsequently resolved into expressions by various researchers [33] [34], as follows:

$$F = 1 \qquad \left\{if\ \frac{1}{X_{tt}} \leq 0.1\right\}$$
$$F = 2.35\left(\frac{1}{X_{tt}} + 0.213\right)^{0.736} \qquad \left\{if\ \frac{1}{X_{tt}} > 0.1\right\} \tag{2-16}$$

In the above equation set, the Lockhart-Martinelli parameter (X_{tt}) establishes the two-phase pressure gradient or pressure drop due to effects of forced convection (assuming homogeneous flow). As reported in practice, that if the liquid phase is turbulent, then the vapour phase will usually be turbulent as well [35]. In this case, the Lockhart-Martinelli parameter is:

$$X_{tt} = \left(\frac{1-x}{x}\right)^{0.9}\left(\frac{\mu_l}{\mu_v}\right)^{0.1}\left(\frac{\rho_v}{\rho_l}\right)^{0.5} \tag{2-17}$$

The vapour quality (x) is determined by:

$$x = \left(h_l - h_{l,sat}\right)/h_{lv} = c_p\Delta T/h_{lv} \tag{2-18}$$

Chen also originally correlated the suppression S factor acting on h_{pool} to the two-phase Reynolds number (Re_{TP}) experimentally and presented it graphically. Other researchers subsequently expressed the Chen S factor in equation format [36] [34] [37]. The first three equations have been widely cited but restrict the application to within stipulated Re_{TP} range limitations. However, the correlation per Eq. (2-20) was not widely reported in the literature but was formulated to be inclusive of all ranges of Re_{TP} and therefore finds application later on in this dissertation.

$$S = \frac{1}{1 + 0.12Re_{TP}^{1.14}} \qquad (if\ Re_{TP} \leq 32.5)$$
$$S = \frac{1}{1 + 0.42\ Re_{TP}^{0.78}} \qquad (if\ 32.5 < Re_{TP} \leq 70) \tag{2-19}$$
$$S = 0.1\ \ (if\ Re_{TP} > 70)$$

$$S = \frac{1}{1 + 2.53 \times 10^{-6}\, Re_{TP}^{1.17}} \quad (can\ be\ used\ for\ all\ ranges\ of\ Re_{TP}) \tag{2-20}$$

The two-phase Reynolds number (Re_{TP}) is defined for a fluid in which vapour bubbles are present. In the following equation, the expression for Re_{TP} is:

$$Re_{TP} = Re_l F^{1.25} \tag{2-21}$$

where

$$Re_l = \frac{10^{-4}\dot{m}(1-x)D_o}{\mu_l} = \frac{G\, D_o(1-x)}{\mu_l} \tag{2-22}$$

The subcooled flow boiling equation for the Chen correlation is:

$$\dot{q} = \dot{q}_{nb} + \dot{q}_{fc} = h_{nb}(T_w - T_s) + h_{fc}(T_w - T_b) \tag{2-23}$$

in which

$$h_{nb} = 0.023\, Re_l^{0.8}\, Pr_l^{0.4} \left(\frac{k_l}{D_H}\right) F$$

and

$$h_{fc} = 0.023\, Re_l^{0.8}\, Pr_l^{0.4} \left(\frac{k_l}{D_H}\right)$$

In the above equations, the wall (T_w) and bulk fluid (T_b) temperatures are typically measured. The saturation temperature (T_s) is typically obtained from water property tables [20] or calculated from equations [38].

2.4.2.2 Shah Correlation

Shah (1977) advanced a graphical method (*CHART*) for saturated boiling in which the convection coefficient (Co) was introduced [39]. Four dimensionless parameters were defined for the use of this method, namely:

i. Heat transfer enhancement factor (ψ):

$$\psi = \frac{h_{TP}}{h_l} \tag{2-24}$$

ii. Convection coefficient (Co):

$$Co = \left(\frac{x}{1-x}\right)^{0.8} \left(\frac{\rho_v}{\rho_l}\right)^{0.5} \tag{2-25}$$

iii. Boiling number (Bo):

$$Bo = \frac{\dot{q}}{G\, h_{fg}} \tag{2-26}$$

iv. Froude number (Fr_l):

$$Fr_L = \frac{G^2}{\rho_l^2\, g\, D} \tag{2-27}$$

For vertical pipe flow, Shah proposes that the Froude number be at unity. For a flow condition, that has a low vapour quality and hence a higher Co value, Shah proposes the following simple equation to determine the heat transfer enhancement factor:

$$\psi = 230\, Bo^{0.5} \tag{2-28}$$

In the case of flow conditions that generate lower Co values with associated higher vapour qualities, the following equation is proposed:

$$\psi = \frac{1.8}{Co^{0.8}} \tag{2-29}$$

The Dittus-Boelter equation per Eq. (2-15) yields the heat transfer coefficient h_l.

Shah (1977) also suggests the use of the effective diameter (D_e) when analysing flow through annuli using the above sets of equations, stated as follows:

$$D_e = \frac{4\,(flow\ area)}{heated\ perimeter} \quad (clearance\ < 4) \tag{2-30}$$

$$D_e = \frac{4\,(flow\ area)}{wetted\ perimeter} \quad (clearance\ > 4) \tag{2-31}$$

where $clearance = (D_o - D_i)/2$, in which D_o and D_i represent the outside and inside diameters of the annulus respectively.

For fully developed heat transfer in subcooled flow boiling, Shah (1983) proposes an equation for a heat flux that will result in a specific wall temperature, as follows [40]:

$$\dot{q} = \left[230\left(\dot{m}h_{fg}\right)^{-0.5} h_l (T_w - T_s)\right]^2 \tag{2-32}$$

where

$$h_l = 0.023\left[\frac{G\, D_o(1-x)}{\mu_l}\right]^{0.8} Pr^{0.4}\,\frac{k_l}{D_o} \tag{2-33}$$

2.4.2.3 Gungor and Winterton Correlations

The authors used a similar approach to that adopted by Chen [30]. Their correlation also includes the enhancement and suppression factors for the saturated boiling heat transfer coefficient (HTC), as follows [41]:

$$h_{TP} = Eh_l + Sh_{nb} \tag{2-34}$$

The forced convection heat transfer coefficient (h_l) is the same as for the Dittus-Boelter equation in Eq. (2-15) but the nucleate pool boiling heat transfer coefficient (h_{nb}) is the same as Cooper's correlation [42], expressed as:

$$h_{nb} = 55 p_r^{0.12}\, \dot{q}^{0.67} (-log_{10}\, p_r)^{-0.55} M^{-0.5} \tag{2-35}$$

In the above equation, p_r represents the reduced pressure value in the test section and M the molecular weight of the coolant.

The enhancement and suppression factor equations are respectively:

$$E = 1 + 24 \times 10^3\, Bo^{1.16} + 1.37(1/X_{tt})^{0.86} \tag{2-36}$$

and

$$S = \frac{1}{(1 + 1.15 \times 10^{-6} E^2 Re_l^{1.17})} \tag{2-37}$$

The following equation states the expression for the subcooled heat flux for a specific wall temperature:

$$\dot{q} = h_l(T_w - T_b) + Sh_{pool}(T_w - T_s) \tag{2-38}$$

The above correlations are still widely cited by various scholars. A subsequent correlation by Gungor and Winterton (1987) provides a more simplified model to determine the heat transfer coefficients for saturated boiling [43]. The equation set is as follows:

$$h_{TP} = (SS_2 + FF_2) h_{SP,l} \tag{2-39}$$

$$h_{SP} = 0.023\, Re_l^{0.8}\, Pr_l^{0.4}\; k_l/D_H \tag{2-40}$$

The suppression multiplier is:

$$S = 1 + 3 \times 10^3 \, Bo^{0.86} \tag{2-41}$$

in which the boiling number (Bo) is:

$$Bo = \dot{q}/\left(h_{fg} G\right) \tag{2-42}$$

The equation to determine the F multiplier in which x still represents the vapour quality as:

$$F = 1.12 \, (x/(1-x))^{0.75} \, (\rho_l/\rho_v)^{0.41} \tag{2-43}$$

The following limitations frames F_2 and S_2 variables applications:

$$S_2 = \begin{cases} Fr_l^{(0.1-2Fr_l)} & [for\ horizontal flow\ and\ if\ Fr_l < 0.05] \\ 1 & [for\ vertical\ flow\ and\ all\ other\ cases] \end{cases}$$

$$F_2 = \begin{cases} Fr_l^{0.5} & [for\ horizontal\ flow\ and\ if\ Fr_l < 0.05] \\ 1 & [for\ vertical\ flow\ and\ all\ other\ cases] \end{cases} \tag{2-44}$$

2.4.2.4 Liu and Winterton Correlation

Liu and Winterton [44] combined some of the concepts proposed by Kutateladze [45] and Chen [30] in an effort to develop a generalised model to predict the subcooled flow boiling heat flux. The authors propose the expression of the saturated heat transfer coefficient as a combination of the single-phase forced convection heat transfer and the pool boiling heat transfer as follows:

$$h_{TP}^2 = [F h_l]^2 + \left[S h_{pool}\right]^2 \tag{2-45}$$

The Liu and Winterton enhancement (F) and suppression (S) factors respectively are:

$$F = \left[1 + xPr_l \left(\frac{\rho_l}{\rho_v} - 1\right)\right]^{0.35} \tag{2-46}$$

$$S = \left[1 + 0.055 F^{0.1} Re_l^{0.16}\right]^{-1} \tag{2-47}$$

The single-phase heat transfer coefficient is provided by the Dittus-Boelter equation in Eq. (2.15) and the pool boiling correlation is as per Cooper's correlation as was expressed previously in Eq. (2-35).

Liu and Winterton claim that their correlation accurately predicts surface temperature and that the correlation clearly distinguishes between nucleate boiling and forced convection effects. As such, the correlation facilitates a starting point for understanding the performance of surfaces designed to enhance heat transfer. The correlation promotes an explicit boiling term rather than an empirical boiling number dependence. In their findings, the authors also state that the correlations that use the boiling number term Bo (as discussed previously in Subsection 2.4.2.2) prevent application to subcooled boiling analysis [44].

2.4.2.5 Kandlikar Correlations

Kandlikar (1990) proposed a correlation, refined from his earlier work (1983), which could predict the h_{TP} versus x relationship (x is as defined earlier) [46]. The correlation, as verified for both water and R-113 refrigerant, was valid for predicting saturated flow boiling heat transfer coefficients inside vertical and horizontal tubes. The equation includes familiar parameters: h_l, Co and Bo (defined previously) together with constants (C_i) in an explicit equation as follows:

$$\frac{h_{TP}}{h_l} = C_1\, Co^{C_2} (25\, Fr_{lo})^{C_5} + C_3\, Bo^{C_4}\, F_{fl} \tag{2-48}$$

The F_{fl} variable is a fluid-dependent parameter, which for water is equal to unity. **Table 2-1** provides details for the values of the other constants in the equation.

Table 2-1: Constants for use in the Kandlikar (1990) correlation [46]

Constant	Convection Region	Nucleate Boiling Region
C_1	1.1360	0.6683
C_2	-0.9	-0.2
C_3	667.2	1 058
C_4	0.7	0.7
$C_5{}^*$	0.3	0.3

$C_5{}^* = 0$ for vertical tubes and for horizontal tubes with $Fr_l > 0.04$

In the above equation, Kandlikar states that the h_{TP}/h_l factor represents the larger yielded value for either the forced convection region or nucleate boiling region group of constants, as determined by evaluation of the Co value. The heat transfer in convective boiling region dominants when $Co > 0.65$. For $Co < 0.65$, the nucleate boiling region dominants the heat transfer. The respective column of

constants in **Table 2-1** should be selected for use in the correlation. The author suggests that this method provides a continuity between the convective and nucleate boiling regions.

For the case of subcooled flow boiling, Kandlikar (1998) proposes the following equation to correlate with the heat flux [47]:

$$\dot{q} = \left[1\,058(\dot{m}h_{lv})^{-0.7}F_{fl}h_{lo}(T_w - T_s)\right]^{\frac{1}{0.3}} \tag{2-49}$$

The single-phase heat transfer coefficient (h_{lo}) is determined by assuming all mass flow as liquid only and is provided by the Petukhov and Popov (1963) equation according to $0.5 \leq Pr \leq 2 \times 10^3$ and, $10^4 \leq Re_l \leq 5 \times 10^6$ in the following equation [48]:

$$h_{lo} = \frac{Re_L\, Pr_l(f/2)}{[1.07 + 12.7(Pr^{2/3} - 1)(f/2)^{0.5}]}\,\frac{k_l}{D} \tag{2-50}$$

The friction factor (f) in Eq. (2-51) is:

$$f = [1.58\ \ln(Re_l) - 3.28]^{-2} \tag{2-51}$$

2.5 Clad Tube Surface Temperature

A common theme emanating from the literature survey is the requirement for the physical surface temperatures measurements along the heated clad surfaces. This parametric value is key to determining the required heat transfer coefficients. To achieve this, the heated surface of the clad walls had to be fitted with appropriate temperature measurement probes. This aspect of the project required quite an in-depth analysis and related experimentation to determine the most suitable solution. Subsection 4.2 discusses suitable methods to obtain this parametric value.

2.6 Dissolved Air/Gases

The amount of air, gas or other impurities dissolved in the water affects the properties of the water and hence the boiling process. Experiments by Kandlikar *et al*. (2007) [49] showed that if the fluid body was maintained at or close to the desorption temperature, then there would be a reduced chance of air or gas (including vapour) being absorbed back into the fluid body. This technique was thus adopted in the design and operating considerations of the flow loop. The water in the system was first heated to levels above the required test condition and then allowed to cool to the required operating temperature. This was repeated a few times before final testing commenced.

2.7 Survey of Thermal-Hydraulic Flow Loops in other Facilities

A survey of other facilities provided the basis for the configuration of the UP-THFC as well as the recognition of industry best practices. The following sections highlight the findings from the survey.

2.7.1 Subcooled Flow Boiling Loop at City College New York (CCNY)

The experiments performed on the CCNY flow loop included pool boiling from platinum wire, subcooled flow boiling in a vertical tube and single air bubble injection into a turbulent water stream based on a vertical up flow configuration. Kawaji *et al*. (2011) used the experimental results [50] to develop an advanced thermal finite element lattice Boltzmann model in order to predict the pool and flow boiling experiments.

The CCNY flow loop makes use of the main tank equipped with a 1.5 kW immersion heater to store degassed water. A gear pump caters for a flow rate with a range of 5 to 55 litres per minute as measured by a flow meter. This provides for a maximum bulk velocity of water in the annular channel test section of 1.48 m/s. A condensation tank located downstream of the test section allows for any steam bubbles to be condensed and for the liquid to be cooled down. The adjusting of the cooling water flow rate through a condensation tank and in conjunction with adjustments to the immersion heater power in the main tank facilitates the inlet subcooling temperature control. During steady-state experiments, the main tank bulk temperature is constant.

The cross-section of the CCNY flow loop test section consists of an annular flow channel. A single 9.53 mm outer diameter (OD) aluminium tube with a 0.9 mm wall thickness is located concentrically inside a 19.04 mm inner diameter (ID), 25.4 mm OD polycarbonate tube forming an annular gap of 4.80 mm between the tubes. The aluminium tube is heated by means of a 750 W cartridge heater (6.3 mm OD, 254 mm length), located concentrically inside the tube, and provides a maximum heat flux of 100.3 kW/m^2. A thermally conductive grease fills the approximately 0.72 mm gap between the cartridge heater and inner wall of the aluminium tube. A T-type thermocouple measures the tube wall temperature. The thermocouple is embedded inside the aluminium tube wall by inserting it via a 0.5 mm hole drilled through the wall and filled with an aluminium repair epoxy.

2.7.2 The University of California, Los Angeles (UCLA) Flow Loop

Basu and co-workers (2002) [23] used the flow loop at UCLA for subcooled flow boiling experiments. The experiments included the investigation and study of ONB and active nucleation site density during

subcooled conditions. These experiments used two formats consisting of a flat copper plate surface and nine-rod Zircaloy-4® cladding bundle configurations. Distilled water constituted the flow medium. The flow configuration was vertical up flow through a 1.83 m long flow channel.

The flow loop consisted of two tanks of 1.25 m^3 liquid volume each. The main supply tank was fitted with immersion heaters of 13.5 kW total power for aiding the preheating and degassing of the distilled water. A centrifugal pump recirculated the water through the system with the flow rate measured by means of a turbine flow meter. The main preheater (210 kW, 480 V, 3-phase) was also of the immersion type and was located vertically in a stainless steel container and upstream of the test section entrance. At the inlet and exit of the test section, pressure transducers and thermocouples measured pressure and temperature, respectively.

The flat copper plate surface and nine-rod bundle formats had different test section configurations. In the case of the flat copper plate surface, the test section was almost square in cross-section consisting of a 16.33 cm^2 flow channel with the heated length being 0.3 m long. Flow development and flow transition sections of approximately 0.6 m and 0.3 m respectively were provided upstream of the heated section. Similar sections, but of 0.3 m lengths each, were provided downstream of the heated section. Pyrex glass, fitted into frames on three sides of the test chamber, allowing for visual observations. A copper block heated with embedded cartridge heaters and mounted flush onto the channel formed the fourth wall of the flow duct.

For the nine-rod bundle configuration, the heated lengths were 0.91 m Zr-4 cladding rods with 1.11 cm outside diameters. The upstream flow development and transition sections were 0.36 m and 0.20 m respectively. Corresponding downstream sections were 0.15 m and 0.20 m respectively. Glass windows provided for visual observations on all four sides of the square cross-section test section.

The 3 x 3 square lattice arrangement of the rods had a 1.43 cm pitch typical in PWRs. Copper bus bars located at the entrance and exit sides of the heated sections connected power to the rods. Rods were heated by means of Joule heating using a 100 kW DC power supply. The bus bars created a flow obstruction in the flow channel, however, Basu *et al*. (2002) [23] deemed this the best alternative for providing power to the rod bundle.

2.7.3 KAIST Experimental Low-pressure Critical Heat Flux (CHF) Test Loop

A number of researchers used the low-pressure CHF test facility at Korea Advanced Institute of Science and Technology (KAIST) in order to conduct studies of CHF in annuli under low-pressure low-flow

conditions, which had relevance to certain research reactors and heating reactors used for the provision of process heat [51]. These researchers included Mishima *et al*. (1982-1987), Rogers *et al*. (1982), El-Genk *et al*. (1988), and Park *et al*. (1996). Park and co-workers progressively modified the loop to a version eventually used.

The loop used filtered subcooled water fed into the test section via a throttling valve. This method created a large pressure drop in order to obtain stable inlet flow conditions. A combination of valves directed the flow for either vertical -upflow or -downflow configurations. The boiling off the water in the loop for about half an hour prior to any tests allowed for the control of the amount of entrained non-condensable gases in the water. A 5 kW electrical resistance preheater controlled the amount of inlet subcooling. The condenser/cooler-type heat exchanger, located downstream of the test section, was employed to cool the two-phase water/steam back into subcooled liquid. A centrifugal pump recirculated water through the loop.

A large volume surge tank with controlled water level maintained a nearly constant pressure in the test section. The large liquid volume of the surge tank also suppressed any rapid change of water temperature. An open steam vent valve at the top of the surge tank systematically released the steam to maintain atmospheric-type pressure conditions in the loop. A 64 kW DC power supply provided power for the heated sections of the test section. A turbine flow meter was used for flow rate measurements and T-type thermocouples were used for temperature measurements.

2.7.4 Modified KAIST Experimental Low-pressure Loop

Another modification of the KAIST low-pressure test loop led to the version used by Kim and co-workers [52]. The experimental parameters that were required for the experiments conducted by Kim *et al*. (2000) [52] included a pressure range of 106 to 951 kPa, mass flux range of 20 to 277 kg/m^2.s, and inlet subcooling capability of between 50 to 654 kJ/kg.

In this new modified version of the KAIST low-pressure flow loop, a pressuriser unit connected to the top of the surge tank via a conduit pipe that was fitted with a shut-off valve to control the pressure in the loop. Water was filled in the pressuriser vessel to a predetermined height. To pressurise the system required the injection of compressed nitrogen gas from a high-pressure cylinder into the upper part of the pressuriser, which, in turn, provided a compressible volume to the loop (via the surge tank with the shut-off valve fully opened). This method catered for the maintenance of the desired pressure condition in the system.

2.8 Chapter Summary

The main objective of the present work was to develop a suitable experimental test rig to conduct comparative heat transfer testing of nuclear fuel clad tubes consisting of existing and new proposed material types. Studies of the heat transfer characteristics of the test specimen clad tubes subjected to subcooled and saturated forced convection flow conditions were of focal interest. Studies focusing on the heat transfer performances of the clad tubes during critical heat flux (CHF) conditions form the focus of future research. In order to fulfil these goals, the experimental hypothesis test was to evaluate the test parameter requirements and thereafter to design a system for the extraction of the required heat transfer information. The literature survey thus identified the different measurands that were required for use within relevant equation sets for the evaluation of the heat transfer phenomena. The information gleaned from the literature survey thus guided the design of the experimental set-up and test section, as discussed in the following chapter.

3 Test Section and Experimental Set-up

3.1 Introduction

This chapter presents a description of the UP-THFC experimental rig and test section set-up. The UP-THFC test facility had to be purpose designed and built from the ground up to meet the specific testing requirements of the current study initiative. Existing designs for such facilities were propriety in nature with little information available. From a survey of other closed-loop test facilities (Chapter 2) which conducted forced convection heat transfer experiments, the necessary operational features were investigated and evaluated for use in the UP-THFC. Calculations for the design of the UP-THFC are included in Appendix A. This chapter also discusses the instrumentation used for the measuring of the various test parameters, as well as the data collection and system control methods.

3.2 System Requirement Analysis of the University of Pretoria – Thermal-Hydraulic Flow loop Cell (UP-THFC)

The test section was the key component of the flow loop. Because the main heat transfer studies were set to be conducted in this section, the design and configuration of the rest of the flow loop were derived from the operation parameter and conditions of the test section. In the establishment of the test section dimensions and parameters, a point of reference was required, from which the system analysis could proceed.

That reference point was identified as being at the geometric centre of the test section. By specifying the operating parameters at that reference point, the system condition at any other point in the loop, both upstream and downstream of the reference, could then be determined analytically. The range of values stipulated in **Table 3-1** was thus used for initial estimates of the size and configuration of the system, which specified the respective operating condition at the designated reference point.

Table 3-1: Design operating condition ranges of UP-THFC

Operating Parameter	Range
Pressure (absolute)	Up to 200 kPa
Bulk coolant temperature	Ambient to 120 °C
Mass flux	500 to 3 000 kg/m^2.s

The next major component that was required and identified in the survey was a condenser or heat exchanger. This item was required in order to maintain the necessary inlet temperatures to the pump and/or the test section. The component was identified to be located downstream of the test section but just upstream of the flow loop recirculation pump. The heat exchanger was thus required to be configured according to the level of subcooling required in the system.

The selection of a suitable pump was deemed one of the main design considerations of the flow loop. In the flow loop systems that were surveyed in the literature, different types of pumps were used in each of the respective test rigs per their individual operational requirements. In the selection of a suitable pump for the UP-THFC, a detailed pumping requirement analysis was conducted according to best practices [57]. Some of the details and calculations are available in Appendix A.

It was also extracted from the literature survey that the test facilities that operated at higher internal pressure conditions than the local ambient pressure required an auxiliary pressurising method. The modified KAIST loop (Subsection 2.7.4) employs a compressed gas pressuriser system for these purposes. This mechanism provides for the overall pressure control of the system and ensures that the required inlet pressure of the pump is met. It was thus envisaged that such a mechanism would also be adopted for the UP flow loop.

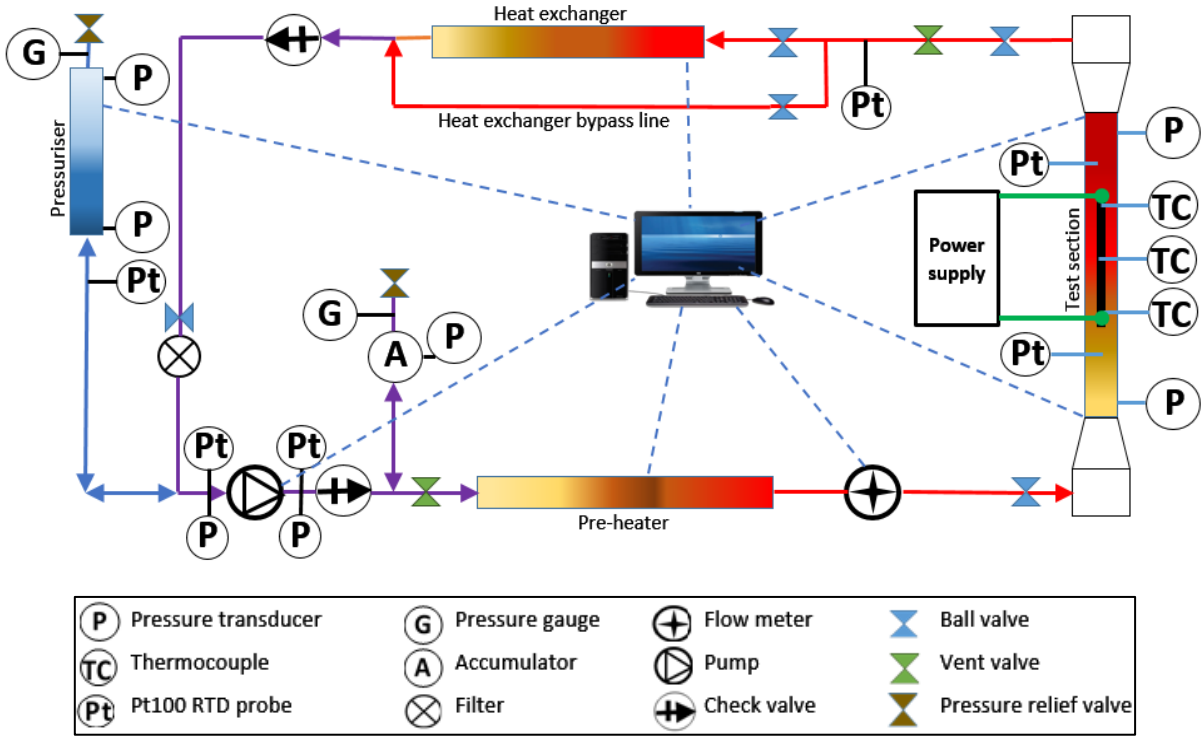

Figure 3-1: Schematic representation of the UP-THFC experimental setup.

The above four components, namely the test section, heat exchanger, pressuriser and pump, constituted the major components of the UP flow loop. A purpose-built pipe network interconnected

these components. A schematic representation of the UP-THFC experimental setup is depicted in **Figure 3-1**. Other components and equipment such as flow meters, pressure sensors, temperature sensors, valves, and filters were also included and connected at pre-determined locations into the flow loop. Suitable data recording facilities, operator interfaces and safety equipment was also required and hence was developed for the effective operations of the loop.

For natural convection heat transfer studies, a continuous flow loop path involving just the vertically orientated test section and certain pipe sections was to be isolated from the rest of the system. At a later stage, an auxiliary pump would be incorporated into the selected flow path for circulation of the preheated working fluid according to the vertical downflow configuration. Once the required flow speed was attained, the auxiliary pump would be switched off, thus allowing the buoyancy forces in the bulk fluid to dominate the flow and in so doing reverse the flow direction through the test section. This portion of the work is scheduled for a future undertaking.

3.3 Evolution of the UP-THFC

A number of conceptual iterations led to a final optimised composite system configuration that would sufficiently cater for each of the four flow circuit requirements. The composite system used a singular test section that could be rotated into either a vertical or horizontal orientation. In the horizontal orientation, an additional pipe section was required to facilitate the connection of the pump to the inlet of the test section. Flow direction through the test section was controlled by a set of valves and was similar to the method adopted in the KAIST loop as discussed in Subsection 2.7.3.

The above-mentioned layout configuration of the composite system formed the foundation for the complete UP flow loop design. As part of the adoption of the final design, the necessary materials and components first needed to be evaluated and selected. The physical influence of these materials and components within the flow loop also needed to be accounted for in the analytical processes with the aim of providing the expected system performances. Calculations for the pump selection and the system pressure drop are detailed in the appendices. From this analysis, an Ebara 3M 50-160/7.5 centrifugal pump [53] was evaluated to be reasonably suitable for the majority of the flow requirements of the UP-THFC.

In the as-built system with the test section orientated vertically, the rig occupied a space of approximately 5 m long, 2 m wide, and 4.5 m high with the centre of the test section at approximately 2.35 m above the floor of the room, **Figure 3-2 (a)**. In the horizontal test section orientation, as shown in **Figure 3-2 (b)**, the occupied length extended to approximately 7.0 m with the centre line of the test

section levelled at approximately 1.78 m above the floor of the room. A 2.4 m^2 and 0.8 m high-elevated platform was installed to provide an ergonomic working height of approximately 1.55 m to the centre of the test section in the vertical orientation and 1.0 m for the horizontal layout.

(a) (b)

Figure 3-2: As built and installed UP-THFC experimental rig (shown without elevated work platform) for the following test section orientations: (a) vertical orientation and (b) horizontal orientation.

3.4 Test Section Configuration

In consideration of the range of tests involving different pin array configurations, a flow channel with a square cross-section and flat panelled walls was selected as the test section channel profile. Shown in **Figure 3-3** is the general cross-sectional arrangement for the test section channel. The graphic indicates the locations of the visual viewing ports as well as a typical fuel pin arrangement.

The 80 mm x 80 mm cross-sectional area of the test section is capable of accommodating pin arrays up to a maximum 7 x 7 array of typical Zircaloy® pins with an outer diameter and pitch spacing of 9.8 mm and 11.43 mm respectively or a 4 x 4 array of the currently available SiC tubes with outer

diameter and pitch spacing of 15.5 mm and 20 mm respectively. Pin lengths were of 530 mm for Zr-4 and 540 mm for the SiC clad tubes.

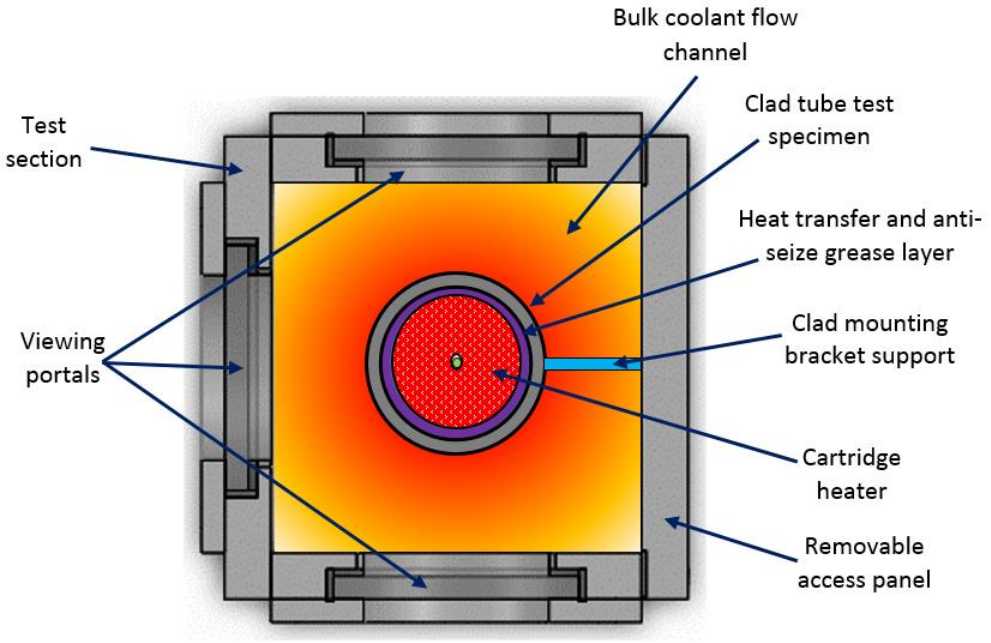

Figure 3-3: Typical cross-sectional schematic of the UP-THFC test section (not to scale) depicting a single heated pin within the bulk coolant flow channel.

The hydrodynamic entrance length for the test section duct was designed according to an accepted criterion [13], namely that for turbulent flow, the entrance length becomes insignificant beyond a length of approximately 10 hydraulic diameters and that both the hydrodynamic and thermal entry lengths could be considered to be:

$$L_{h,turb} = L_{t,turb} = 10D_H \tag{3-1}$$

Since the facility had to accommodate both vertical up flow and down flow forced convection conditions, the entrance and exit lengths were selected to be of the same length to reduce the tedious rotation of the test section. An overall length of 3 m for the flow duct, inclusive of the centrally located 530 mm heated test section length, allowed for an effective $15.44D_H$ equivalent length of the hydrodynamic entrance and exit lengths.

The heated test section portion was fitted with a removable access panel, as shown in **Figure 3-4**, to allow for access into the test section flow channel. The removable access panel also served as a mounting platform for the test specimen(s) and measuring instruments. The arrangement allowed for the external pretesting of the installed cartridge heater and test instruments in an auxiliary test tank to conduct equipment functionality and water tightness tests prior to the panel being installed in the test section flow channel. This provided for a quicker turnaround time between experiments.

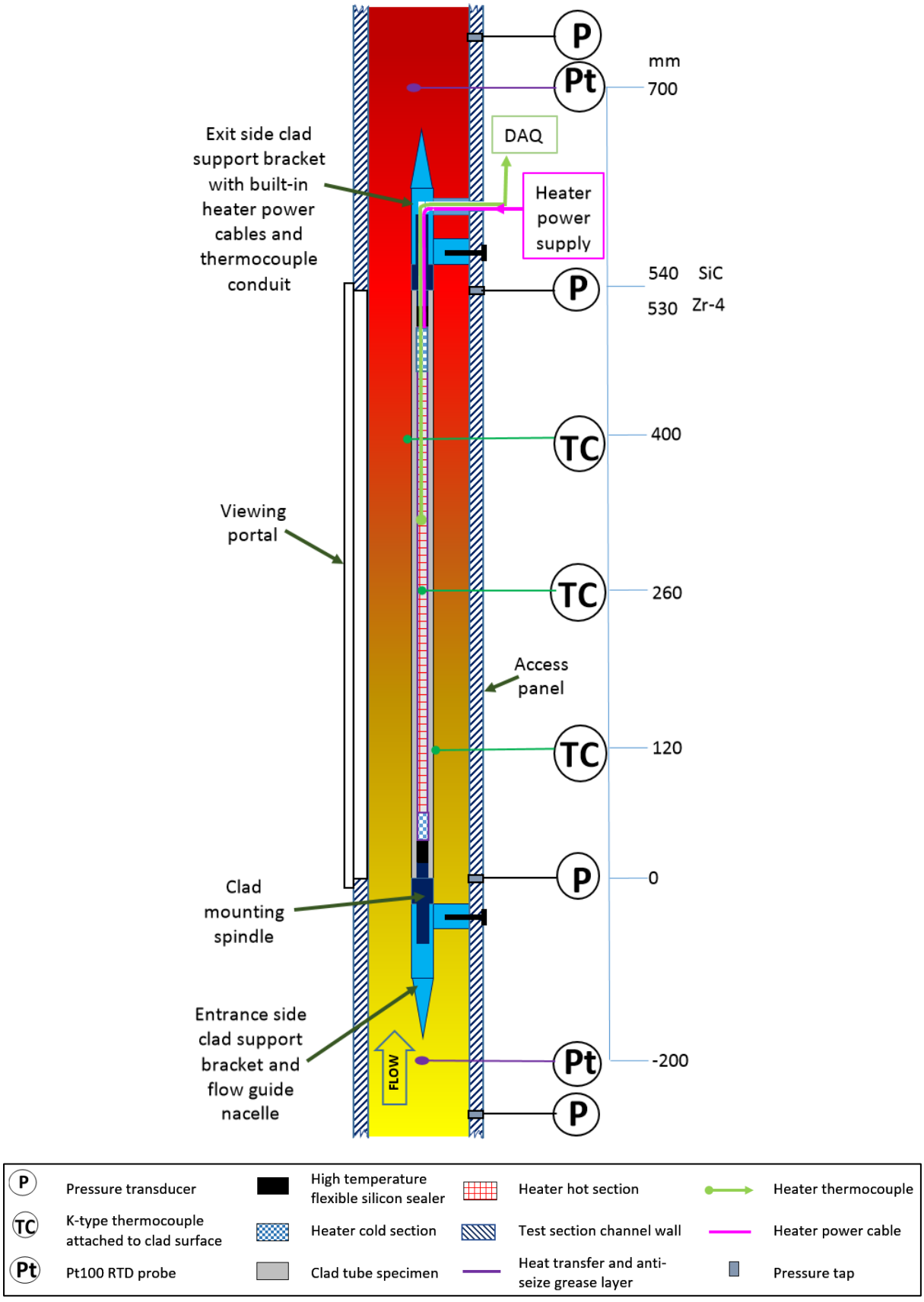

Figure 3-4: Schematic of the heated portion of the UP-THFC test section (not to scale) showing a general longitudinal cross-sectional view of a single clad-tube test specimen mounted in place between support brackets. The locations and general layout of various test instruments are indicated in the schematic.

3.5 Instrumentation, Data Logging and System Control

The test section was equipped with inlet and outlet Pt100 temperature sensing probes to measure the inlet- and outlet-bulk fluid temperatures and electronic pressure transducers to measure the absolute static pressure at those locations as shown in **Figure 3-4**. The test section could be readily populated with additional temperature and pressure probes. Other temperature probes and pressure transducers were employed in the loop for system and performance monitoring. All instruments were supplied as calibrated or calibrated in-house where necessary.

A Venturi flow meter primary element coupled to a high-precision electronic differential pressure transducer (DPT) secondary element was used to measure the bulk flow in the system. Endress+Hauser [54] kindly donated the DPT and the company sponsored the calibration of the compound flow-measuring device.

Control of the flow in the system was achieved electronically via user input to a variable frequency drive (VFD), which was connected to the pump.

The power supply to the cartridge heater located inside the test clad tubes was by means of an adjustable solid-state relay (SSR) that could supply a maximum of 25 A at 230 VAC. The SSR was manually controlled via a potentiometer. Observation and monitoring of the voltage and current drawn by the cartridge heater were via high-precision analogue voltmeter and ammeter respectively. The output values of these were also electronically monitored and logged. The cartridge heater had a built-in J-type thermocouple for the monitoring of the heater temperature and to gauge the operational status of the heater.

The pressurisation of the flow loop was achieved by means of introducing high-pressure compressed air into the pressuriser unit only when the flow loop was filled with the required water inventory. The process was manually controlled by means of adjustments of a conventional pressure regulator valve. Depressurising was via a remotely activated solenoid valve, which was fitted at the top of the pressurising unit. The depressurising of the system was also aided by carefully purging small volumes of thermally expanded water from the system via the manually controlled bleed/drain valves. Electronic pressure transducers were used to monitor the pressure levels in the system. For redundancy, dial pressure gauges were fitted to the pressuriser and accumulator units. These units were also equipped with pressure relief valves, which were pre-set to release pressure at specific threshold levels.

The electronic output signals from all instruments employed in the test rig were relayed to an Agilent data logger linked to a desktop computer system. The signals from non-temperature devices were in voltage (VDC) format and required conversion to reflect the correct units of measure of the respective

instruments. A graphical user interface (GUI) program configured with Labview software was used for this purpose. The GUI also acted as the main control interface for the system health monitoring, and test specific data display and recording interface. The GUI was coded with an audio-visual alarm suite to alert the operator whenever any of the flow loop performance thresholds were reached or exceeded.

3.6 Chapter Summary

This chapter provided some insight into the design and development of the UP-THFC. Apart from the pump, all other components were designed and built in-house exclusively for the flow loop. The system was configured to function within the performance requirements as stipulated in the design directives as stated in Chapter 1. An appropriate control suite was designed and installed to provide operational and data recording functions. The next chapter discusses the system validation and data analysis.

4 Data Analysis and System Validation

4.1 Introduction

The experimental test procedures and data reduction methodologies are discussed in this chapter. The method to determine the heat transfer coefficients and the clad tube outer-surface temperatures are also described. Importantly, the validation of the experimental set-up is detailed to ensure that accurate measurement can be obtained.

4.2 Data Reduction for Heat Transfer Calculations

4.2.1 Heat Flux

The heat flux ($\dot{q}$) was determined from the relation between the input electric power to the heater ($\dot{Q}_{in}$), which is equivalent to the product of the root mean square (RMS) value of the voltage and current drawn by the heater and the outer heated surface area of the clad tube specimen (A_s) as follows:

$$\dot{q} = \frac{\dot{Q}_{in}}{A_s} = \frac{V_{in}.I_{in}}{\pi D_o L_{heated}} \tag{4-1}$$

On this basis, the magnitude of the heat input and resultant heat flux is shown in **Table 4-1**.

4.2.2 Clad Surface Wall Temperature

Following an extensive investigation as detailed later on in Subsection 4.5.6, the wall temperature (T_w) on the heated clad surface was determined from the measured film or interface temperature (T_f) and the average bulk coolant temperature (T_b) in the test section as shown in the following equation:

$$T_w = 2T_f - T_b \tag{4-2}$$

4.2.3 Heat Transfer Coefficient

The average heat transfer coefficient was determined from the following equation:

$$h_{avg} = \frac{\dot{q}}{\Delta T_b} \tag{4-3}$$

$$\Delta T_b = T_w - T_b$$

Table 4-1: Heat flux on test clad-tube specimen outer surface area.

Electric Power Inputs			Heat Flux [kW/m^2]	
Input Voltage [VAC]	Input Current [A]	Heater Power [kW]	Zr-4	SiC
100	5.0	0.50	40.4	25.6
125	6.5	0. 8	63.2	40.0
150	7.5	1.1	90.9	57.6
175	9.0	1.6	124	78.4
200	10.0	2.0	162	102
220	11.0	2.4	196	124

4.2.4 Wall Superheat (Excess) Temperature

The difference between the temperature on the clad wall (T_w) and the saturation temperature (T_{sat}) of the water at a particular pressure is referred to as the superheat (excess) temperature (ΔT_s). The following equation was used to determine the ΔT_s values:

$$\Delta T_s = T_w - T_{sat} \tag{4-4}$$

4.3 Uncertainties

Uncertainties for the test instruments were established within the 95 % confidence level and are tabulated in **Table 4-2**. The full uncertainty analysis is detailed in Appendix B and follows the procedures set out by Moffatt (1988) [55] and Dunn (2010) [56].

Table 4-2: Test instrument uncertainties.

Instrument/Equipment	Range	Uncertainty
Thermocouples T-type	50 to 150 °C	0.1 °C
Pt100 RTD	95 to 150 °C	0.1 °C
Pressure transducers	0 to 250 kPa 0 to 1 000 kPa	0.025 kPa 0.1 kPa
Flow meter	2.5 to 11.5 kg/s	0.012 kg/s
Voltmeter	0 to 230 VAC	0.1 to 0.5 V
Ammeter	0 to 25 A	0.1 to 0.25 A

4.4 Validation of the Experimental Set-up

Isothermal and diabatic testing was conducted to characterise the thermal hydraulic flow in the test section. These are discussed in the following sections.

4.4.1 Isothermal Test Section Validation

For the isothermal validation, the Reynolds number at the prevalent flow rates was used to verify that the resultant pressure drop across the test section corresponded to the relevant friction factor for the channel walls of the test section. The isothermal friction factors were used for the validation of the experiments with the coolant flow at close to the local ambient conditions at around 29 °C. This was done in order to reduce the influences from heat transfer activities, such as varying density and viscosity effects, which could be disregarded for the flow properties. The pressure drop results emanating from these tests were compared with recognised flow models, as depicted in **Figure 4-1**.

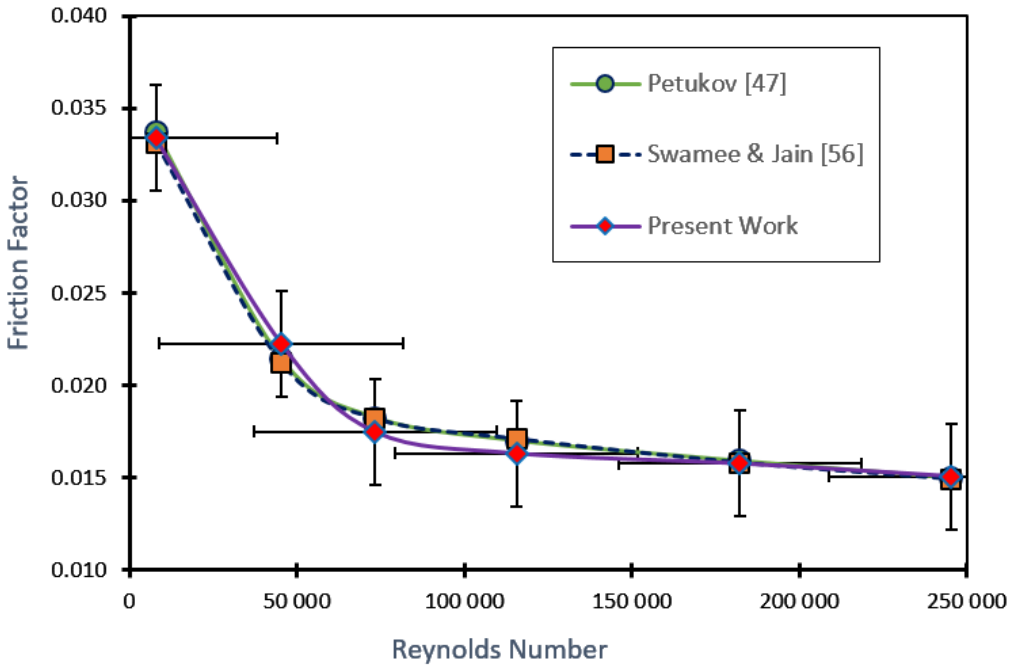

Figure 4-1: Reynolds number versus isothermal friction factor.

The friction factor (f) data was obtained over a Reynolds number (Re) range spanning from about 7.80×10^3 to around 2.45×10^5. The calculated friction factors in the middle of the range have an average deviation of approximately 5.5 % from both the Swamee and Jain [57] and the Petukhov [48]

friction correlations respectively. The error bars indicate the uncertainty in the pressure difference measurements as well as mass flow measurements. These results thus indicate that the flow in the test section could be reasonably accurately determined using the pressure difference measured by the pressure probes on the test section in combination with the Venturi flow meter instrumentation.

4.4.2 Diabatic Test Section Validation

In the diabatic validation of the test section, an energy balance method was used to verify the heat transfer in the system. For a measured inlet temperature, and assuming that all of the heat produced by the clad heater was transferred into the bulk coolant water flow, the outlet temperature was then calculated and compared with the measured outlet temperature by using the following equation:

$$T_{b,out} = \frac{\dot{Q}_w}{\dot{m} \, . \, C_p} + T_{b,in} \tag{4-5}$$

The measured outlet temperature was marginally higher than the corresponding calculated value but was within the uncertainty limits of 0.1 °C for the reference Pt100 resistance temperature-measuring device. Due to the closeness of fit to the calculated values and the uncertainty and tolerances of the outlet Pt100 instrument, the calculated values were subsequently utilised in the data processing and analysis of the heat transfer in the system.

4.5 Clad Wall Surface Temperature and HTC Determination

In Chapter 2, it was established that the clad surface temperature was one of the fundamental factors required to determine the heat transfer capability and characteristics of the cladding tubes. The method to measure the temperature on both the Zr-4 and SiC clad tubes had to be identical in technique in order to claim the validity of the heat transfer results. The capability to utilise the same set of calibrated measuring instruments for all comparative testing was also recognised as being vital to reduce or eliminate the experimental error. In addition, it was essential that the selected surface measuring technique would not adversely affect the flow and thermal surface conditions.

However, efforts to measure the clad surface temperature proved to be quite challenging. Little information was available in the literature regarding suitable surface temperature measurement techniques on heated surfaces exposed to external forced convection conditions. Thus, applicable methods had to be evaluated both experimentally and analytically to select the most appropriate method to attain these surface temperatures. The following subsections provide more details.

4.5.1 Non-Contact Surface Temperature-measuring Methods

The use of pyrometers and infrared laser temperature-measuring devices required a direct line of sight to the respective temperature-emitting surfaces. Although the observation windows in the test section catered for this, the effectiveness of these devices was shown to be incapable of measuring the actual surface temperature on the clad tubes while these were subjected to test conditions within in the flow loop.

Experimental testing results revealed that the heated surfaces of the windows, as well as the heated convective bulk water flow within the test section, produced a thermal barrier that ineffectively restricted the surface temperature measurements on the clad tubes by these devices. This method was subsequently abandoned.

4.5.2 Externally (wetted surface) Mounted Probes

This method entailed the fixing or attaching of temperature-sensing probes to the clad outer surface (wetted surface). Welding or brazing of probes onto the clad surfaces was considered non-feasible, as this could not be achieved on the SiC surfaces.

Clearly, this method would have also been further restrictive as the test probes would have been non-reusable or transferable due to these being permanently attached to the respective clad surface. This method also had the potential of causing a significant permanent velocity and thermal boundary layer disturbance on the clad surfaces.

Thermowell or sheathed-type temperature probes that were in contact and positioned normal with the clad surface in non-permanent-type arrangements were found to respond in a manner resembling cooling fins whereby the output signals of these related the convective bulk water temperature more than the actual clad surface temperatures.

In using this method, it was also relatively difficult to maintain constant contact of the probe-sensing points on the clad surface (bar permanently attaching the probes to the surface as discussed above) due to the bulk coolant flow strength and thermal expansion effects.

The option to locate or position temperature-sensing probes on the external surfaces of the clad tubes was not completely abandoned and was re-evaluated at a later stage, the results of which are discussed in Subsection 4.5.4.

4.5.3 Internally (non-wetted surface) Mounted Probes

It was hypothesised that by measuring the inner clad wall temperature, the external clad wall temperature could then be obtained with the use of analytical extrapolation methods. This entailed the location of temperature probes within the interface space between the heater and the inner clad wall (air gap).

In order to attain the best heater to clad wall heat transfer performances, it was necessary to maintain this gap at the absolute minimum of less than equal to 0.1 mm (as was also recommended by the heater manufacturer). This was found to be necessary in order to reduce premature heater failure owing to poor heat transfer across larger gaps – even when the air gap was completely filled with heat transfer compounds. Due to the space limitations within the very narrow air gap, it was then necessary to groove either the heater or clad inner wall in order to accommodate the most compact temperature-sensing probes available at the time. For structural and thermal stress reasons, the walls of the Zr-4 were deemed too thin (0.5 mm thick) to effectively produce grooves into them and nor was it possible to machine such internal grooves into the SiC owing to its poor post-manufacture machining qualities. Hence, square-shaped grooves of around 0.8 mm wide and to a maximum depth of 0.5 mm were milled into the heater wall (about 1 mm thick) and axially along its length. These were sufficient to accommodate insulated thermocouples with a wire size of 36 to 40 AWG. Sheathed thermocouples of the same size or smaller could not be obtained at the time.

Experiments revealed that these internally mounted thermocouples were highly susceptible to electromagnetic force (EMF) interferences, which were emitted from the cartridge heater during powered-up operations. The EMF effects produced erratic output temperature signals from the thermocouples, which could not be used further for the heat transfer analysis. In addition, during certain test conditions, the gap temperature exceeded 200 °C. This caused the insulation on thermocouple leads to melt leading to short-circuiting and hence malfunctioning of the thermocouples. In this particular case of application, it was hence concluded that it was not feasible to measure the internal clad wall temperature and thereafter to analytically obtain the external clad wall surface temperature.

4.5.4 Adopted Surface Temperature-measuring Technique

After considerable deliberation, it was thus an unavoidable option to attach temperature probes on the outer surfaces of the clad tubes notwithstanding the disturbances that such an arrangement would offer to flow and thermal boundaries. It was assessed that in order to deal with this concern,

the smallest possible probes that were available had to be utilised for the intended purpose with the base condition that these could easily be removed without damaging the clad surface finish. For this purpose, pre-calibrated K-type stainless steel 318L sheathed thermocouples with an overall length of 350 mm and 0.75 mm outer diameter were selected.

Prior to attaching the probes onto the clad surfaces, the access panel had to be removed from the test section and the appropriate clad tube mounted in place. A sheathed thermocouple was then routed via a compression gland on the access panel. Next, a thermal expansion and strain relief loop was fashioned on the probe lead. This was done to compensate for any potential thermal expansion of the sheathed probe lead that would be in contact with the heated convective flow in the test section. Thereafter, a length of approximately 25 mm of the sheathed probe, starting from its tip (sensor point), was located and axially aligned on the clad tube. Predetermined lengths of solid 0.25 mm diameter stainless steel wire were then looped around the clad tube and sheathed thermocouple. The ends of the wire were then carefully twisted together until it was deemed that the probe was sufficiently affixed onto the clad tube or when it could be reasonably assumed that there was a negligible air gap in between. Care was taken to locate the wire ties at least 15 mm downstream from the sensor tip to avoid tripping the flow at the temperature measuring point. A mechanical shakedown was conducted thereafter to ensure that the probe did not move out of place. The assembled access panel was then pretested in the auxiliary test tank to check equipment functionality and water tightness of fittings. The access panel was then relocated to and fastened in place onto the test section. Thereafter, the relevant connections to the instrument and control systems were completed.

The above method provided a very reasonable, cost-effective, and non-permanent option to affix the thermocouple probe onto the test specimen clad surface. The probes could easily be removed when the heat transfer studies required minimal or no flow disturbances over the clad surfaces. This method also allowed for the same set of test instruments to be used for all tests. As compared to previous attempts to measure the clad surface temperatures, the test results using this method yielded excellent results. The findings are discussed in more detail next.

4.5.5 Analysis of Temperature Measurements on Clad Surfaces

A series of tests were conducted to evaluate the acceptability and validity of measuring surface temperature with the adopted technique as discussed in the above subsection. The evaluations included tests in the air (testing conducted inside a vertical furnace), pool boiling (mock tank set-up) as well as forced convection conditions within the flow loop. For brevity, only the outcomes of the forced convection tests are discussed, as they are most relevant to the present study. For obvious

reasons, no additional insulation could be installed over the temperature probe to isolate it from the bulk coolant flow effects.

In the forced convection studies, the average operating pressure in the test section (inclusive of the pump-induced flow velocity pressure) was initially set at around 198 kPa at a bulk coolant flow velocity of around 0.25 m/s. This allowed for a saturation temperature of around 120 °C. The system operating pressure was not increased with further increases in the bulk coolant flow velocity. This allowed the flow-induced pressure to influence the behaviour of the boiling phenomena on the clad heated surfaces. It was reasoned that the inclusion of these effects would be a valuable contribution to the validation of the heat transfer processes in the UP-THFC. However, the analysis of the test data took into consideration the variations of saturation temperature in terms of the respective operating pressure conditions. Hence, it was hypothesised that for the same set of measured temperatures, the experimental results could be interpreted as follows:

a) the measured temperature correlates with the actual surface temperature, or
b) the measured temperature correlates with an interface (film) temperature in the boundary layer between the clad-tube surface and the bulk water stream.

The merits of the above study cases are discussed in the following sections.

4.5.5.1 Visual Observations of the Boiling Phenomena

The experimental data for the evaluations of the two hypotheses were derived from physical flow boiling experiments conducted in the UP-THFC. The testing criteria included cycling through four predetermined velocities in the test section coupled with four heater power inputs with associated heat fluxes. The boiling activity was visually observed for each permutation with the observations tabulated in **Table 4-3**. Instances of a few selected flow-boiling activities are shown in the photographic plates in **Figure 4-2**.

Table 4-3: Summary of visually observed boiling activity.

Flow Velocity [m/s]	Mass Flux [kg/m^2.s]	Heat Flux [kW/m^2] (Heater Power Input [kW])				Average Test Section Pressure [kPa]	Saturation Temperature [°C]
		104 (0.9)	142 (1.2)	191 (1.6)	237 (2.0)		
0.25	234	PNB with numerous bubbles	Bubble sliding, coalescing and lift-off (OSV)	Mass bubbles coalescing and lifting-off (PNB)	Rapid ebullition (FDNB)	199	120
0.5	477	Small amount of bubbles forming	NB with numerous bubbles	Bubble sliding, coalescing and lift-off (OSV)	Mass bubbles coalescing and lifting-off (PNB)	205	121
0.75	717	No Bubble activity	Small amount of bubbles forming	PNB with numerous bubbles lift-off but no coalescing	Bubble sliding, coalescing and lift-off (OSV)	208	122
1	958	No Bubble activity	No bubble activity	No bubble activity	Slight ONB activity	213	122

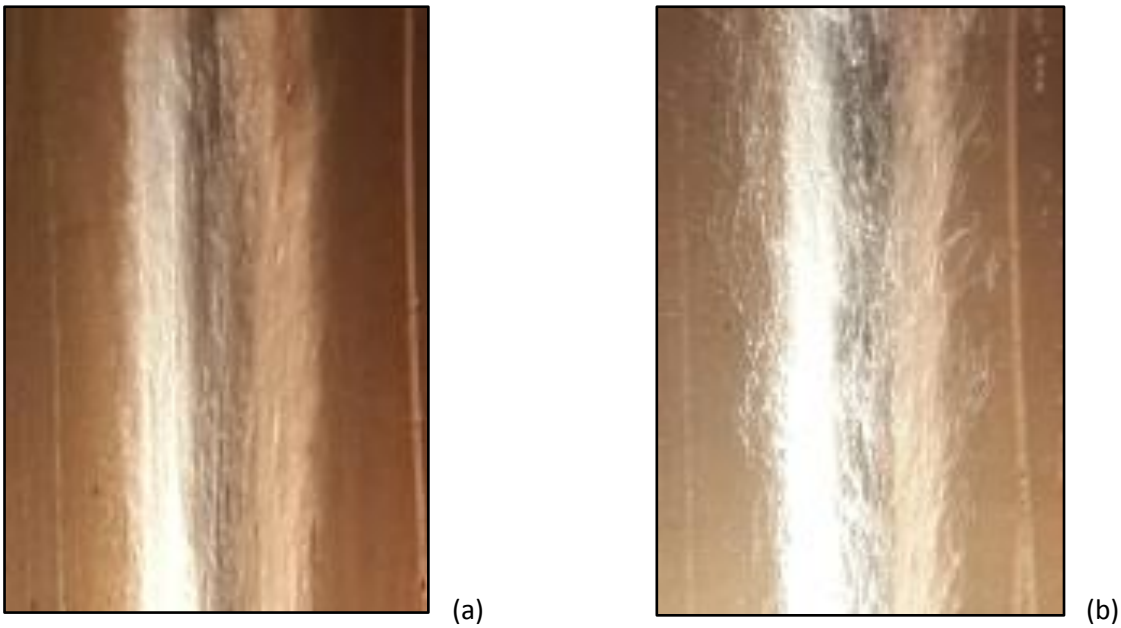

Figure 4-2: Flow boiling phenomena at $T_{in} = 120$ °C, heat flux of 237 kW/m^2, and flow velocities at (a) 0.5 m/s and (b) 0.25 m/s.

4.5.5.2 Analysis of Measured Temperature Results Correlated as Actual Surface Temperature

It is widely accepted that the incipience of the onset of nucleate boiling (ONB) initiates at around a superheat temperature of 5 °C (or 5 °C above the saturation temperature of a liquid at a particular pressure) [13] [14].

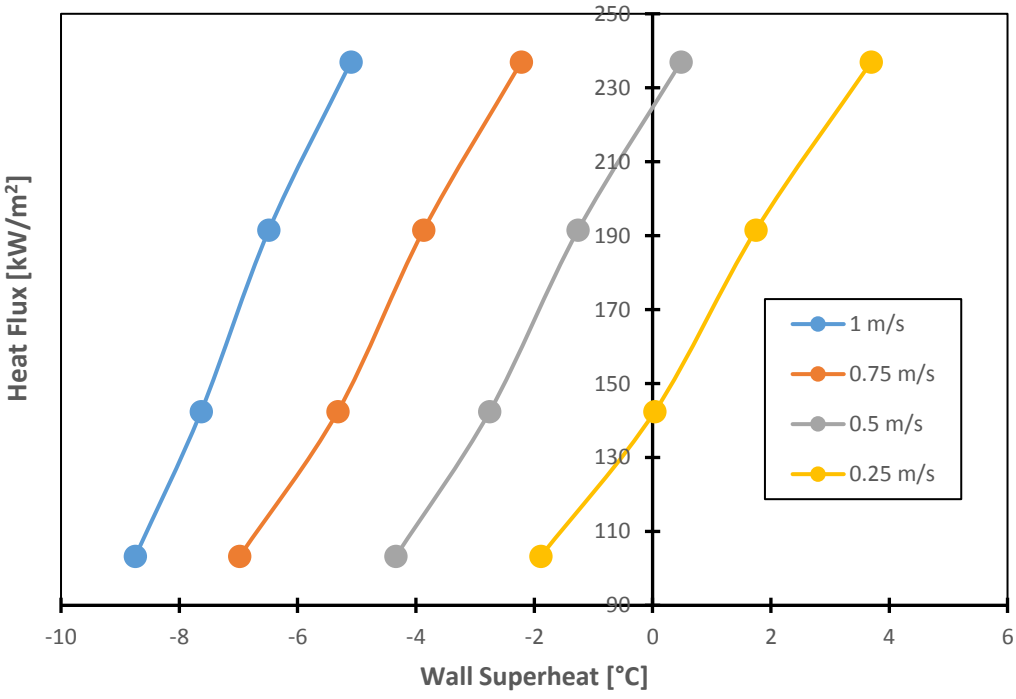

Figure 4-3: Boiling curves for measured temperature correlated as actual surface temperature.

With the measured temperature data assumed as stated above, the wall superheat temperature was calculated using Eq. (4-4) and plotted against the corresponding input heat flux values to produce the relevant boiling curves, as shown in **Figure 4-3**.

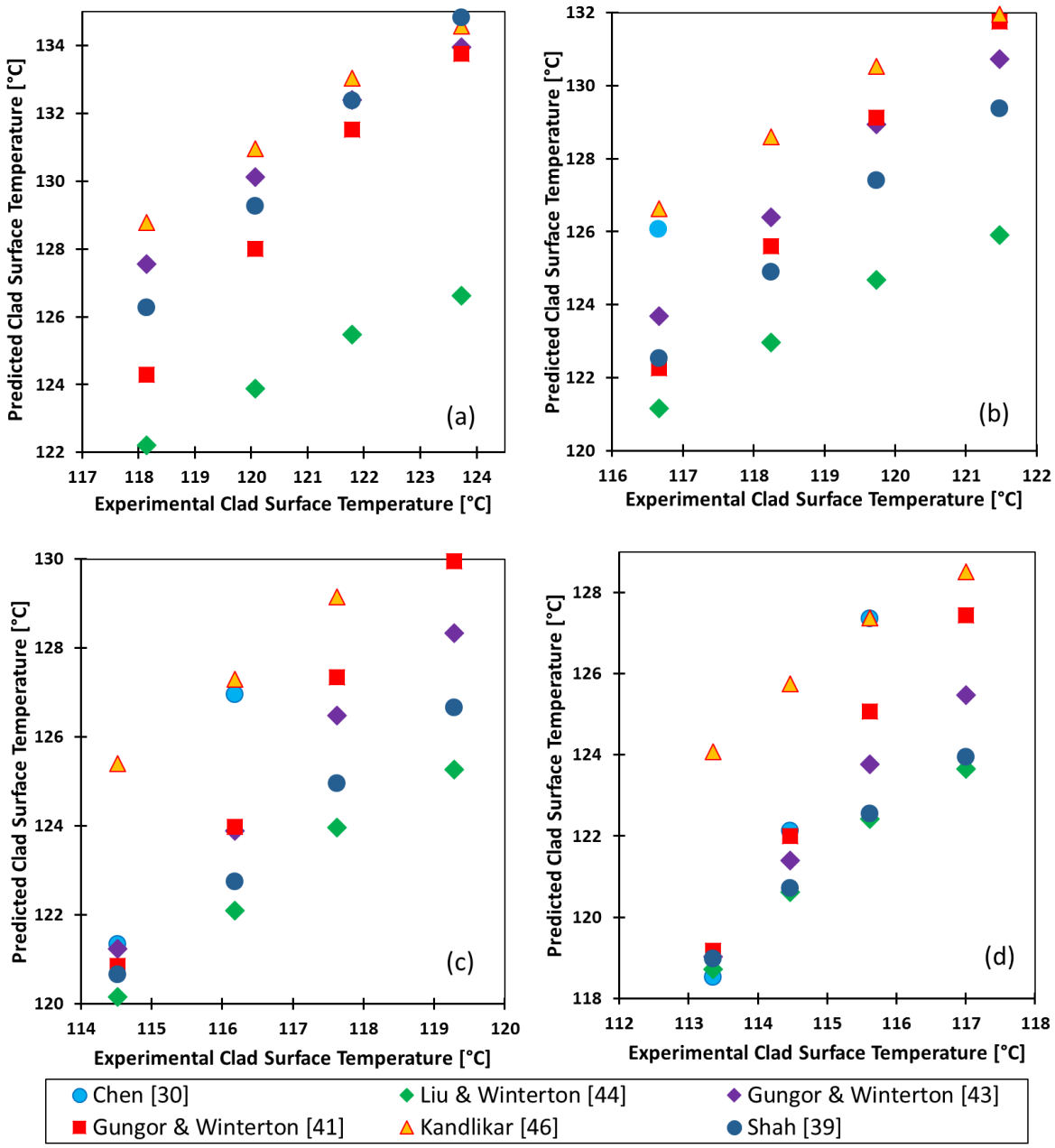

Figure 4-4: Comparison of experimental and predicted wall surface temperature for the case of measured temperature correlated as actual surface temperature for test section flow velocities at (a) 0.25 m/s, (b) 0.5 m/s, (c) 0.75 m/s, and (d) 1 m/s.

The boiling curves in **Figure 4-3** are indicative of typical flow boiling heat transfer trends. The results show that with increasing heat flux, the wall temperatures increase accordingly. The boiling curves

also follow predictable behaviour in that the heat transfer associated with the lowest flow rates (bulk coolant velocity) at a particular heat flux setting produces the largest wall superheat values. To ascertain the level of rationality of these experimental results, a comparison was conducted against values predicted using the various flow boiling correlations that were discussed in Chapter 2. The findings from this comparison are presented graphically in **Figure 4-4**.

For this study case, it is quite evident from **Figure 4-4,** according to this comparison, that all of the predicted results over predict the wall temperature as compared with the corresponding experimental value. The results using the Liu-Winterton correlation predicts the closest associated values to that obtained experimentally. Most of the predicted values over predicts the surface temperature.

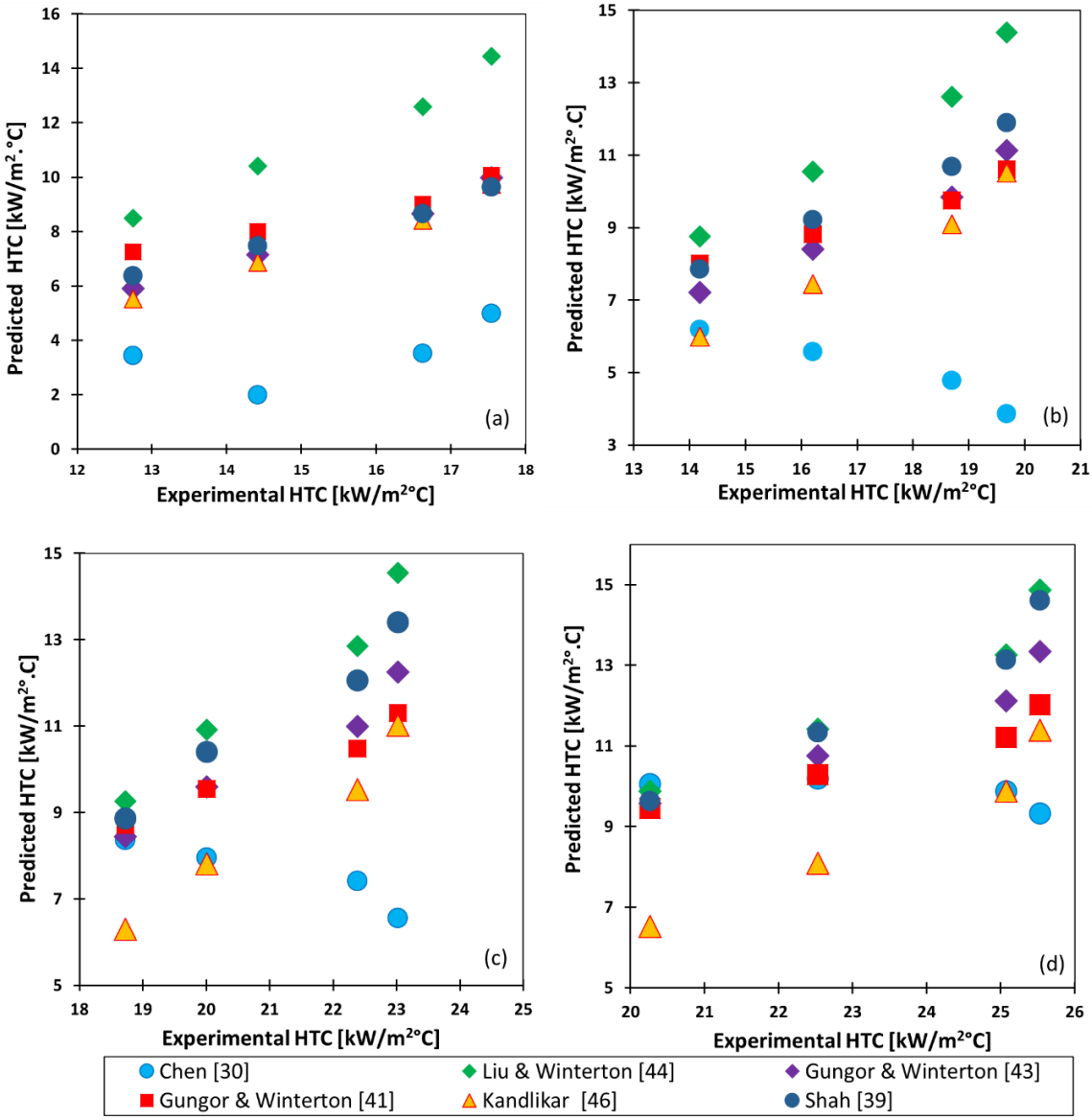

Figure 4-5: Comparison of experimental and predicted HTC for the case of measured temperature correlated as actual surface temperature for test section flow velocities at (a) 0.25 m/s, (b) 0.5 m/s, (c) 0.75 m/s, and (d) 1 m/s.

The experimental heat transfer coefficients (HTCs) were evaluated in comparison with the predicted results as calculated from the correlations in Subsection 2.4.2 and is plotted accordingly in **Figure 4-5**. The corresponding experimental heat transfer coefficients were computed according to Eq. (4-3). As can be seen, the outcomes of most of the yielded predicted to experimental results show relatively poor agreement. The best overall comparative result for this case was obtained with the Liu-Winterton correlation.

4.5.5.3 Measured Temperature Correlated as Equivalent Film Temperature

In this case, it was hypothesised that the measured temperature could be evaluated as being representative of the interface zone temperature rather than the physical clad surface temperature. The reasoning was justifiable due to most of the surface area on the thermocouple probe at the sensing point is more in contact with the stratified bulk coolant flow than the heated surface (not considering the boiling phenomena occurring on the heated surface at the time). Given this assumption, the wall surface temperature and hence wall superheat were then calculated using Eq.s (4-2) and (4-4) respectively.

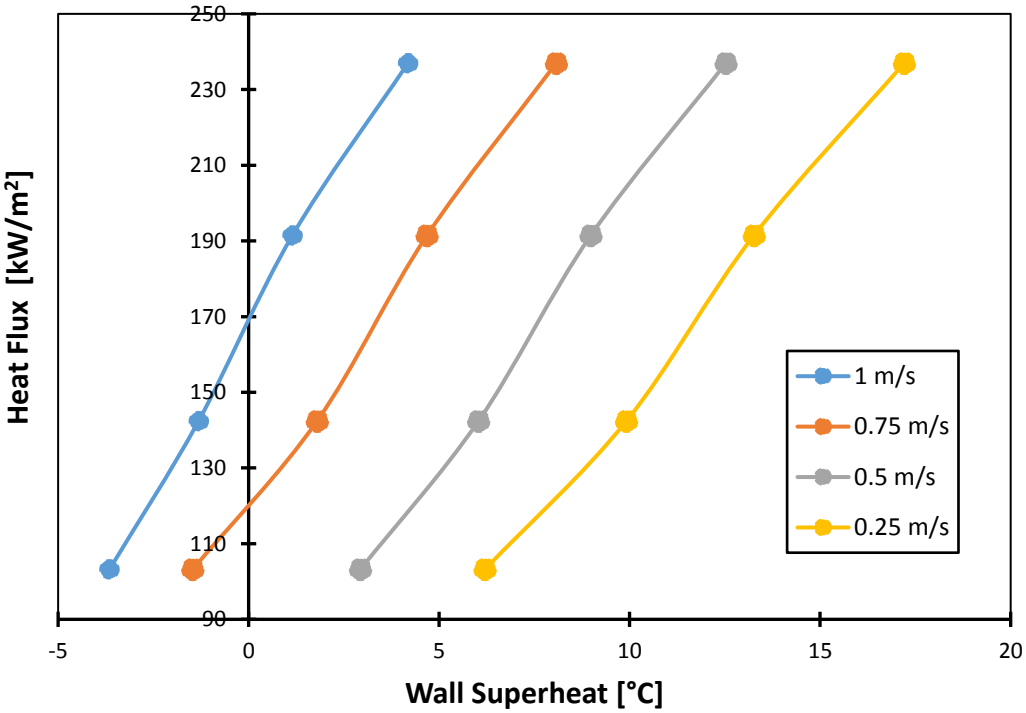

Figure 4-6: Boiling curves for measured temperature correlated as film or interface temperature.

The yielded results of this case study are presented in terms of the boiling curve trends in **Figure 4-6**. As for the earlier case, the results obtained in this case also mimicked typical flow boiling trends for

such typical boiling activity and conditions. However, for the same heat flux input and bulk coolant flow conditions, the new results showed significantly higher wall superheat characteristics than those obtained previously.

Further comparisons between the experimental and predicted clad surface temperatures are presented in **Figure 4-7** in which the solid line indicates the line of best-fit between experimental and predicted results. The results show much better agreement between the predicted and experimental results and almost near-perfect agreement when the Gungor-Winterton methods are applied.

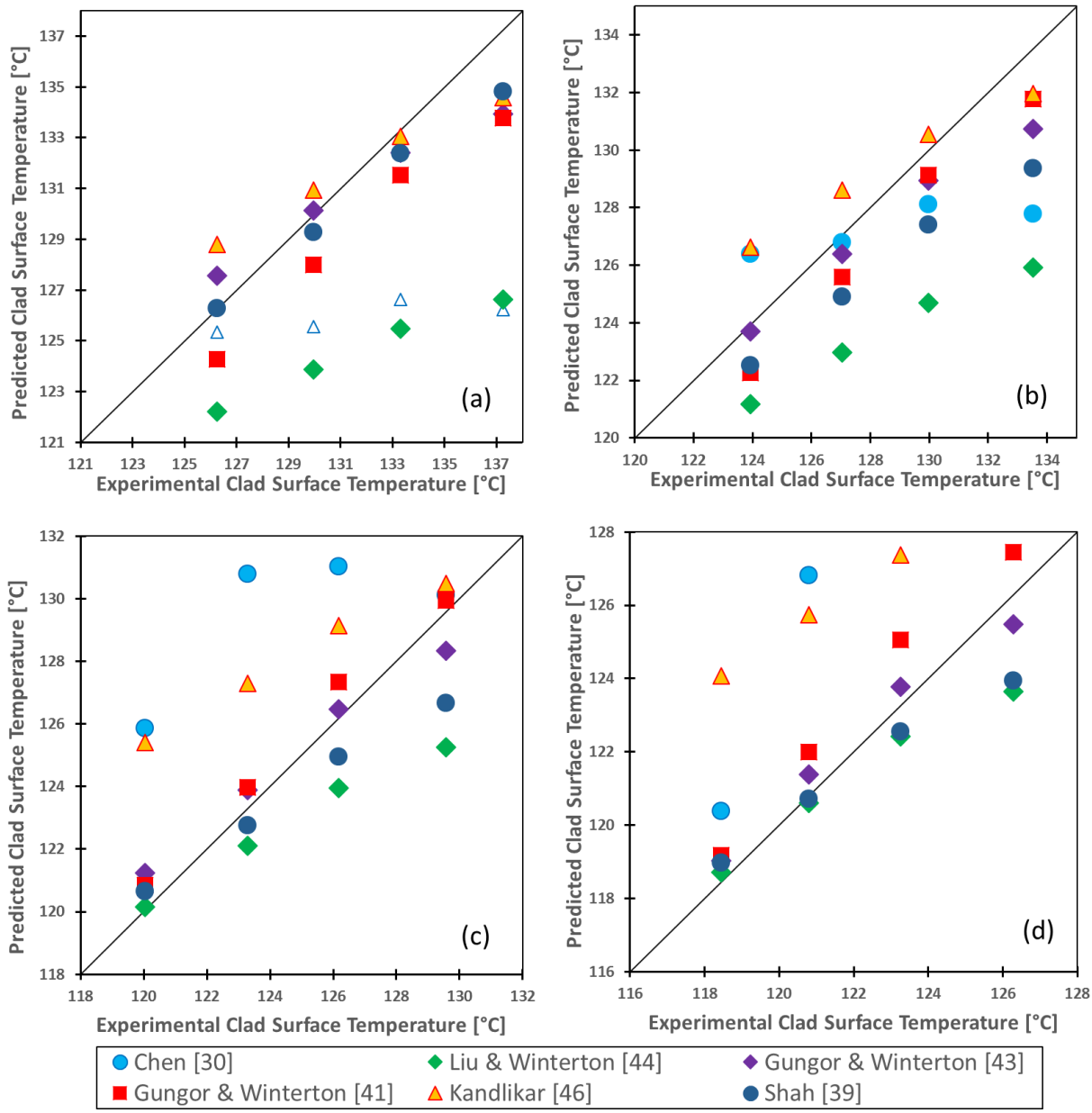

Figure 4-7: Comparison of experimental and predicted wall temperature for the case of measured temperature correlated as a film or interface temperature. The solid line indicates the line of best-fit.

The respective experimental HTC results were also compared with those predicted using the flow boiling correlations in Subsection 2.4.2 with the results shown graphically in **Figure 4-8.** Most of the predicted results show greater parity with the experimental results as compared with the previous case study. Except for the HTC results derived using the Chen and the Liu-Winterton correlations, it is quite evident from **Table 4-4** that all the other correlated results trend well within a 10 % absolute deviation band in comparison with the experimental results.

The results obtained using the Chen (1966) correlation [30] produced some of the worst results but were much improved over those in the previous case study. Given the subtleties of determining the enhancement and suppression factors for each of the correlations, the only other major difference between the Chen correlation and the others is the use of the Forster-Zuber correlation for the nucleate boiling component, while all of the other correlations (except Shah) use the Cooper correlation for the nucleate boiling component. It would be an interesting study to substitute the Cooper correlation for the nucleate boiling term in the Chen HTC equation and re-analyse the results, but at this stage, it is beyond the scope of the present work.

The HTC results as determined using the Shah (1977) correlation [39] yielded relatively good agreement with the experimental values at an absolute deviation of just over 5 %. This result was forthcoming even thou Shah did not include an explicit nucleate boiling term in his correlation. His inclusion of a boiling number term instead is reasoned to have contributed to such small variation with the experimental HTC values.

Surprisingly, both of the Gungor and Winterton correlations [41] [43] yielded an excellent agreement as compared with the experimentally derived results in this particular case study. Interestingly, Gungor and Winterton's (1986) earlier correlation [41] has been shown to deliver the best corresponding fit in terms of consistency, linearity and accuracy and has a maximum average deviation of just 2.8 % across all measured ranges. The later Gungor-Winterton correlation (1987) [43] had a better overall average deviation result than the former [41] but was analysed to have lower linearity compared with the former correlation.

The results computed using Kandlikar's correlation (1990) [47] showed good overall linearity and producing some of the smallest mean average deviations especially at the lowest tested flow velocity. This correlation exhibited a trend to generally underpredict the HTC results versus the experimental values. The overall computed average deviation was determined to be around 8.5 %, which indicated reasonable agreement with that of the experimental threshold values.

It was anticipated that the results using the Liu-Winterton (1991) [44] correlation would have produced much better outcomes since their work is thought to have progressed from that which was previously conducted by Gungor-Winterton [41] [43]. This was thus an unexpected result, which, in this particular case, yielded one of the worst evaluated average deviations of around 16 %. No explanation is proffered for these noticeably larger deviations except perhaps the use of a root sum square approach to determine the HTC values, as promoted in this correlation. It must be stated though that this is not a conclusive finding against the Liu-Winterton approach but there exists sufficient merit to study this further in the future.

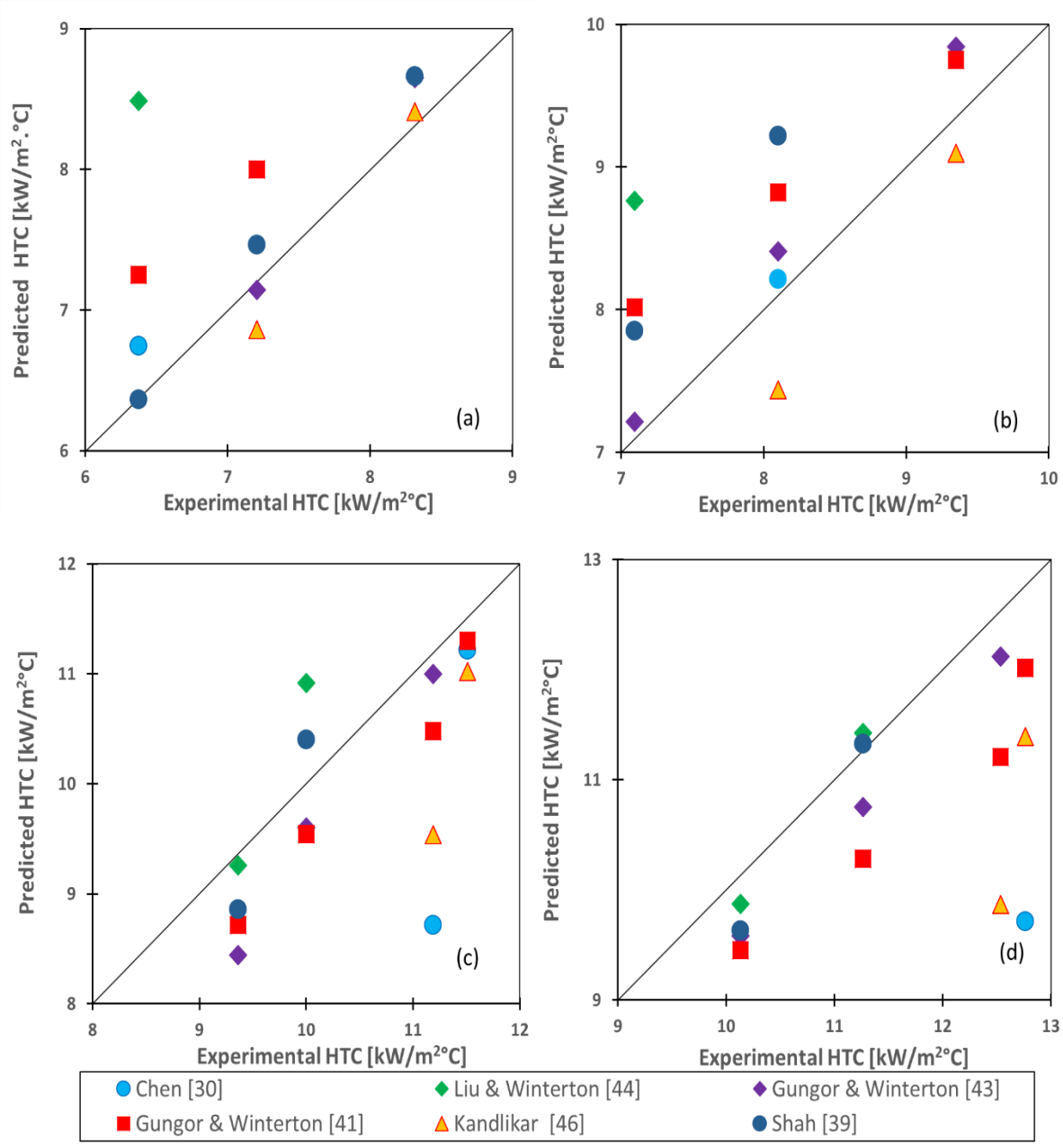

Figure 4-8: Comparison of experimental and predicted HTC for the case of measured temperature correlated as a film or interface temperature. The solid line indicates the line of best-fit.

Table 4-4: Mean absolute deviation (MAD) and average deviation (Avg) comparisons of predicted HTC versus experimental values.

Correlation	Lui & Winterton [44]		Gungor and Winterton [43]		Gungor and Winterton [41]		Kandlikar [46]		Chen [30] [36]		Shah [39]	
Deviation	MAD	Avg	MAD	Avg	MAD	Avg	MAD	Avg	MAD	Avg	MAD	Avg
%	25	16	5.62	2.83	8.35	2.80	15	8.50	26	14	8.48	5.13

Mean absolute deviation (MAD) = $\mathbf{1/N}\ \sum_{i=1}^{N}\left|\left[\boldsymbol{HTC_{exp}}-\boldsymbol{HTC_{pred}}\right]/\boldsymbol{HCT_{pred}}\right|\times\mathbf{100\%}$

Average deviation(Avg)= $1/N\ \sum_{i=1}^{N}\left[HTC_{exp}-HTC_{pred}\right]/HTC_{pred}\times 100\%$

4.5.6 Discussion and Conclusion of the Techniques to Determine Wall Temperature on the Heated Clad Surface

The approaches that were taken to ascertain the temperature on the heated clad tube surface were explored in the above subsections. The extensive investigations that were conducted pursuant with the required outcomes of the present work revealed that it was quite necessary to position the temperature-sensing probes directly onto the surface on which the wall temperature was required to be measured. The method, as described in Subsection 4.2.4, was evaluated to be the most appropriate technique but which produced a conundrum as to how to evaluate the measured value.

Through the analysis of the outcomes of the two hypotheses, it became quite evident that the case whereby the measured temperature that was correlated with that of the interfacial or film temperature from which the wall temperature was thenceforth determined, was most acceptable. This assessment is supported by the excellent agreement between the experimental results and the results from the two significantly different Gungor-Winterton correlations [41] [43] for the evaluation of the wall temperature and HTC. Results from the other applied correlations also showed acceptable agreement with the experimentally derived results. It must be noted that almost all the correlations that were used in the present work-study for the prediction of the forced convection flow boiling criteria were mainly derived for internal forced convection within heated tubes. The outcomes from the analysis in the previous subsection thus showed that these correlations could be relatively successfully applied to external forced convection flow boiling cases.

It is thus concluded that the hypothesis relating the measured temperature to that of the film or interface temperature has been proved the correct approach. In addition, the visual observations and photographic evidence in Subsection 4.2.5.1 show excellent agreement with the assessed outcome. Since the heat transfer phenomena were shown to be predictable by various appropriate correlations, this outcome is thus also considered as contributing to the validation of the effective functioning of the UP-THFC. This is a justifiable conclusion since the heat transfer results of both the experimental and predicted values were based on various explicit operating conditions such as bulk inlet

temperature, mass flux, and at super-atmospheric pressure, which had to be well regulated within the test section in order to achieve such agreeable outcomes.

4.6 Chapter Summary

In the fully built and commissioned UP-THFC facility, preliminary tests were conducted to determine the actual system performances against the system design calculations. The system performance data was recorded from the installed measuring instrumentation and then analysed in order to ascertain the performance characteristics of the flow loop. The tests were conducted at or near the operating design temperature and pressure. The results obtained from specific tests were utilised for the thermal-hydraulic validation of the UP-THFC system performances. The results presented in this chapter show that the UP-THFC had operational performance characteristics comparable with the predicted design calculations, some of which are detailed in Appendix A. A method to accurately determine the clad surface temperature was also investigated. The results from this experiment based investigation proved that the method could be successfully applied to obtain accurate clad surface temperatures.

5 Experimental Results

5.1 Introduction

For the current work, a series of tests were conducted in order to establish and demonstrate the range of system performances as well as experimental heat transfer testing capacities and capabilities of the UP-THFC. Qualifying tests were performed with single heated clad tubes located on the axial centre line of the test section. One of the test criteria was based on pump performance at different bulk water temperature conditions.

5.1.1 Test Section Bulk Water Flow Characteristics

The UP-THFC was conceptualised with the primary aim of providing a test facility in which a wide range of mainly forced convection heat transfer experiments could be conducted with water as the heat transfer and flow medium. A key requirement was that the water had to circulate through the flow loop at flow rates and test section inlet temperatures that were selected according to the stipulations of a particular experiment. These test conditions, with respect to the operational water properties, ranged from around ambient conditions to saturation temperature and pressure of around 120 °C and 200 kPa respectively.

It was accepted that no single pump solution was available that could provide (cost-effectively) a uniform performance characteristic across such an operating range. The most appropriate pump for the system was selected as a compromise. The convective bulk coolant flow characteristics of the UP-THFC were established experimentally according to the operational capabilities of the selected pump. The upper forced convection flow characteristics of the UP-THFC were plotted graphically as depicted in **Figure 5-1** and were based on diabatic testing conducted with single rods of Zr-4 and SiC respectively. The results relate the pump speed with the equivalent test section velocity and corresponding mass flux values for the respective test specimen clad tube under test and the different bulk water inlet temperatures.

The bulk water density effects with respect to the pump performances are quite evident in **Figure 5-1**. In the subcooled operating ranges, the system bulk coolant flow characteristics were predictable with higher pump flow capacities for a given pump speed occurring at increasing levels of bulk coolant subcooled temperatures. At inlet test section temperatures closer to the saturation level, the pump performance did not increase for pump speeds of more than 1 500 rpm. This characteristic could be

attributed to the pump reaching its threshold-operating limit owing to the density and viscosity of the water at that operating point(s). Further testing would be required to verify this.

It was also noted that the flow direction through the test section had an effect on the overall test section velocities and hence heat transfer capacities. For a given clad geometry and pump speed setting, the vertical upflow test section velocities were on average more than those of the vertical downflow configurations. This operational condition was expected as the longer pipe network of the latter required a higher pump head to handle the larger pressure drop across the flow loop in that configuration.

The test section velocities were also influenced by the effects of reducing water density with a corresponding increase of heater power input. The effects of water density change with respect to the test section velocities are observable in **Figure 5-1**. It is noticed that for specific pump speed, clad specimen type, and flow direction, that the test section velocity and/or equivalent mass flux reduces with increasing bulk coolant inlet temperatures.

Therefore, the heat transfer test results that are discussed in the following sections relate the heat transfer removal performances according to the respective pump capacities at a test section pressure of around 200 kPa and a corresponding saturated bulk water temperature of around 120 °C.

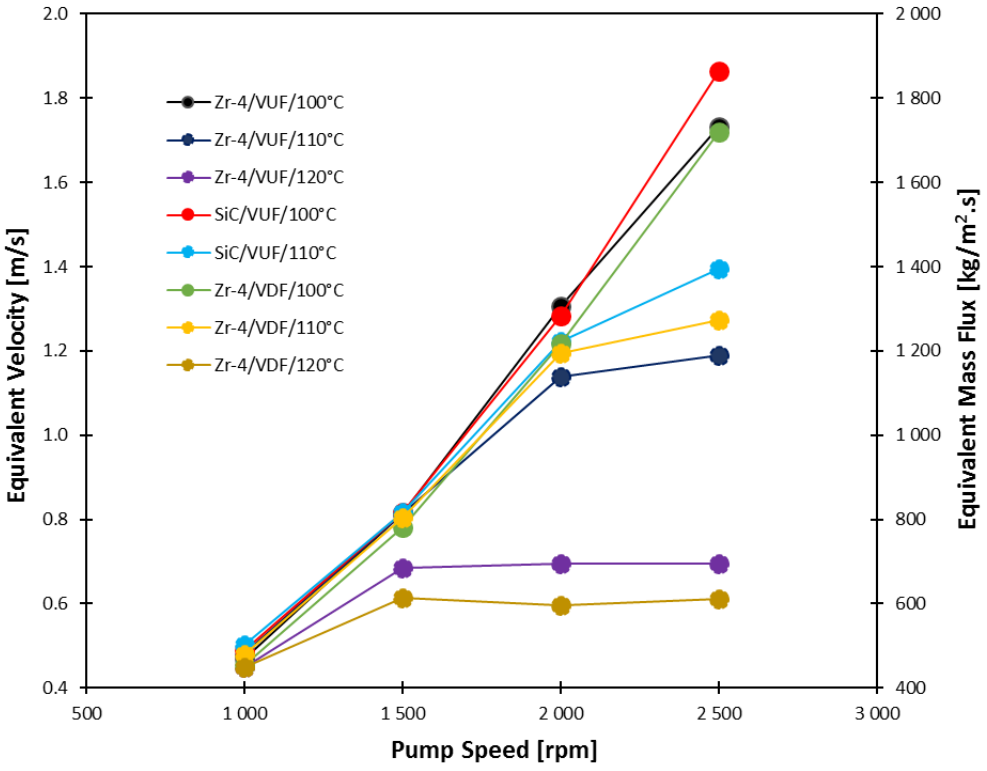

Figure 5-1: Flow characteristics in the test section at mean test section pressure of 200 kPa showing the influences of density change on flow velocity and/or mass flux for clad specimens subjected to vertical upflow (VUF) or downflow (VDF).

5.2 Comparative Heat Transfer Performances: Experimental Procedure

All test procedures followed a standardised experimental method for consistency in the experimental data and test results. Prior to testing in the flow loop, the test section and test specimen clad tubes had to be prepared according to the required test specification. The details of the specimen-clad tubes used in the present study are listed in **Table 5-1**. The surface roughness properties presented in the table were obtained with the use of an atomic force microscope at the University of Pretoria.

Table 5-1: Test specimen clad tube properties.

Properties	Zr-4	SiC
Inside diameter (ID) [mm]	8.3	8.3
Outer diameter (OD) [mm]	9.8	15.5
Heated length [mm]	420	420
Overall length [mm]	530	540
Thermal conductivity [W/m.°C]	13.7	130
Roughness [nm]	31.4	754.4
Standard deviation [nm]	31.9	747.4

The experimental procedure described next is for the set-up for a single-tube specimen but is readily applicable to multi-tube arrays. The procedure starts with the flow loop drained and the access panel removed from the test section duct.

First, the cleaned outer surfaces of the cartridge heater and the inner surface of the clad tube were lubricated with a thermally conductive anti-seize paste and the heater inserted inside the bore of the specimen-clad tube. A high-temperature silicon-based sealing compound was filled into each end of the clad tube to seal the heater into the tube. The lead cables for the heater power and heater thermocouple were fed through the cable access provided on the exit side tube support bracket. Thereafter, the rod assembly was braced into position between the support brackets that were already fixed to the access panel (see **Figure 3-4**). The thermocouples to measure the wall temperature were then fitted to the clad surface.

The assembled panel was subjected to pretesting of the test instruments and heater functionality in a separate purpose-built auxiliary tank. A test for water tightness of the clad tube assembly and cable/instrument access points was also conducted in the auxiliary tank prior to fixing the assembled panel into the test section duct. The instrumentation signal output wiring was then routed into the data acquisition system and the cartridge heater was connected to a regulated power supply.

Prior to filling of the flow loop with the water, all drain valves were closed and all vent valves opened. In addition, all flow control valves in the pipe network were fully opened to prevent voids and air pockets from being created in dead legs of the pipe network. The graphical user interface (GUI) was operational during the entire filling process with all instruments active.

The water inventory was obtained from the building supply water but that which was first prepared by filtering for solids, heavy metals and added chemicals using reverse-osmosis technology. The prepared water was stored in a reservoir tank from which it was pumped through a deionising module and into the fill point located at the top of the pressurising unit. As the system filled, the air inside the pipes was vented through the vent valves, which were located at different elevation points on the flow loop. These valves were sequentially closed off manually when the water bled out through each, observed through transparent pipes that directed the discharged water to auxiliary holding tanks. The system was completely filled when only water bled out from the vent valves at the highest points in the system located respectively on top of the pressurising unit and/or the test section assembly when orientated vertically.

The system was ready for testing when the flow loop was confirmed leak free. The flow control valves were then set to attain the correct flow direction through the test section for the specific experiment. Thereafter, the pump, cartridge heater, and preheaters were powered on and turned up to around 80 to 90 % operational limit of each to heat up the water to the required bulk inlet water temperature. For a single heated pin, around four hours was required to increase the water temperature from around 30 °C to 100 °C. A further two hours were required to get the temperature to 120 °C.

On attainment of the required bulk water inlet temperature, the system was then adjusted to the required test conditions for each experimental test point according to mass flow rate, test section pressure, bulk water inlet temperature, and cartridge heater power input. The system conditions were then allowed to attain a steady state before testing commenced. Each incremental test parameter adjustment thereafter resulted in around two minutes for the system to settle and converge to the steady operational condition. A steady operational condition is defined as when at least five consecutively recorded data points show negligible differences for the bulk water inlet temperature value as observed and recorded by the data acquisition system. The sequence of data logging commenced on achieving a steady operating condition. The physical test data was then recorded for the next 60 seconds. Following this, the next test point was set and a settling period of around 120 seconds (or more if necessary) was observed before commencing the next data logging event. The sequence was repeated until the required data set was recorded. Due to operational limitations of the data acquisition equipment, the data was recorded at a sampling frequency of around 0.4 Hz giving approximately 24 data points per minute. The output signals from 28 instrument channels were

recorded at each data point. In the data post-processing, the first four data points were normally disregarded.

5.3 Diabatic Testing Matrix

The selection of testing points for the current work was both to demonstrate the heat transfer testing capacities of the UP-THFC and to validate the experimental rig. The test parameter ranges are detailed in **Table 5-2**. Except for the heater power input, the listed test parameter ranges fall into the upper band of the as-designed system operating and performance limits. The heater power input depends on the rating of the heater used and can range between 2 to 7.5 kW. A heater rated at 3 kW at 240 VAC (mains voltage-alternating current) was used in the current testing schedule. For consistency and standardisation purposes, the same heater was used in all of the clad tubes tests.

Table 5-2: Parameters for experimental testing points.

Test Parameter	Range
Pressure at test section mid-point (P_{sat})	200 kPa absolute
Bulk inlet water temperature ($T_{b,in}$)	100 °C, 110 °C, 120 °C
*Mass flux (G)	450 to 1 800 kg/m^2.s
**Cartridge heater power input ($\dot{Q}_{in}$)	500 to 2 450 W

*(set according to pump speed (rpm) values) **(set according to voltage input values)

In the present work, tests were conducted on a single Zr-4 clad tube for the vertical upflow and downflow forced convection flow regimes. Due to time constraints, the horizontal forced convection flow regime tests were not conducted nor were the SiC tubes tested at the 120 °C bulk inlet temperature or in the vertical downflow conditions. No natural convection tests were conducted. The omission of these tests does not indicate deficiencies of the system or detracts from the overall system performance capabilities. Time constraints also limited the number of tests at each test point and only three data sets were recorded for each test point for statistical and repeatability analysis.

All diabatic tests were conducted with the static pressure adjusted and maintained at around 200 kPa (absolute) at the mid-point of the test section. This set the mean saturation temperature (T_s) of the water to around 120 °C in the test section for all test conditions except for the clad wall temperature parameters. Testing was conducted with three bulk water inlet temperatures ($T_{b,in}$) set at 100 °C, 110 °C and 120 °C respectively. The mass flux testing range was selected from 450 to 1 800 kg/m^2.s which was set using four pump speeds set via the electronic VFD pump speed controller. The pump

speeds ranged from 1 000 to 2 500 revolutions per minute (rpm). The corresponding flow velocities and mass flux values for each pump speed setting and in terms of the selected bulk coolant inlet temperatures are presented in the graphical format in **Figure 5-1**.

Power input settings to the cartridge heater were set up at specific intervals comprising input voltage adjustments of 25 V incremental steps over a range from 100 to 220 VAC to create six power set points. This was achieved using the tuneable SSR potentiometer in conjunction with observations from the analogue voltmeter and GUI display. The current drawn by the cartridge heater was proportional to each voltage input setting and did not require any additional adjustment.

One typical test point setting consisted of a heated clad tube specimen exposed to flow in a particular direction in the test section while simultaneously being subjected to a specific single bulk water inlet temperature, mass flux, and heater power setting.

A data set consisted of six singular test points in which only the heater power parameter was different (corresponding to the six power set points that were mentioned earlier). In this manner, 32 data sets (not including repeatability data sets) comprising a total of 192 data test points were recorded for the system performance and heat transfer analysis in the present study.

5.4 Forced Convection Heat Transfer Results and Analysis

In the current work, and as mentioned earlier, the SiC tubes could not be obtained in the same external dimensions as those of the Zr-4 tubes and hence were tested as supplied. The available SiC tubes had an outer diameter of 15.5 mm, which was about 60 % larger than the Zr-4 tubes with an outer diameter of 9.5 mm. However, both sets of clad tubes had the same inner diameter of 8.3 mm. Therefore, for the same heater power settings, the computed heat fluxes yielded smaller values for the SiC clad tubes as compared with the values of the Zr-4 tubes. Hence, the heat transfer coefficients were evaluated with respect to the comparative flow and heat flux conditions. Thus, the analysis of the heat transfer performances took into account the influences and effects of the bulk coolant flow condition, heat flux levels, flow orientation, and the effects associated with the different clad tube materials. These are discussed further in the following subsections.

The methods discussed in Section 4.5 were used to determine the wall temperatures using experimentally measured values such as mass flow rates, bulk coolant inlet and outlet temperatures, heat flux as determined from measured power input values, heated surface areas on the clad tube specimens, and absolute pressure in the test section.

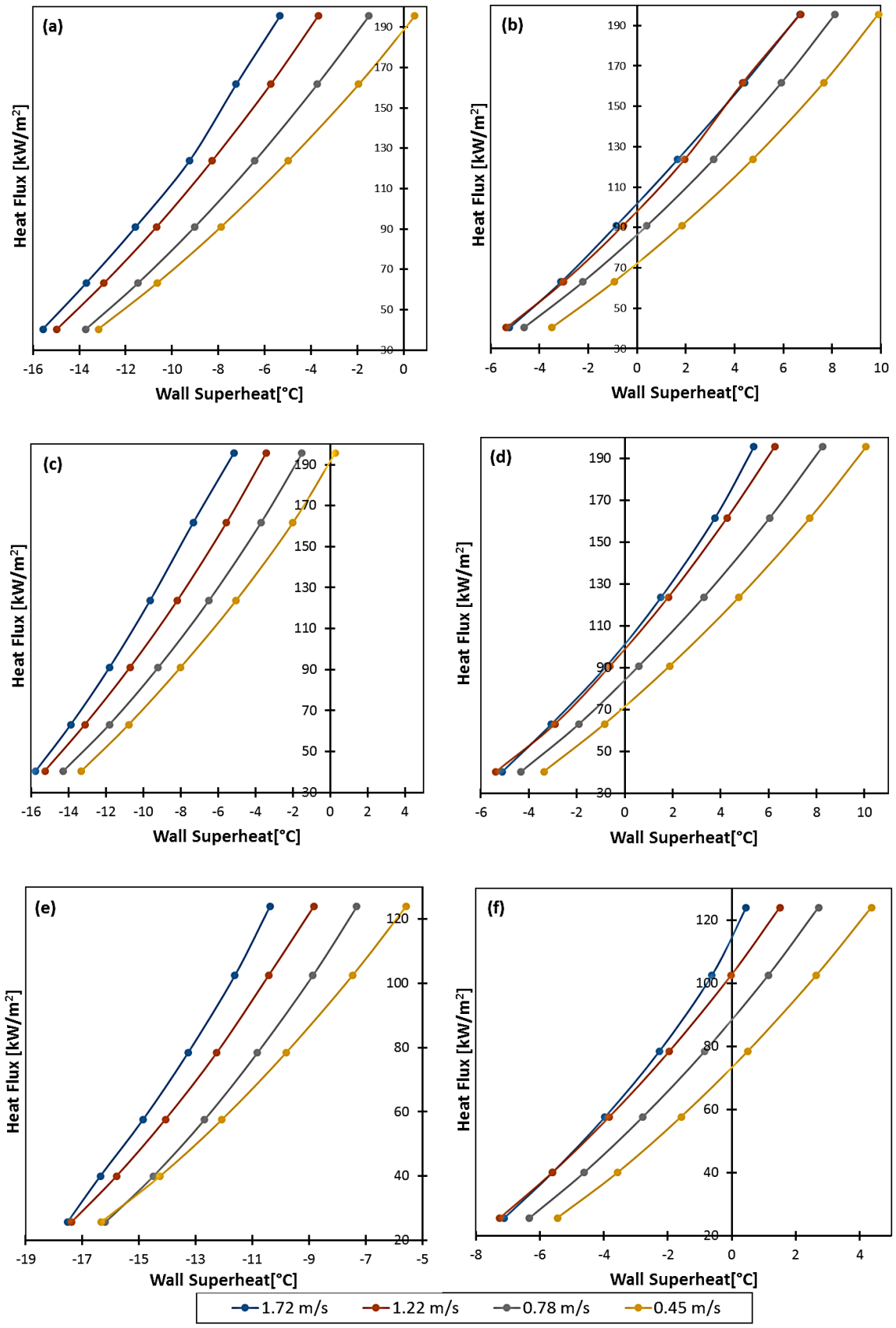

Figure 5-2: Subcooled boiling curves according to clad tube material, flow direction, and bulk coolant inlet temperatures at (a) Zr-4, VUF and T_{in} = 100 °C; (b) Zr-4, VUF and T_{in} = 110 °C; (c) Zr-4, VDF and T_{in} = 100 °C; (d) Zr-4, VDF and T_{in} = 110 °C; (e) SiC, VUF and T_{in} = 100 °C; (f) SiC, VUF and T_{in} = 100 °C.

In the heat transfer experiments in the present study, six precise input heater power settings were used for the cartridge heater located inside the respective clad tube bores and having a heated length of 420 mm. This catered for heat flux ranges from about 40 to 196 kW/m^2 for the Zr-4 tubes, and 25 to 125 kW/m^2 for the SiC tubes, as listed in **Table 4-1**. Four flow rate settings were also used for all tests in order to gauge overall heat transfer as well as system performances. The wall superheat, when compared with the respective heat flux levels, yielded the boiling curves, as shown in **Figure 5-2**. The data is presented for four flow rate settings and must be read in conjunction with the pump speed and mass flux equivalent values in **Figure 5-1**.

The flow boiling curves appear consistent with trends in the literature and show progressively lower overall superheat values for the same heat flux as the coolant flow rates were increased.

For the subcooled boiling cases, no noticeable nucleate boiling activity occurred on the clad surfaces for all cases tested with bulk inlet water temperatures at around 100 °C. The partial nucleate boiling activity occurred on the Zr-4 surfaces when tested with 110 °C inlet water conditions.

For the test conditions with the SiC clad tubes, only ONB-type activity was observed and mainly at the lower flow rate settings. The difference in wall superheats for the Zr-4 clad tubes averages around 1.6 % higher for the downflow cases as compared with the up flow test cases and is attributed to possible buoyancy effects. The SiC yielded around an average 3.8 % lower wall superheat versus that of the Zr-4 tubes at the same up flow conditions and equivalent heat flux values and was estimated at around 3.6 % lower when compared with the downflow condition of the Zr-4. The computed HTC differences yielded that the SiC was approximately 5.4 % lower than that of the Zr-4 clad-tubes.

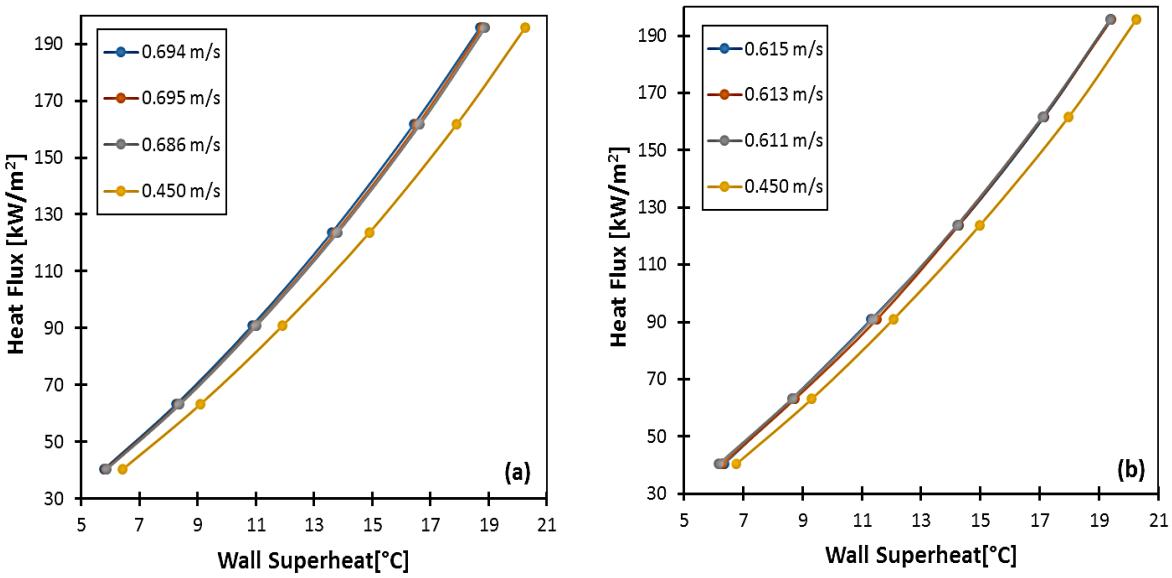

Figure 5-3: Saturated boiling curves for Zr-4 clad-tube material and according to flow direction and bulk coolant inlet temperatures for (a) Zr-4, VUF and T_{in} = 120 °C; (b) Zr-4, VDF and T_{in} = 120 °C.

Concerning the saturated flow cases, as shown in **Figure 5-3,** various stages of boiling up to the onset of significant void (OSV) were observed on the Zr-4 tubes. Generally, lower heat fluxes were required in the saturated flow condition to attain nucleate boiling. This could be attributed to the smaller ΔT_s for the initiation of nucleate boiling due to the larger heat transfer coefficient. Although the SiC tubes were not tested under the saturated bulk coolant conditions, all indications were that it would produce similar offsets as previously determined for the subcooled cases.

5.5 Uncertainties

The results for the uncertainties of the various measured and calculated heat transfer-related values for both Zr-4 and SiC clad tubes are tabulated in **Table 5-3**. Further details are available in Appendix B. Generally, the uncertainty of the heat transfer coefficient was found to decrease with increasing heat flux levels. This could mainly be attributed to the test equipment uncertainties.

Table 5-3: Uncertainty of measured and calculated values.

Parameter	Uncertainty
Minimum heat flux	± 1.8 % at 0.5 kW heat input
Maximum heat flux	± 2.25 % at 2.45 kW heat input
Heat transfer area	± 0.04 × 10^{-3} m² (Zr-4) ± 0.06 × 10^{-3} m² (SiC)
Heat transfer coefficient - lowest	± 4.07 % at 6 kW/m².°C
Heat transfer coefficient - highest	± 3.8 % at 14.1 kW/m².°C

5.6 Chapter Summary

A series of tests were conducted with test conditions maintained at comparative operating levels in order to gain a general overview of the heat transfer characteristics of Zr-4 versus SiC clad tube materials in the UP-THFC test facility as well as to evaluate its operational performance envelope.

Generally, the SiC tubes exhibited lower heat transfer coefficients for the same process conditions as compared with zirconium alloy-based tubes. Although the SiC tubes on hand were only tested in the vertical up flow test configuration with subcooled flow conditions, there was little indication that their heat transfer characteristics would improve significantly in comparison with the Zr-4 in any of the other test conditions. It still had to be determined whether the SiC clad tubes, if it was possible to manufacture them with similar dimensions to those of the Zr-4 clad tubes, would have better heat transfer capability than that of the standard SiC tubes that were tested. Overall, the SiC clad tubes exhibited relatively good heat transfer performance characteristics and hence potential as a replacement fuel clad tube for the currently used zirconium alloy-based tubes.

6 Summary, Conclusions and Recommendations

6.1 Summary

This project was initiated on the premise of contributing to international research and the investigation of better accident tolerant fuel for typical light-water nuclear reactors. The study program was primarily set to investigate the heat transfer properties of the proposed silicon carbide (SiC) alternate nuclear fuel clad material in the quest to replace the somewhat problematic zirconium-based material. This required a suitable experimental test rig within which the relevant tests could be conducted.

In fulfilling the needs of the study program, a closed-loop thermal hydraulic flow loop (UP-THFC) was designed, manufactured, and tested. The fully installed and operating system is capable of providing a closed-loop flow through a custom-built test section. Flow through the test section can be selected in either the up-, down- or horizontal-flow directions. This capability allows for the test and evaluation of particular fuel clad samples according to flow directional conditions found in most types of NPP that are currently operational. However, due to budgetary restrictions, the exact operating conditions of the UP-THFC were not designed to replicate the general NPP operating conditions but merely to conduct tests that could be used to predict the conditions occurring in commercial nuclear power plants.

6.2 Conclusions

An analytical method based on the use of spreadsheet solvers was developed to solve for the system performance requirements and/or characteristics of closed-loop flow circuits. The spreadsheet solver set was successfully utilised (as demonstrated experimentally) to aid the design of the UP-THFC for forced and natural convection boiling experiments involving water as the flow medium. The designed and built 80 mm x 80 mm channel test section cross-section of the UP-THFC allows for a wide variety of boiling heat transfer experiments to be carried out in a single facility.

Although initially designed to study the external boiling and heat transfer characteristics of certain nuclear fuel pin configurations of particular cladding material structures, the facility can readily be adapted for other experimental test studies requiring forced convection experiments involving fully submerged external and/or internal surface heat transfer studies such as the analysis of heater elements for liquid heating. The study of other fully submerged flow experiments can also be accommodated in the system and include fluid-structure interactions, porous flow analysis, secondary

flow analysis around structures and pin arrays, and general fluid dynamics studies such as natural- and forced- convection experiments.

Due to the approximately 1 300 m altitude at which the University of Pretoria is located, the average local barometric pressure is about 87 kPa at which the saturated boiling point of water is typically around 95.6 °C. The pressurised UP-THFC has thus been conceived and designed to cater to super-atmospheric forced and natural convection boiling experiments that are independent of altitude-associated working properties of the water flow medium. The system was designed and rated for continuous operations in terms of the limits, as listed in **Table 6-1.**

Table 6-1: Operating specification for the UP-THFC

OPERATING CONDITION	LOCATION IN FLOW LOOP	OPERATING RANGE/VALUE
Design pressure	• Test section	87 to 200 kPa (Abs.)
	• Pump discharge port	400 kPa (Abs.)
	• Pump inlet port	100 to 200 kPa (Abs.)
	• Pressuriser	250 kPa (Abs.)
Design temperature	Inlet to Test Section	Ambient to 120 °C
*Design volumetric flow rate	System	100 to 975 L/min
*Mass flow rate	System	1.6 to 15.3 kg/s
Heated pin length	Test section	550 mm maximum
Test section configuration	Test section	80 mm x 80 mm Square
Maximum pin array configurations	Test section	7 x7 Array of 9.8 mm Zr-4 Pins, or 4x4 Array of 15.5 mm SiC pins
*Flow velocities	• Test section	Depends on pin array configuration and flow rate condition in the test section. Nominal 0.2 to 2.5 m/s.
	• System pipeline	0.2 to 2.6 m/s

*Bulk water temperature dependent

The test section was designed for the accommodation of various heated/non-heated pin arrays with working lengths of up to 550 mm if the inlet flow must be fully developed turbulent at the inlet to the test specimens. Longer test specimen lengths of up to 3 m can also be accommodated if the above flow regime is not required to be a stringent test condition limitation The modular test section can easily be replaced with other test section designs, e.g. annular tube-type test sections, and is only limited by the operating limits of the current installation.

The initial theoretical analysis and calculations (Appendix A) of the system, together with the design and selection of the various components and systems, were verified and validated by experimental

and test performances of the fully built and installed system. These were successfully accomplished according to the design and operational constraints that were stipulated in the initial design directives.

Preliminary experimental testing and results indicated that the SiC cladding material exhibited a generally lower heat transfer coefficient as compared with that of the Zr-4. The lower HTC capacities of the SiC are not necessarily a disadvantage to the clad material. Characteristics (under current prevailing test conditions) of lower vapour bubble volume generation were observed on the SiC as compared to the Zr-4. This could be advantageous in PWRs since vapour bubble production within the narrow hot channels in the reactor core is undesirable. Excessive vapour could restrict bulk coolant flow and lead to the creation of voids in the hot channels with the consequence of reduced heat transfer from the fuel to the bulk coolant flow. It was however observed that vapour bubble generation was quite significant on new SiC clad tube surfaces but that which reduced over time. This may be due to the wearing down of surface roughness on the SiC over a period of testing. Further experimenting is required to explore more comprehensively the heat transfer-based characteristics of SiC within the operational envelope of the UP-THFC.

6.3 Recommendations

The UP-THFC was developed within limited budget and time constraints parameters. There are thus considerable improvements that can be accomplished to optimise and extend the experimental testing performances of the UP-THFC. Accordingly, the following improvements and alterations to the UP-THFC are recommended:

1. A multi-channel data acquisition system (40+ channels) with simultaneous channel scanning capabilities coupled with higher scanning frequency rates per instrument channel would be desirable for more precise data measurements.
2. Different test section size/s and/or configurations should be explored per individual experimental investigation.
3. Non-contact or other surface temperature technologies should be investigated and/or employed in place of the current contact-type temperature measurement with thermocouples. Fibre-optic-based temperature-measuring technology, with fibre Bragg grating/s (FBG), has been demonstrated to be unaffected by EMF interferences and is therefore highly recommended for future measurement of component temperature in the test section. Further work is also required to investigate the influences of boundary layer thickness on the measured film/interface temperatures.

4. Dissolved gases and impurities in the bulk fluid should be investigated further with respect to their effect on the heat transfer process.
5. The inclusion of a separate flow meter in the test section assembly would cater for experiments in the laminar and transient flow regimes. It would be desirable to employ instrumentation that is more precise for these purposes and consideration should be given to the use of either a Coriolis or ultrasonic-type flow meter.
6. In the present constructed state of the UP-THFC, the set-up and configuration of the required test conditions are controlled mainly by operator input. For better productivity and performance of the system, a fully integrated automated system for the control of the thermal hydraulic test conditions would be ideal. This automated system would control aspects such as pump speed, heat exchanger performance, heater levels, and pressuriser conditions in order to achieve more stable operating conditions in the flow loop.
7. The loop should be modified to include the possibility to study unrestrained natural convection heat transfer from heated components following pump stoppage.

7 References

[1] J. Voglewede, Nuclear Fuel Safety Criteria Technical Review, 2nd Edition, Organisation for Economic Co-operation and Development (OECD); Nuclear Energy Agency (NEA), 2012.

[2] J. Lamarsh and A. Barrata, Introduction to Nuclear Engineering, 3rd Edition, New Jersey, USA: Prentice-Hall, 2001.

[3] J. Buongiorno, "Technical Lessons Learned from the Fukushima-Daichii Accident and Possible Corrective Actions for the Nuclear Industry: An Initial Evaluation," Center for Advanced Nuclear Energy Systems, MIT-NSP-TR-025, May 2011.

[4] H. Anglart, "Applied Reactor Technology," 2011. [Online]. Available: http://www.diva-portal.org/smash/get/diva2:500610/fulltext01.pdf.

[5] A. McMinn, E. C. Darby and J. S. Schofield, "The Terminal Solubility of Hydrogen in Zirconium Alloys," in 12th International Symposium on Zr in the Nuclear Industry, Toronto, 1998.

[6] A. Nechaev, "Corrosion of Zirconium Alloys in Nuclear Power Plants," IAEA-TECDOC-684, www.iaea.com, 1993.

[7] Y. Lee, T. McKrell and M. Kazim, "Key Structural Challenges for SiC as Fuel Cladding for LWRs," in Proceedings of ICAPP, Charlotte, USA, 2014, April 6-9.

[8] D. Carpenter, K. Ahn, S. Kao, P. Hejzlar and M. Kazimi, "Assessment of Silicon Carbide Cladding for High-Performance Light Water Reactor," Nuclear Fuel Cycle Program, Vol. MIT-NFC-TR-098, 2007.

[9] S. Nishio, "Fusion Power Reactor Designs Adopting SiC/SiC Composite as the Structural Material," The Journal of Plasma Science and Nuclear Fusion Research, 80, vol. 80, pp. 1-14, 2004.

[10] Y. Sukjai, K. Shirvan, E. Pilat and M. Kazimi, "The effects of SiC cladding thickness on advanced PWR fuel rod performance," in Proceedings of ICAPP 2014, Charlotte, USA, 2014, April 6-9.

[11] H. Feinroth, M. Ales, E. Barringer, G. Kohse, D. Carpenter and R. Jaramillo, "Mechanical Strength of CTP Triplex SiC Fuel Clad Tubes After Irradiation in MIT Research Reactor under PWR Coolant Conditions," in The 33rd International Conference on Advanced Ceramics and Composites, 2009.

[12] G. Hewitt, "Chapter 15 - Boiling," in Handbook of Heat Transfer, New York, McGraw-Hill, 1998.

[13] Y. Cengel, Heat and Mass Transfer - A Practical Approach, 3rd Edition, New York: McGraw-Hill, 2007.

[14] S. Nukiyama, “The Maximum and Minimum Values of the Heat Transmitted from Metal to Boiling Water under Atmospheric Pressure,” International Journal of Heat and Mass Transfer, vol. 9, no. 12, pp. 1419 - 1433, 1966.

[15] R. Bowring, “Physical Model Based on Bubble Detachment and Calculation of Steam Voidage in the subcooled Region of a Heated Channel,” OECD Halden Reactor Project, 1962.

[16] J. Ribatski and G. Jabardo, “Experimental Study of Nucleate Boiling of Halocarbon Refrigerants on Cylindrical Surfaces,” International Journal of Heat and Mass Transfer, pp. 4439-4451, 2000.

[17] P. Berensen, “Experiments in Pool Boiling Heat Transfer,” International Journal of Heat and Mass Transfer, vol. 83, pp. 351-358, 1961.

[18] T. Sato and H. Matsumura, “On the Conditions of Incipient Subcooled-Boiling with Forced Convection,” Bulletin of Japan Society of Mechanical Engineers, pp. 392-398, 1963.

[19] M. Shiutso and K. Hama, “Film Boiling Heat Transfer from a Vertical Cylinder in Forced Flow of Liquids under Saturated and Subcooled Conditions at Pressures,” Nuclear Engineering and Design, vol. 200, no. 1-2, pp. 23-80, 2000.

[20] Y. Cengel, Heat and Mass Transfer: A Practical Approach, 2nd ed, New York: McGraw-Hill, 2006.

[21] N. Basu, “Modeling of Experiments for Wall Heat Flux Partitioning during Subcooled Flow Boiling of Water at Low Pressures, PhD Thesis,” University of California, Los Angeles, USA, 2003.

[22] V. Dhir, “Nucleate and Transition Boiling Heat Transfer Under Pool and External Flow Conditions,” Internation Journal Heat and Fluid Flow, vol. 12, no. 4, pp. 290-314, 1991.

[23] N. Basu, G. R. Warrier and V. K. Dhir, “Onset of Nucleate Boiling and Active Site Density During Subcooled Flow Boiling,” ASME, Journal of Heat and Mass Transfer; Vol 124, pp. 717 - 728, 2002.

[24] N. Basu, G. Warrier and V. Dhir, “Wall Heat Flux Partitioning During Subcooled Flow Boiling at Low Pressures,” in Proceedings of HT2003 - ASME Summer Heat Transfer Conference, Las Vegas, Nevada, USA, 2003.

[25] R. Situ, Y. Mi, M. Ishii and M. Mori, “Photographic study of bubble behaviours in forced convection,” International Journal of Heat and Mass Transfer, vol. 47, pp. 3659–3667, 2004.

[26] Z. Wang, P. Gao, D. Yu, Z. Yang, H. Chen, C. Zou and C. Chen, "Recognition Statistic and Analysis of Bubbles in Flow Boiling," in Proceedings of the 2014 22nd International Conference on Nuclear Engineering, Prague, Czech Republic, 2014.

[27] L. ZOU, "Experimental Study on Subcooled Flow Boiling on Heating Surfaces with Different Thermal Conductivities," The University of Illinois at Urbana-Champaign, Illinois, USA, 2010.

[28] H. Schlichting, Boundary Layer Theory, New York: Mcgraw-Hill, 1955.

[29] W. Rosenow, "A Method of Correlating Heat Transfer Data for Surface Boiling Liquids," Transactions of ASME, vol. 74, pp. 969-976, 1952.

[30] J. C. Chen, "Correlation of Boiling Heat Transfer to Saturated Fluids in Convective Flow," I&EC Process Design and Development, vol. 5, no. 3, pp. 322-329, 1966.

[31] H. Forster and N. Zuber, "Dynamics of Vapor Bubbles and Boiling Heat Transfer," Journal of American Institute of Chemical Engineering (AIChE), vol. 1, no. 4, pp. 531-535, 1955.

[32] F. Dittus and M. Boelter, "Heat Transfer in Automobile Radiators of the Tubular Type," University of California Publications on Engineering, vol. 2, pp. 433-461, 1930.

[33] J. Collier and J. Thome, Convection Boiling and Condensation, 3rd Edition, Oxford: Clarendon Press, 1994.

[34] D. Groeneveld and C. Snoek, "A Comprehensive Examination of Heat Transfer Correlations Suitable for Reactor Safety Analysis," Multiphase Science and Technology, vol. 2, pp. 181-274, 1986.

[35] R. Serth and T. Lestina, Process Heat Transfer: Principles, Applications and Rules of Thumb, Academic Press, 2014.

[36] W. Chen and X. Fang, "A Note on the Chen Correlation of Saturated Flow Boiling Heat Transfer," Internation Journal of Refrigeration, vol. 48, pp. 100-104, 2014.

[37] H. Steiner, A. Kobor and L. Gebhard, "A Wall Heat Transfer Model for Subcooled Boiling Flow," International Journal of Heat and Mass Transfer, vol. 48, no. 19-20, pp. 4161-4173, 2005.

[38] C. Popiel and J. Wojtkowiak, "Simple Formulas for the Thermophysical Properties of Liquid Water for Heat Transfer Calculations (from 0 °C to 150 °C)," Heat Transfer Engineering, vol. 19, pp. 87 - 101, 1998.

[39] M. Shah, “A General Correlation for Heat Transfer During Subcooled Boiling in Pipes and Annuli,” ASHRAE Trans, vol. 83, pp. 205 - 215, 1977.

[40] M. Shah, “Generalized Prediction of Heat Transfer During Subcooled Boiling in Annuli,” Heat Transfer Engineering and Design, vol. 4, no. 1, pp. 24-31, 1983.

[41] K. Gungor and R. Winterton, “A General Correlation for Flow Boiling in Tubes and Annuli,” International Journal of Heat and Mass Transfer, vol. 29, no. 3, pp. 351-358, 1985.

[42] M. Cooper, “Saturation Nucleate Boiling. A Simple Correlation,” 1st UK National Conference on Heat Transfer, 1984.

[43] K. Gungor and R. Winterton, “Simplified General Correlation for Saturated Flow Boiling and Comparison with Data,” Chemical Engineering Research and Design, vol. 65, no. 2, pp. 148-156, 1987.

[44] Z. Liu and R. Winterton, “A General Correlation for Saturated and Subcooled Flow Boiling in Tubes and Annuli, Based on a Nucleate Pool Boiling Equation,” International Journal of Heat and Mass Transfer, vol. 34, no. 11, pp. 2759-2766, 1991.

[45] S. Kutateladze, “Boiling Heat Transfer,” in International Journal of Heat and Mass Transfer, 1961.

[46] S. Kandlikar, “A General Correlation for Saturated Two-Phase Flow Boiling Heat Transfer Inside Horizontal and Vertical Tubes,” Journal of Heat Transfer, vol. 112, pp. 219-228, 1990.

[47] S. Kandlikar, “Heat Transfer Characteristics in Partial Boiling, Fully Developed Boiling, and Significant Void Flow Regions of Subcooled Flow Boiling,” Journal of Heat Transfer, vol. 120, pp. 395 - 401, 1998.

[48] B. Petukhov and V. Popov, “Theoretical Calculation of Heat Exchange in Turbulent Flow in Tubes of an Incompressible Fluid With Variable Physical Properties,” High Temperature, vol. 1, no. 1, pp. 69-83, 1963.

[49] S. Kandlikar and M. Steinker, “Control and Effect of Dissolved Air in Water During Flow Boiling in Microchannels,” Int. Journal of Heat and Mass Transfer, Vol. 47, pp. 1925-1935, 2007.

[50] M. Kawaji, R. Samaroo, j. Kreynin, T. Lee and S. Banerjee, “Subcooled Flow Boiling Experiments and Numerical Simulation for a Virtual Reactor Development,” in The 14th International Topical Meeting on Nuclear Reactor Thermal Hydraulics, Toronto, Canada, 2011, September 25-30.

[51] K. Mishima and M. Ishii, “Flow Regime Transition Criteria for Upward Two-Phase Flow in Vertical Tubes,” International Journal Heat and Mass Transfer, vol. 27, no. 5, pp. 723-737, 1984.

[52] H. C. Kim, W. Baek and S. Chang, “Critical Heat Flux of Water in Vertical Round Tubes at Low Pressure and Low Flow Conditions,” Nuclear Engineering and Design, Vol. 199, pp. 49 - 73, 2000.

[53] “Ebara 3M Series Centrifugal Pumps Specifications,” 2016. [Online]. Available: www.ebara.com.

[54] “Endress+Hauser,” [Online]. Available: www.endress.com.

[55] R. Moffat, “Describing the Uncertainties in Experimental Results,” Experimental Thermal and Fluid Science, vol. 1, no. 1, pp. 3-17, 1988.

[56] P. Dunn, Measurement and Data Analysis for Engineering and Science, Boca Raton: CRC Press, 2010.

[57] P. Swamee and A. Jain, “Explicit Equations for Pipe-flow problems,” Journal of the Hydraulics Division, American Society of Civil Engineers, vol. 102 (HY5), pp. 657-664, 1976.

[58] W. Kays and H. Perkins, “Forced Convection, Internal Flow in Ducts,” in Handbook of Heat and Mass Transfer, New York, Mcgraw-Hill, 1985.

[59] S. Kakac, R. Shah and W. Aung, Handbook of Single-Phase Convective Heat Transfer, New York: Wiley-Interscience, John Wiley & Sons, 1987.

[60] S. G. Kandlikar, V. Mizo and M. Cartwright, “Bubble Nucleation and Growth Characteristics in Subcooled Flow Boiling of Water,” ASME, 1997.

[61] B. R. L. Petukhov, “Relationships for Heat Transfer in a Turbulent Flow of a Gas in Tubes of Annular Section,” High Temperature (USSR), vol. 2, pp. 65-68, 1964.

[62] V. Gnielinski, “New Equations for Heat and Mass Transfer in Turbulent Pipe and Channel Flow,” International Chemical Engineering, vol. 16, pp. 359 - 368, 1976.

[63] L. Moody, “Friction Factors for Pipe Flow,” in Trans. ASME, Vol. 66, 1944.

[64] N. Cambell, “Predictions for Nucleate Boiling - Results From a Thermal Bench Marking Exercise Under Low Flow Conditions,” SAE International, 2002.

[65] Swift Heat and Control, “www.swiftheat.co.za,” [Online].

[66] American Society of Mechanical Engineers (ASME), ASME-MFC-3M-2004, Measurement of Fluid Flow in Pipes Using Orifice, Nozzle, and Venturi, ASME, 2004.

[67] Y. Hsu, “On the Size Range of Active Nucleation Cavities on a Heating Surface,” Journal of Heat Transfer, vol. 84, pp. 207-212, 1962.

[68] J.W. Park, W.P. Baek and S.H. Chang, “Critical Heat Flux and Flow Pattern for Water Flow in Annular Geometry,” Nuclear Engineering and Design, Vol. 172, pp. 137-155, 1997.

[69] R. Mott, Applied Fluid Mechanics, 6th Edition in SI Units, Singapore: Pearson Prentice Hall, 2006.

[70] R. Johnson, Probability and Statistics for Engineers, Upper Saddle River, New Jersey: Pearson Prentice Hall, 2005.

Appendix A: Calculations

A.1 Test Section Analysis and Sizing Calculations

The design criteria for the test section were discussed in Chapter 3. In this section, the actual calculations that were conducted to derive the various dimensions of the test section are described. **Table A-1** indicates the data that was used as input to the various calculations. The subscripts "op" indicates selected or derived operational values. The symbol $\dot{V}$ indicates the volumetric flow rate.

Table A-1: Input data for calculating the test section dimensions.

Variable	Value or Range	Units of Measure	Variable	Value or Range	Units of Measure
T_{op}	Ambient to 120	°C	v_{op}	0.5 to 3	m/s
ρ_{op}	943.4 to 994	kg/m^3	P_{op}	87 to 200	kPa (absolute)
$C_{p,op}$	4 180 to 4 245	J/kg.°C	μ_{op}	0.23 to 0.72	$\times 10^{-3}$ kg/m.s
A_c	0.08	m^2	$\dot{V}$	3.2 to 19.2	$\times 10^{-4}$ m^3/s
D_{Zr-4}	9.8	mm	D_{SiC}	15.5	mm

A.1.1 Hydraulic Diameters

In commencing the calculations for the test section dimensions, the first step was to determine the dimensions within the flow channel of the test section in conjunction with the various pin configurations that will be accommodated in the channel. Hence the hydraulic diameter (D_H) of the flow channel is determined by using the following equation in which A_c is the cross-sectional flow area, p is the wetted perimeter, w is the width of the test section duct, D_o is the pin outer diameter(s), and N is the number of pins [A1][A2][A17]:

$$D_H = 4A_c/p = (4w^2 - N\pi D^2)/(4w + N\pi D) \quad \text{(A-1)}$$

Hydraulic diameter sample calculation:

Given: 80 mm square flow channel with a 3X3 Zr-4 pin matrix configuration:

$$D_H = 4A_c/p = \frac{(4w^2 - N\pi D^2)}{(4w + N\pi D)}$$

$$= \frac{4(80)^2 - (9 \times \pi \times 9.8^2)}{4(80) + (9 \times \pi \times 9.8)}$$

$$= 38.3 \text{ mm}$$

Following the above method, the rest of the hydraulic diameters for the various other pin configurations were calculated. The results are shown in **Table A-2**.

Table A-2: Hydraulic diameters for the heated test section duct.

Hydraulic Diameters (D_H) [mm]		
Pin Configuration	Material	
	Zr-4	SiC
1 Pin	72.0	67.0
3 x 3 Array	38.3	23.8
4 x4 Array	25.6	11.3
5 x 5 Array	16.6	-
6 x 6 Array	10.3	-
7 x 7 Array	5.9	-

A.1.2 Flow Rates

Next, the flow rates through the pin configurations are determined. The following equations are used to determine the required flow rates [A1] [A2]:

Volumetric $Flow\ Rate$: $\dot{V} = vA_c$ (A-2)

Mass Flow Rate: $\dot{m} = \rho\dot{V} = \rho A_c v$ (A-3)

Mass Flux: $\dot{G} = \frac{\dot{m}}{A_c} = \rho\dot{V}$ (A-4)

Flow rate sample calculation:

Given: v = 0.5 m/s with 80 mm x 80 mm flow channel (with no pins) at $T_{op} = 120$ °C

$$\dot{V} = vA_c$$

$$= 0.5 \times 0.08^2$$

$$= 3.2 \times 10^{-3}\ \mathrm{m^3/s}$$

$$= 11.5\ \mathrm{m^3/h}$$

$$\dot{m} = \rho \dot{V}$$

$$= 943.4 \times (3.2 \times 10^{-3})$$

$$= 3.0 \text{ kg/s}$$

$$\dot{G} = \frac{\dot{m}}{A}$$

$$= \frac{3.0}{0.08^2}$$

$$= 472 \text{ kg/m}^2 \text{.s}$$

The flow ranges for the other pin configurations were calculated accordingly. Only the mass flow rates are tabulated in **Table A-3.**

Table A-3: Mass flow rate ranges for various pin array configurations in the test section.

Mass Flow Rate ($\dot{m}$) [kg/s]									
Material		**Zr-4**				**SiC**			
Velocity : v [m/s]		**0.5**		**3**		**0.5**		**3**	
Temp: T [°C]		**20**	**120**	**20**	**120**	**20**	**120**	**20**	**120**
Pin array configuration in test section	No pins	3.24	3.0	19.22	18.13	3.24	3.0	19.2	18.1
	1 pin	3.2	3.0	18.9	17.9	3.1	2.9	18.6	17.5
	3x3	2.9	2.7	17.1	16.2	2.3	2.2	13.7	13.0
	4x4	2.61	2.5	15.5	14.7	1.6	1.5	9.5	9.0
	5x5	2.3	2.1	13.5	12.8				
	6x6	1.8	1.7	11.0	10.4				
	7x7	1.3	1.3	8.1	7.7				

A.1.3 Reynolds Number (*Re*)

Calculation of the Reynolds number for the various pin configurations is required to establish the turbulence model of the ensuing flow stream through the test section. The following equation was used to calculate these values [A1] [A11]:

$$Re = \frac{\rho v D_H}{\mu} \qquad \text{(A-5)}$$

Reynolds number sample calculation:

Given: v = 0.5 m/s with 80 mm x 80 mm flow channel at $T_{op} = 120$ ℃ and a 3 x 3 Zr-4 pin array configuration:

$$Re = \frac{\rho v D_H}{\mu}$$

$$= \frac{943.4 \times 0.5 \times 38.3 \times 10^{-3}}{2.32 \times 10^{-4}}$$

$$= 78 \times 10^3$$

Similarly, values for the Reynolds number ranges are calculated and tabulated in **Table A-4**.

Table A-4: Reynolds number ranges for various pin configurations at specified test section velocities and bulk coolant inlet temperatures.

Reynolds Number Ranges ($\times 10^3$)									
Material		**Zr-4**				**SiC**			
Velocity : v [m/s]		**0.5**		**3**		**0.5**		**3**	
Temperature: T_{in} [°C]		**20**	**120**	**20**	**120**	**20**	**120**	**20**	**120**
Pin array configuration in test section	no pins	40	163	239	976	40	163	239	976
	1 pin	36	147	215	880	33	136	200	817
	3x3 array	19	78	115	468	12	5	71	290
	4x4 array	13	52	76	312	6	23	34	138
	5x5 array	8	34	50	202				
	6x6 array	5	21	31	126				
	7x7 array	3	12	18	72				

A.1.4 Entrance/Exit Length Calculations

Table A-4 indicates that the bulk of the flow within the expected operating conditions is much greater than the critical Reynolds number of 4 000 for internal flow regimes ($4\,000 \ll Re$). Thus, the flow is in the turbulent flow domain and well developed at the entrance to the heated part of the test section. From Eq. (4-5), the entrance length [A2] [A11] is at least:

$$L_{ent,ext} \geq 10 D_H$$

$$= 10\ (0.080)$$

$$= 0.8\ \text{m}$$

A physical measurement of the location venue revealed that the following maximum entrance/exit length was possible:

$$L_{ent,ext} = 15.44 D_H \gg 10 D_H$$

$$L_{ent} = L_{ext} = (15.44 \times 0.08) = 1.235\ \text{m}$$

Total Test Section Duct Length is therefore:

$$L_{T/S,\ Tot} = L_{ent} + L_{heated} + L_{ext}$$
$$= 1.235 + 0.530 + 1.235$$
$$= 3.0 \text{ m}$$

A.1.5 Friction Factor

The friction factor is calculated from the Swamee and Jain friction equation [A8] (Eq. (2-32). For this equation, the highest Reynolds number is used with the surface roughness (ε) of the stainless steel wall being from literature [A2][A5][A15].

Data Input: Surface roughness $\varepsilon = 4.6 \times 10^{-5}$ m (Table 8.2 in[A2])

$$f = \frac{0.25}{\left[\log\left(\frac{1}{3.7\,(D_H/\varepsilon)} + \frac{5.74}{Re_{D_H}^{0.9}}\right)\right]^2}$$
$$= \frac{0.25}{\left[\log\left(\frac{1}{3.7\,(0.08/4.6\times10^{-5})} + \frac{5.74}{976\times10^{3\,0.9}}\right)\right]^2}$$
$$= 0.018$$

A.2 Heat Exchanger Calculations

A double pipe heat exchanger for the UP-THFC was analysed. In determining the appropriate dimensions of the required double pipe heat exchanger, the results were achieved by using the effectiveness – number of transfer units (ε–NTU) method [A-11]. **Figure A-1** depicts a schematic representative cross-sectional sketch of the double pipe heat exchanger that was used in the UP-THFC. The nominal dimensions and other operating condition criteria that were used in the calculations are also shown.

$$\varepsilon = \frac{1 - exp[-NTU(1-c)]}{1 - c\ exp[-NTU(1-c)]} \quad \text{(A-7)}$$

$$NTU = \frac{1}{c-1} \ln\left(\frac{\varepsilon-1}{\varepsilon c-1}\right) \quad \text{(A-8)}$$

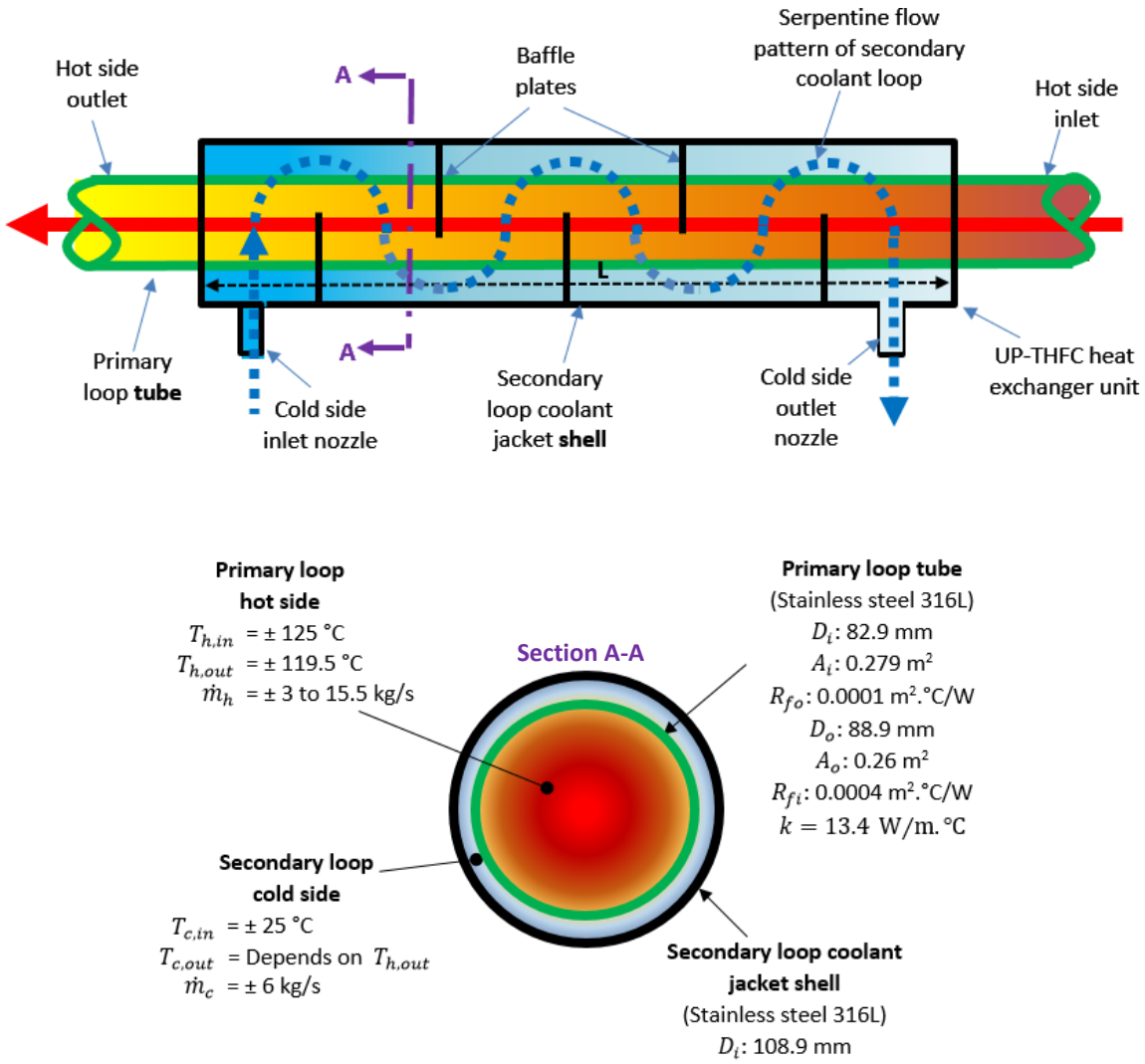

Figure A-1: Schematic representative sketch (not to scale) of a double pipe heat exchanger for the UP-THFC indicating nominal sizes and operating values of the heat exchanger sections.

Table A-4: Data input values for heat exchanger calculations.

Variable	Value	Units of Measure	Variable	Value	Units of Measure
$T_{c,in}$	25	°C	$T_{h.in}$	125	°C
ρ_c	996	kg/m^3	ρ_h	939	kg/m^3
$C_{p,c}$	4 186	J/kg.°C	$C_{p,h}$	4 254	J/kg.°C
$\dot{m}_c$	6	kg/s	$\dot{m}_h$	3	kg/s

$$C_h = \dot{m}_h c_{p,h} = 12.76 \text{ kW/°C} \quad \text{(A-9)}$$

$$C_c = \dot{m}_c c_{p,c} = 25.11 \text{ kW/°C} \quad \text{(A-10)}$$

$$c = C_{min}/C_{max} = 12.76/25.11 = 0.51 \quad \text{(A-11)}$$

Calculation of the energy balance of the system:

$$\dot{Q} = C_h\left(T_{h,in} - T_{h,out}\right) \tag{A-12}$$

$$\dot{Q} = C_c\left(T_{c,in} - T_{c,out}\right) \tag{A-13}$$

$$C_h\left(T_{h,in} - T_{h,out}\right) = C_c\left(T_{c,in} - T_{c,out}\right) \tag{A-14}$$

$$T_{c,out} = \frac{C_h}{C_c}\left(T_{h,in} - T_{h,out}\right) + T_{c,in} \tag{A-15}$$

$$T_{h,out} = 119.5\ ℃\ (\text{max}) \tag{A-16}$$

$$T_{c,out} = \frac{12.76}{25.11} \times (125 - 119.5) + 25 = 27.8\ ℃ \tag{A-17}$$

$$\begin{aligned} \dot{Q} &= \left[\dot{m}C_p\right]_c \times (T_{out} - T_{in})_c \\ &= \left[6 \times 4\ 185\right] \times (27.8 - 25) \\ &= 70.2\ \text{kW} \end{aligned} \tag{A-18}$$

$$\begin{aligned} \dot{Q}_{max} &= C_{min}\left(T_{h,in} - T_{c,in}\right) \\ &= 12\ 760 \times (125 - 25) \\ &= 1\ 276\ \text{kW} \end{aligned} \tag{A-19}$$

$$\varepsilon = \frac{\dot{Q}}{\dot{Q}_{max}} = \frac{70.2}{1\ 276} = 0.055 \tag{A-20}$$

$$\begin{aligned} NTU &= \frac{1}{0.51 - 1}\ \ln\left(\frac{0.055 - 1}{(0.51 \times 0.055) - 1}\right) \\ &= 0.063 \end{aligned} \tag{A-21}$$

$$A_s = \frac{NTU \times C_{min}}{U_{avg}} \tag{A-22}$$

$$U_{avg} = \frac{1}{\frac{1}{h_i} + \frac{1}{h_o}} \tag{A-23}$$

$$U_{avg}A_s = \frac{1}{R} \qquad or \qquad R = \frac{1}{U_{avg}A_s} = \frac{1}{U_iA_i} = \frac{1}{U_oA_o} \tag{A-24}$$

$$R = \frac{1}{h_i A_i} + \frac{R_{f,i}}{A_i} + \frac{\ln(D_o/D_i)}{2\pi kL} + \frac{R_{f,o}}{A_o} + \frac{1}{h_o A_o} \quad \text{(A-25)}$$

Heat transfer coefficients (water properties at T_{avg} values) [A3][A11]:

$$h_i = \frac{k}{D_i} Nu = \frac{k}{D_i}(0.023 \times Re^{0.8} Pr^{0.3}) \qquad (Cooling) \quad \text{(A-26)}$$

$$h_o = \frac{k}{D_o} Nu = \frac{k}{D_o}(0.023 \times Re^{0.8} Pr^{0.4}) \qquad (Heating) \quad \text{(A-27)}$$

$$Re_i = \left(\frac{\rho v D_H}{\mu}\right)_i = \frac{939 \times 0.7 \times 0.083}{0.232 \times 10^{-3}} = 235\,155 \quad \text{(A-28)}$$

$$Re_o = \left(\frac{\rho v D_H}{\mu}\right)_o = \frac{996 \times 1.94 \times 0.2}{0.89 \times 10^{-3}} = 434\,211 \quad \text{(A-29)}$$

$$h_i = \frac{0.683}{0.0828}\left(0.023 \times 235\,155^{0.8} 1.44^{0.3}\right)$$

$$= 4.2 \text{ kW/m}^2.\text{℃} \quad \text{(A-30)}$$

$$h_o = \frac{0.607}{0.089}\left(0.023 \times 434\,211^{0.8} 6.14^{0.4}\right)$$

$$= 10.5 \text{ kW/m}^2.\text{℃} \quad \text{(A-31)}$$

$$R = \frac{1}{4\,200 \times 0.26} + \frac{0.0004}{0.26} + \frac{\ln(88.9/82.8)}{2\pi \times 13.4 \times 1} + \frac{.0001}{0.28} + \frac{1}{10\,500 \times 0.28}$$

$$= 1.6 \times 10^{-3} \text{ ℃/W} \quad \text{(A-32)}$$

$$U_i = \frac{1}{RA_i} = \frac{1}{1.6 \times 10^{-3} \times 0.26} = 2.4 \text{ kW/m}^2.\text{℃} \quad \text{(A-33)}$$

$$U_o = \frac{1}{RA_o} = \frac{1}{1.6 \times 10^{-3} \times 0.28} = 2.2 \text{ kW/m}^2.\text{℃} \quad \text{(A-34)}$$

$$U_{avg} = \frac{U_i + U_o}{2} = \frac{2.4 + 2.2}{2} = 2.3 \text{ kW/m}^2.\text{℃} \quad \text{(A-35)}$$

$$A_s = \frac{0.063 \times 12\,760}{2\,300} = 0.35\ \text{m}^2 \quad \text{(A-36)}$$

$$A_s = \pi D L \qquad or \qquad L = \frac{A_s}{\pi D} \quad \text{(A-37)}$$

$$L = \frac{0.35}{\pi \times 0.089} = 1.25\ \text{m} \quad \text{(A-38)}$$

Heat Exchanger Analysis Conclusion

The design aspects of the heat exchanger were discussed in Section 5.9. As calculated above, a length of 1.25 m of the standard NB3 Sch10S pipe was determined to be adequate for the use as the main heat exchange interface between the hot and cold streams of the prospective double pipe heat exchanger. The calculation was based on the maximum expected thermal hydraulic operating conditions of the system. At any other conditions, part of the flow would be redirected via a bypass line for recombination at a downstream point with the portion of the flow passing through the actual heat exchanger. The amount of flow to be bypassed is to be determined experimentally.

A.3 System Head Loss Analysis for UP-THFC

The system head calculations were conducted in order to determine both the frictional losses that would be expected in the system as well as to establish the pump performance that would be required. Initially setting the pressure, temperature, and velocity at a particular point in the system and then calculating the respective upstream and downstream conditions at particular locations from this reference point would accomplish these. For a specified mass flow rate, the vertical downflow (VDF) circuit had the longest flow length and hence the highest flow resistance and pumping requirements of all the flow circuits. The VDF circuit was thus analysed to determine its performance requirements and characteristics that in turn would define the performance envelope limits of the UP-THFC. A schematic of the circuit is shown in **Figure A-2**. The circuit was divided into a few sections and the relevant reference points were labelled accordingly as is also indicated in **Table A-5**. The main reference point mentioned above was chosen at the mid-point (3) of the test section location, as this was where the required operating conditions were specified for the experimental tests.

The steady flow energy equation in Eq. (A-39) was used to determine the number of performance values for the system. The subscripts i and j in Eq. (A-39) indicate the start and end respectively of a particular pipe section under analysis. In the above equation, the values of the various pressures ($P_{i,j}$),

the elevation heads ($z_{i,j}$), and the head losses (h_L), at the different reference points, need to be determined. The head added by the pump (h_A) is initially unknown and is thus initially ignored. The velocities $v_{i,j}$ are calculated using the continuity equation and are based on the velocity specified at the mid-test section reference. Starting at the pump outlet port and using the operating conditions specified at the mid-test section reference point, Eq. (A-6) is then used to determine the required outlet pressure of the pump. The calculations follow the downstream direction in order to determine the inlet pump pressure condition. The elevation at each reference point in **Figure A-2** is shown in **Table A-6** with the component breakdown of each pipe section shown in **Table A-7**.

$$\left(\frac{P}{\gamma}+\frac{v^2}{2g}+z\right)_i=\left(\frac{P}{\gamma}+\frac{v^2}{2g}+z\right)_j+h_L-h_A \tag{A-39}$$

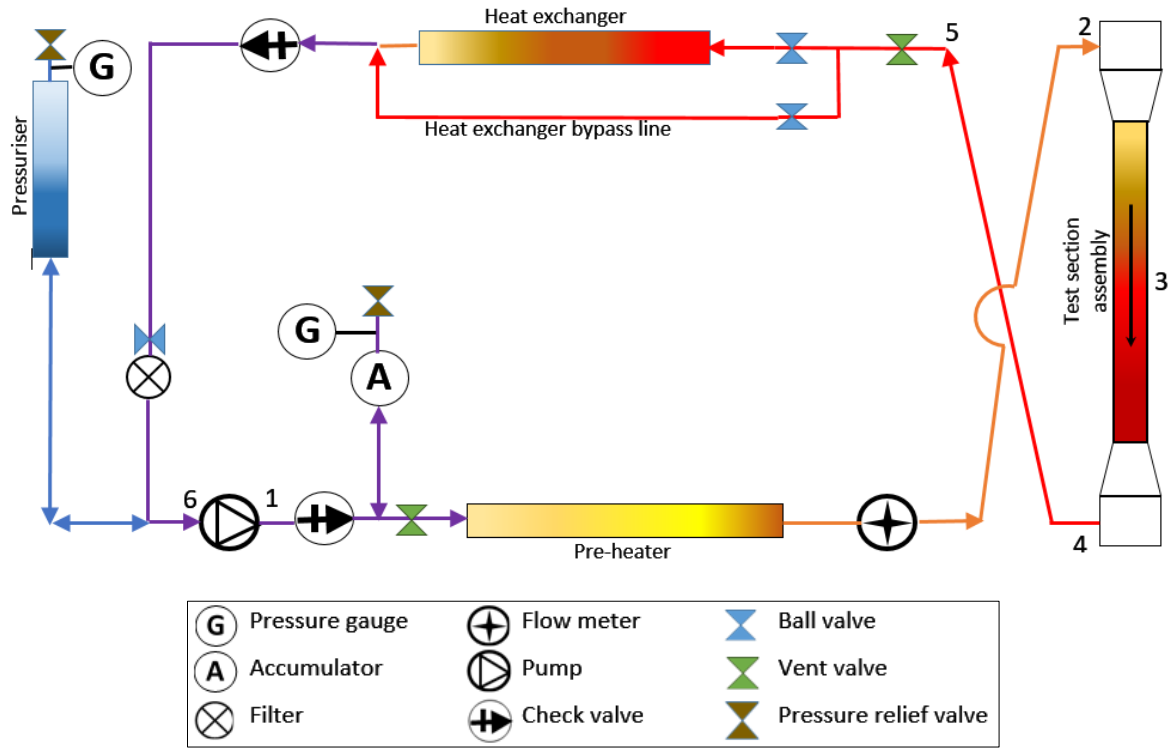

Figure A-2: Schematic of the VDF flow circuit

Table A-5: Pipe section details for VDF flow circuit

Pipe Section	Location	Pipe Section Description
A	1 – 2	Pump exit to test section entrance
B	2 – 3	Test section entrance to mid-point of test section
C	3 – 4	Mid-point of test section to test section exit
D	4 – 5	Test section exit to return leg T-junction
E	5 – 6	Return leg T-junction to pump inlet

$$\Delta h_{tot} = h_f + \sum h_m = \frac{fL}{d}\frac{v^2}{2g} + \sum\left(K\frac{v^2}{2g}\right) \quad \text{(A-40)}$$

hence $$h_A = \frac{\Delta P_{sys}}{\gamma} + \frac{fL}{d}\frac{v^2}{2g} + \sum\left(K\frac{v^2}{2g}\right) \quad \text{(A-41)}$$

$$K = f_T\frac{L_e}{D} = Loss\ coefficients\ for\ pipe\ components \quad \text{(A-42)}$$

For stainless steel 316L 3NB Sch10S pipe the turbulent friction factor is[A13]:

$$f_T = 0.018 \quad \text{(A-43)}$$

Table A -6: Elevation height of reference points for VDF flow circuit from floor level.

Reference Point	Description	Elevation in metres [m] from ground level
1	Pump outlet port	0.16
2	Test section inlet port (VDF)	4.27
3	Mid-test section	2.35
4	Test section outlet port (VDF)	0.34
5	Return leg T-junction	1.32
6	Pump inlet port	0.16

Table A -7: Component composition per pipe section (Table A-5) of VDF flow circuit.

Component Description	No. of Components per Pipe Section				
	A	B	C	D	E
T-junction line flow	2				1
Elbows- long radius	4			1	2
3-inch ball valves (fully opened)	1			1	2
Eccentric reducer					1
Gradual concentric expander	1				
Lift-type check valve	1				1
T-junction branch flow				2	2
Y-strainer/filter					1
Inlet plenum box		1			
Outlet plenum box			1		
(ISO 5167-1) AMCA honeycomb flow straightener		1	1		
3NB Sch10S SS316L pipe length [m]	10			3	7
80 mm SS 316L Square Duct [m]		1.5	1.5		

Typical resistance in valves and fittings as indicated in **Figure A-2** is expressed as the equivalent length in pipe diameters, (L_e/D) and tabulated in **Table A-8**.

Table A-8: Resistance in valves and fittings expressed as equivalent length pipe diameters

Pipe Component	(Le/D)
T-junction line flow	20
Elbows-long radius	20
3-inch ball valves (fully opened)	8
Eccentric reducer	2
Gradual concentric expander	1
Lift-type check valve	150
T-junction branch flow	60
Y-strainer	145
Inlet plenum box	20
Outlet plenum box	20
Honeycomb flow straightener	1

The components that were compatible for connection to the pre-selected stainless steel 316L 3NB Sch10S pipe are listed in **Table A-9** and are used in the flow performance computations of the VDF circuit.

Table A-9: Component list for VDF circuit.

Component Type	Quantity
Discharge line pipe sch10s 3nb (m)	10
Suction line pipe sch10s 3nb (m)	10
Test section duct (m)	3
90° elbows	6
T junction-through flow	3
T junction-branch flow	5
Ball valves	5
Eccentric reducer	1
Concentric expander	1
Concentric reducer	1
Non-return/check valve	2
Y-strainer/filter	1
Plenum box assemblies	2

The system head loss calculations commenced from the pump outlet and unknown values were calculated with respect to the specified operating conditions at Reference Point 3 in **Figure A-2** and as listed in **Table A-10**. In order to determine the complete performance characteristics of the UP-THFC,

the calculations were conducted over the entire expected operating ranges of the system. However, due to a large number of iterations that would have been required to define the system requirements, user-defined spreadsheet solvers were used. For the calculations, only the maximum operating pressure and temperature needed to be used. However, the entire flow velocity range had to be considered in order to define the system operating characteristics.

Table A-10: Flow condition values at reference point 3 of the VDF flow circuit

Flow Condition	Description
Fluid Type	Water
Pressure	Up to 200 kPa (absolute)
Temperature	Ambient to 120 °C
Velocity	0.2 to 2.5 m/s

In order to define the system, the following values required computing [A6] [A7]:

1. Section head/head loss: h_L.
2. The pressure at reference points.

To simplify the computations, the calculations were carried out per the pipe section. The values for each pipe section were then added together to yield the total system value for the complete flow circuit. This method also allowed for the pumping requirements for each pipe section to be computed individually and then also summed up to acquire the total pumping requirements of the system at the different flow conditions. The computation and summations of the above data would yield the following values from which the pump requirements of the system could be derived:

3. Total head on the pump: h_A.
4. Power added to fluid: P_A.

These values would then be used to derive and plot the system performance curve, which would then be used to evaluate the different pump options by comparison with the relevant pump performance curves that would typically be obtained from the respective pump manufacturer [A10]. Due to the numerous computations that are required, which would be quite tedious to reproduce in full, only a sample calculation is provided below for key portions of the system in order to show the calculation procedure. The balance of the pre-computed values for a pipe section or the complete system is tabulated in the relevant tables.

Sample Calculation: VDF Closed-loop Operating Parameters

Required: Determine the system operating point for 2.5 m/s flow in the mid-point for the VDF test section orientation at T_{sat} = 120 °C and P = 200 kPa (Absolute).

Solution: Compute values required in 1 to 4 above.

Assumptions: (a) Steady operating condition exists. (b) The working fluid (water) is an incompressible substance with constant properties. (c) Gravitation effects on the water body during flow conditions are considered.

Properties: The properties of water at 120 °C. Specific Weight: $\gamma = 9.25\ \mathrm{kN/m^2}$

References: Specified operational conditions at Reference Point 3 and Pipe Section B in **Figure A-2**.

Analysis: The computation process commences from the pump outlet and proceeds in the downstream direction per pipe section. Subsequent sequential computations would be used to determine the relevant values at the other reference points or pipe sections.

1. Compute total system head losses $(h_{L,tot})$

(a) Pressure loss expressed as an equivalent column of water of inlet plenum box and designated as $h_{L,10}$:

$$h_{L,10} = K_{10} \times \frac{v^2}{2g} = f_T \left(\frac{L_e}{D}\right) \times \frac{v^2}{2g}$$

$$h_{L,10} = 0.018(20) \times \frac{2.5^2}{2(9.81)}$$

$$h_{L,10} = 0.17\ \mathrm{m}$$

(b) Similarly for the honeycomb flow straightener $h_{L,11}$:

$$h_{L,11} = 0.018(1) \times \frac{2.5^2}{2(9.81)} = 0.01\ \mathrm{m}$$

(c) The energy term for the head losses for the square duct test section portion $h_{L,13}$:

$$h_{L,13} = f \left(\frac{L_e}{D}\right) \times \frac{v^2}{2g}$$

$$h_{L,13} = 0.018 \left(\frac{1.5}{0.08}\right) \times \frac{2.5^2}{2(9.81)}$$

$$h_{L,13} = 0.11\ \mathrm{m}$$

Table A-11: Computed pipe section and system head loss values (h_L)

Component Description	h_L per Component per Pipe Section [m]				
	A	B	C	D	E
T junction- line flow: $h_{L,1}$	0.3			-	0.16
Elbows- long radius: $h_{L,2}$	0.6			0.2	0.32
3-inch ball valves (fully opened) : $h_{L,3}$	0.1			0.1	0.13
Eccentric reducer: $h_{L,4}$	0				0.02
Gradual concentric expander: $h_{L,5}$	0.1				0
Lift-type check valve: $h_{L,6}$	1.2				1.2
T junction - branch flow: $h_{L,7}$				1.0	1.0
Y-strainer/filter: $h_{L,8}$					1.25
Inlet plenum box: $h_{L,9}$		0.2			
Outlet plenum box: $h_{L,10}$		-	0.3		
Honeycomb flow straightener: $h_{L,11}$		0.1	0.1		
3NB Sch10S SS316L pipe length: $h_{L,12}$	0.9			0.3	0.7
80 mm SS 316L square duct : $h_{L,13}$	-	0.1	0.1		
Subtotal per pipe section	3.1	0.3	0.3	1.5	4.6
Total system head loss, $h_{L,tot}$	**9.8**				

The head loss values for the components in the other pipe sections are carried out in a similar method as above [A4]. The results are tabulated in **Table A-11**. The head loss value for each pipe section is then computed from the summation of the individual losses of each component in that particular pipe section. A final summation of the pipe section values provides for the system total head loss value per the system operating condition, which in the above case was for a flow velocity of 2.5 m/s in the test section per VDF orientation.

2. Determine static pressure (P) values at other reference points

(a) For Pipe Section B:

$$P_2 = P_3 + \left(\gamma\left(\left(\frac{v_3^2 - v_2^2}{2g}\right) + (\Delta z) + h_{L,B}\right)\right)$$

$$\Delta z = z_2 - z_3 = 4.265 - 2.353 = 1.912$$

Also,

$$v_2 = v_3 \times \frac{A_{c,3}}{A_{c,2}} = 2.5 \times \frac{4 \times 0.08^2}{\pi \times 0.083^2} = 2.96 \text{ m/s}$$

Hence,

$$P_2 = 200 + \left(9.255\left(\left(\frac{2.5^2 - 2.96^2}{2 \times 9.81}\right) + (1.912) + 0.281\right)\right) = 219.11 \text{ kPa}$$

The pressure values at the other reference points are calculated in a similar manner and the results thereof are shown in **Table A-12**:

Table A-12: Computed Static Pressure Values at Reference Points of VDF Circuit at 2.5 m/s

Reference Points	P1	P2	P3	P4	P5	P6
Pressure Value [kPa]	285	219	200	178	156	103

3. Determine head on the pump (h_A)

In deriving the various static pressures in Section 2 above, the flow is assumed constant with the pump at steady operating conditions. The amount of head on the suction side of the pump is also assumed constant and hence is not included in the above static pressure calculations. The pump inlet and outlet pressure values can also be extracted from **Table A-12** per reference points P1 and P6 respectively.

The head on the pump for each pipe section can be calculated by using Eq. (A-3) as follows:

$$h_{A,x} = \frac{\Delta P_{sys}}{\gamma} + \frac{V^2}{2g}\left(\sum \frac{fL}{D} + \sum K\right)$$

$$h_{A,A} = \frac{(P_1 - P_2)}{\gamma} + h_{L,A}$$

$$h_{A,A} = \frac{(285 - 219)}{9.255} + 3.142 = 10.25 \text{ m}$$

The values for the other pipe sections are computed in a similar manner as tabulated in **Table A-13** accordingly. The head on the pump for the entire system (h_{sys}) can be determined in a similar way by considering the pressure differential between Reference Points 1 and 6 and using the h_{tot} of the system [A4].

Table A-13: Head on Pump per Pipe Section

Section	A	B	C	D	E	h_{sys} [m]
h_A [m]	10.3	2.3	2.6	3.9	10.3	29.4

4. Power added to the fluid (P_A)

The power added to the fluid by the pump is not a parameter that is required to define the system performance. However, the yielded values for this parameter would be useful in the selection of an

appropriate pump and are thus included in the system performance calculations. When carried out on a pipe section-to-section basis, then each pipe section can be individually evaluated for system optimisation purposes. For simplicity, only the total system value is calculated below but the values for each pipe section is tabulated in **Table A-14**.

$$P_A = h_A \times W$$

$$P_A = h_{sys} \times (\dot{V} \times \gamma)$$

$$P_A = 29.4 \times \left((2.5 \times 0.08^2)9.255\right) = 4.35 \text{ kW}$$

Table A-14: Power added to the fluid in the VDF circuit at 2.5 m/s in the test section with a single Zr-4 pin.

Section	A	B	C	D	E	$P_{A,sys}$
P_A [kW]	1.52	0.35	0.39	0.57	1.53	4.35

The system performance values over the full flow operating range are derived from the above methodology. A summary of the system values is tabulated in **Table A-15** for the various pin arrays.

Table A-15: Total system performance summary for VDF circuit with single Zr-4 pin configuration

Velocity (m/s) Single Zr-4 Pin	System head Loss h_L [m]	Total Head on Pump h_A [m]	Pump Outlet Pressure [kPa]	Pump Inlet Pressure [kPa]
3	13.9	37.5	296.9	77.9
2.54	10.1	30.0	285.8	101.4
2.5	9.8	29.4	284.9	103.3
2	6.4	22.7	275.1	124.1
1.5	3.8	17.5	267.4	140.3
1	1.9	13.8	261.9	152.0
0.5	0.7	11.5	258.5	159.2
0.1	0.4	10.7	257.3	161.6

The analysis of the results revealed that the 7 x 7 Zr-4 pin array in the VDF flow regime had the highest system head and thus its system performance curve forms the upper operating envelope of the

system. A single Zr-4 pin in the horizontal flow regime had the lowest system head and thus its performance curve defined the lower operational envelope of the system.

Based on these computations, an Ebara 3M 50-160/7.5 pump was selected [A18]. The calculated upper and lower system operating curves is compared with the performance curve for the pump and is shown in **Figure A–4** with the system performance envelope shown for the unpressurised system case. From the figure, the system operating point for 2.5 m/s flow in the mid-point for the VDF test section orientation at T_{sat} = 120 °C and P = 200 kPa (abs) occurs at a pump head of 29.4 m with about 975 L/min (58.5 m^3/h) at approximately 2.5 m/s maximum operating flow velocity in the test section. This was therefore within the operating ranges of the selected pump and was thus considered as the upper operating point of the UP-THFC.

For a system that has been pressurised via the pressurising unit, the net pressure introduced into the system (P_o) would then be in added to the system head or pump head [A10]. **[Answer]**

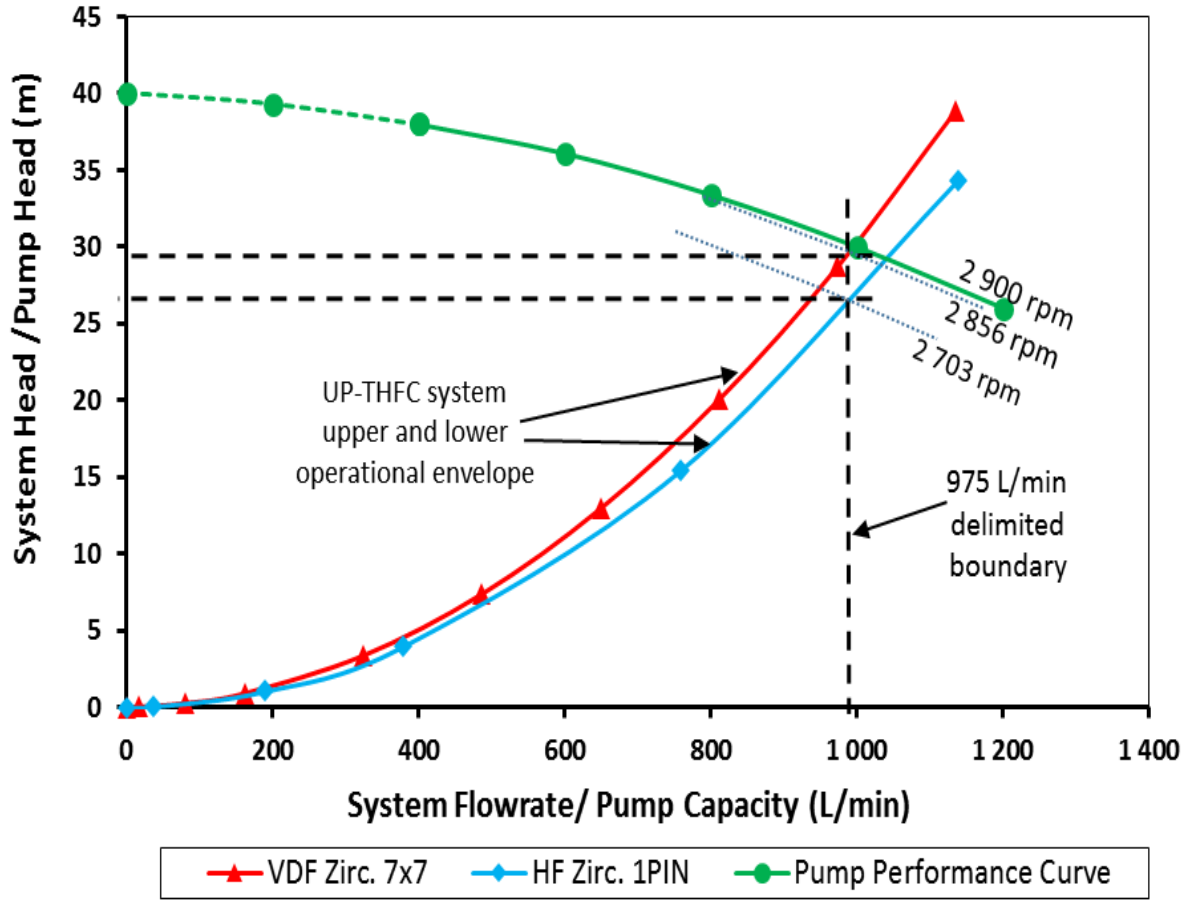

Figure A-4: System performance curve versus pump performance curve (unpressurised system)

Nomenclature: Appendix A

A_c	Cross-sectional area	m^2
$A; A_s$	Surface area, πDL	m^2
C_c, C_h	Heat capacity rate, cold and hot sides	W/°C
C_p	Specific heat	J/kg.°C
c	Capacity ratio	
D	Diameter	m
D_H	Hydraulic diameter	m
$D_o;\ D_i$	Outer diameter; inner diameter	m
f	Friction factor	
f_T	Turbulent friction factor	
G	Mass flux, $\rho \cdot v/A_c$	$kg/m^2.s$
g	Gravitational acceleration	m/s^2
h_{sys}	System pressure head	m
h	Heat transfer coefficient	$W/m^2.°C$
h	Head, $P/(\rho g)$	m
h_A	Head added by pump	m
h_f	Head due to friction	m
h_{fg}	Enthalpy of vaporisation	J/kg
h_L	Head loss	m
h_m	Minor losses	m
K	Loss coefficient (for pipe fittings)	
k	Thermal conductivity	W/m.°C
L	Length	m
L_e	Equivalent length	m
$\dot{m}$	Mass flow rate, $\rho v A_s$	kg/s
N	Number of pins	
Nu	Nusselt number	
P	Pressure	kPa (absolute)
p	Perimeter	m
P_A	Power added to the bulk coolant	W
P_o	Added pressure	kPa
Pr	Prandtl number	
$\dot{Q}$	Heat transfer rate	W
R	Thermal resistance	°C/W
Re	Reynolds number, $\rho v D_H/\mu$	
R_f	Thermal resistance due to the fouling factor	°C/W
T	Temperature	°C
U	The overall heat transfer coefficient	$W/m^2.°C$
$\dot{V}$	Volumetric flow rate	m^3/s
v	Velocity	m/s
W	Power	W
w	Inside width of the test section channel	m
x	Axial position relative to a datum point	m
z	Elevation head	m

Greek Symbols

ϵ	Surface roughness	m
ρ	Density	kg/m^3
ν	Kinematic viscosity	m^2/s
μ	Dynamic viscosity	kg/m.s
ε	Effectiveness	
γ	Specific weight	N/m^3

Subscripts

$1, 2$	Reference points 1, 2,… respectively
abs	Absolute
avg	The average or mean value
c	Cold side
c	Cross-sectional
ent	Entrance side
ext	Exit side
f	Fouling factor
f	Friction factor
h	Hot side
$heated$	Heated test section length
i	Inside or inner-side
$i; j$	Start and end reference points
in	Inlet
$l\ ;\ lo$	Liquid; liquid only condition
max	Maximum
min	Minimum
o	Outer or outside
op	Operational value
out	Outlet
s	Surface
SP	Single-phase condition
sys	System
tot	Total
$T/S\ , tot$	Total test section length
v	Velocity
w	Wall or clad tube surface
x	Axial position relative to a datum point

Abbreviations

NTU	Number of transfer units
SiC	Silicon carbide
UP-THFC	University of Pretoria – Thermal-Hydraulic Flow loop Cell
VDF	Vertical downflow
Zr-4	Zircaloy-4®

References: Appendix A

[A1] F. White, Fluid Mechanics, 6th Edition, New York: McGraw-Hill Int., 2009.

[A2] R. Mott, Applied Fluid Mechanics, 6th Edition in SI Units, Singapore: Pearson Prentice Hall, 2006.

[A3] R. Sonntag, C. Borgnakke and G. Van Wylen, Fundamentals of Thermodynamics, 6th Edition, New Jersey, USA: John Wiley & Sons, 2003.

[A4] B. Hauser, Practical Hydraulics Handbook, 2nd Edition, Boca Raton, USA: CRC, Lewis Publishers, 1996.

[A5] K. Kurganov, "Hydraulic Resistance," [Online]. Available: www. thermopedia.com. [Accessed 03 February 2016].

[A6] G. Jost, Flow Handbook, 3rd Edition, Reinach, Germany: Endress+Hauser Flowtec AG, 2006.

[A7] L. Moody, "Friction Factors for Pipe Flow," in *Trans. ASME, Vol. 66*, 1944.

[A8] P. Swamee and A. Jain, "Explicit Equations for Pipe-flow Problems", Journal of the Hydraulics Division, American Society of Civil Engineers, vol. 102 (HY5), pp. 657-664, 1976.

[A9] EngineeringToolbox, "The Engineering Toolbox," [Online]. www.engineeringtoolbox.com

[A10] Karassik *et al.* , Pump Handbook, 3rd Edition, New York, USA: McGraw-Hill, 2001.

[A11] Y. Cengel, Heat and Mass Transfer: A Practical Approach, 3rd Edition, New York: McGraw-Hill, 2007.

[A12] R. Miller, Flow Measuring Engineering Handbook, New York, USA: McGraw-Hill, 1989.

A13] American Society of Mechanical Engineers (ASME), Power Piping, ASME B31.1-2007, ASME Code for Pressure Piping, ASME, 2007.

[A14] American Society of Mechanical Engineers (ASME), Process Piping, ASME B31.3-2006, ASME Code for Pressure Piping, ASME, 2006.

[A15] American Society of Mechanical Engineers (ASME), Materials Properties (Metric), Section II, Part D, ASME Boiler and Pressure Vessel Code, ASME, 2007.

[A16] E. Meyesy, Pressure Vessel Handbook, 4th Edition, Tulsa, USA: Pressure Vessel Handbook Publishing Inc., 1977.

[A17] Budynas-Nisbett, Shigley's Mechanical Engineering Design, 8th Edition, New York, USA: McGraw-Hill, 2006.

[A18] Ebara 3M Series Centrifugal Pumps Specifications, www.ebara.com [viewed online - February 2016]

Appendix B: Uncertainty Analysis

B.1 Introduction

Due to imperfections in the measurement system, experimental uncertainties are inherent in the measurement stages of calibration, data acquisition and its analysis. In establishing the heat transfer-based results in the present study, parameters such as the heat transfer coefficient, Nusselt number, and heat flux, were subjected to an uncertainty analysis in which the measurable variables (measurands) and/or combinations were analysed. The procedure that was applied followed the methods suggested by Moffat (1998) [B1] and Dunn (2010) [B2]. As is customary for most engineering-based experimental studies, a 95 % confidence level was adopted for the uncertainty analysis.

B.2 Uncertainty Analysis Theory and Procedure

The types of errors that give rise to the measurement uncertainty can be categorised into either systematic errors (commonly known as a bias or fixed errors) or random errors (precision).

Bias errors are typically specified by the instrument/equipment manufacturer and occur due to calibration uncertainties, imperfections in the measuring instruments and/or test equipment, etc. The magnitude of the bias determines the accuracy of the measurement. It can be minimised through the process of calibration, conducted in comparison with a true reference value. The bias error value thus determines the difference between the true mean value and the sample mean value.

The magnitude of random (precision) errors determines the precision or repeatability of the measurement. These errors occur due to factors including scattering in the data owing to discrepancies such as variations during the measuring process (conducted under fixed conditions), noise, or interferences such as electromagnetic force (EMF) and/or radio frequencies (RF), damping. The precision errors thus relate the difference between a confidence limit (either upper or lower) to that of the sample mean value. The uncertainty of a single-sample measurement is the solution of a root-sum-square (RSS) procedure for the combined bias (b) and precision (p) errors and is determined by:

$$\delta x_i = \left(b_i^2 + p_i^2\right)^{\frac{1}{2}} \tag{B1}$$

In probability and statistics, the x_i term represents a single observation with δ being the uncertainty that is obtained from the product of the standard deviation multiplied with Student's t-distribution variable, which is used when estimating the mean of a data set for which the sample size is small (number of degrees of freedom: n < 30) [B2][B3]. The uncertainty for a single measurand or variable ($x_{i,meas}$) can be expressed with odds of 20 to 1 or a 95 % confidence level of probability that the actual error will not be more or less than the estimate. This can be computed via Eq. (B2).

$$x_i = x_{i,meas} \pm \delta x_i \tag{B2}$$

Typically, a parametric result (R) of an experiment is calculated from a set of variables represented by:

$$R = R(x_1, x_2, x_3, \dots, x_n) \tag{B3}$$

For a single known or computed uncertaintyx_i, the uncertainty of R can be determined by:

$$\delta R = \frac{\partial \mathrm{R}}{\partial \mathrm{x_i}} \delta x_i \tag{B4}$$

When there are several independent variables, the uncertainty computation of R is achieved with the combination of the individual terms in an RSS equation:

$$\delta R = \left[\sum_{i=1}^{N} \left(\frac{\partial R}{\partial x_i} \delta x_i \right)^2 \right]^{\frac{1}{2}}$$

$$\delta R = \left[\left(\frac{\partial \mathrm{R}}{\partial \mathrm{x_1}} \delta x_1 \right)^2 + \left(\frac{\partial R}{\partial x_2} \delta x_2 \right)^2 + \left(\frac{\partial R}{\partial x_3} \delta x_3 \right)^2 + \cdots + \left(\frac{\partial R}{\partial x_n} \delta x_n \right)^2 \right]^{\frac{1}{2}} \tag{B5}$$

B.3 Linear Regression Analysis

The bias errors of the pressure transducers and thermocouples that were used in the study were determined via a linear least squares regression analysis [B1] [B2] [B3]. This method was used after calibration in the analysis of the sample data. For the thermocouples, the values of the x-axis variables were the true reference values obtained from a calibrated Pt100 probe with the y-axis variables reflecting the measured sample values of the individual thermocouples. The uncertainty of the y-variables are computed from the following set of equations:

$$\delta y = \pm t S_{yx} \sqrt{\frac{1}{N} + \frac{1}{M} + \frac{\bar{x}^2}{S_{xx}}} \tag{B6}$$

In Eq. (B6), the sum of the squares of the x-values (S_{xx}) is determined by the following equation in which $\bar{x}$ is the mean value of the subset:

$$S_{xx} = \sum_{i=1}^{N} (x_i - \bar{x})^2 \tag{B7}$$

Also, the sum of the product of x and y (S_{yx}) is computed by:

$$S_{xy} = \sum_{i=1}^{N} (x_i - \bar{x})(y_i - \bar{y}) \tag{B8}$$

To establish the expression for the linear regression line of best-fit, the gradient (slope) and intercept terms is then determined. The gradient b is computed from:

$$b = \frac{S_{xy}}{S_{xx}} \tag{B9}$$

The intercept a for the linear line of best-fit is then:

$$a = \bar{y} - b\bar{x} \tag{B10}$$

The standard error of the best-fit S_{yx} can then be determined via:

$$S_{yx} = \sqrt{\frac{\sum_{i=1}^{N} (y_i - y_{ci})^2}{N - 2}} \tag{B11}$$

In Eq. (B11), the calculated value y_{ci} is computed from:

$$y_{ci} = a + b x_i \tag{B12}$$

The uncertainty of the δx variable is then be computed as follows:

$$\delta x = \frac{\delta y}{m} \tag{B13}$$

The value of m in Eq. (B13) is the gradient/slope of the linear regression line of best-fit and is equal to b as in Eq. (B9).

B.4 Equipment and Instrumentation Uncertainty

The results of the heat transfer parameters were obtained primarily from four main measured components, namely temperature, pressure, flow rate, and power input.

T-type thermocouples and Pt100 RTD instruments were employed to measure the various temperature variables. The bias for the temperature probes was taken as the RSS result (u_i), per Equation B14 of the accuracies specified by both the probe manufacturer (u_p) as 1 °C or 0.75 % of full-scale output (FSO) and that of the Agilent data acquisition unit manufacturer (u_{DAQ}) also as 1 °C. Precision magnitudes for the temperature probes were derived from linear regression analysis (Eqs. (B6 to B13)) From statistical data obtained by calibration methods consisting of constant temperature bath method and/or in-situ calibration treatment using quasi-cooling techniques.

$$u_i = \left(u_{p,i}^2 + u_{DAQ}^2\right)^{\frac{1}{2}} \tag{B14}$$

The pressure variables were measured via electronic absolute pressure transducers. The pressure transducers were all supplied with traceable calibration certificates with accuracies of around 1 % of the FSO.

For the flow measurements, a classical Venturi tube primary element (manufactured by the student) was coupled to a high accuracy differential pressure transducer (DPT) secondary element. The coupled flow meter elements were then calibrated as a single entity with a bias of 0.075 % of the FSO.

A solid-state relay (SSR) fitted with a variable resistance potentiometer provided the adjustable single-phase (50 Hz) alternating current (AC) power input to the test specimen fuel rod cartridge heater. The level of power input was determined with inputs from individual measured components of voltage and current, which were indicated by analogue meters. These instruments provided resolutions of approximately 1.0 V for the voltmeter and 0.5 A for the ammeter. Due to electronic data acquisition limitations, the input power data was recorded for statistical purposes only.

For all the instruments except the temperature probes, the bias was considered as the accuracies or resolution specified by the probe/sensor manufacturer. The precision index for these instruments was derived from the standard deviation of around 50 measuring points logged at a frequency of

approximately 0.4 Hz during steady operation, which was then multiplied by a Student's t-variable for a 95 % confidence level.

The uncertainties of the instruments and auxiliary equipment are shown in **Table B-1** for a 95 % level of confidence.

Table B 1: Operational Ranges and Bias of Test Instruments

Instrument/Equipment	Range	Uncertainty
Thermocouples T-type	-200 to 350 °C	± 0.1 °C
Pt100 RTD	-200 to 400 °C	± 0.1 °C
Pressure Transducers (Absolute)	0 to 250 kPa 0 to 1 000 kPa	± 0.025 kPa ± 0.1 kPa
Flow meter	11 to 58.9 m^3/h	± 0.044 m^3/h
Voltmeter	0 to 230 VAC	± 0.1 to 0.5 V
Ammeter	0 to 25 A	± 0.1 to 0.25 A

B.5 Water Properties

The properties of water were computed by the use of empirical correlations developed by Popiel and Wojtkowiak (1998). **Table B2** furnished the uncertainties for the relevant water properties according to these authors [B4]

Table B2: Uncertainties of Water Properties [B4]

Property	$\rho\ [\mathrm{kg/m^3}]$	$C_p\ [\mathrm{J/kg.K}]$	$k\ [\mathrm{W/m.k}]$	$\mu\ [\mathrm{kg/m.s}]$	Pr
Uncertainty (%)	0.004	0.04	2	1×10^{-6}	2.3

B.6 Dimensional Uncertainty

The length and diameter dimensions of the two fuel rod specimens were measured using a tape measure for the former and a Vernier calliper for the latter. The tape measure had a resolution of 1 mm and the resolution of the Vernier calliper was 20 μm.

B.6.1 Heat Transfer Area

The heated surface area of the Zr-4 and/or SiC clad tubes was calculated from the following equation with the uncertainty computed as follows:

$$A_s = \pi \cdot D \cdot L \tag{B15}$$

$$\delta A_s = \left[\left(\frac{\partial A_s}{\partial D}\delta D\right)^2 + \left(\frac{\partial A_s}{\partial L}\delta L\right)^2\right]^{\frac{1}{2}}$$

$$\delta A_s = [(\pi \cdot L \cdot \delta D)^2 + (\pi \cdot D \cdot \delta L)^2]^{\frac{1}{2}} \tag{B16}$$

This resulted in the uncertainty of approximately 4.0×10^{-5} m^2 for Zr-4 and 5.5×10^{-5} m^2 for SiC.

B.6.2 Heat Input

The amount of heat input by the cartridge heater was taken as the amount of power input into the heater. The heat input uncertainty was computed as follows:

$$\dot{Q} = V \cdot I \tag{B17}$$

$$\delta\dot{Q} = \left[\left(\frac{\partial \dot{Q}}{\partial V}\delta V\right)^2 + \left(\frac{\partial \dot{Q}}{\partial I}\delta I\right)^2\right]^{\frac{1}{2}}$$

$$\delta\dot{Q} = [(I \cdot \delta V)^2 + (V \cdot \delta I)^2]^{\frac{1}{2}} \tag{B18}$$

This resulted in the uncertainty of between 25 and 55 W.

B.6.3 Mass Flow Rate

The uncertainty for the mass flow rate was calculated as follows, in which $\dot{V}$ is the volumetric flow rate:

$$\dot{m} = \dot{V} \cdot \rho \tag{B19}$$

$$\delta\dot{m} = \left[\left(\frac{\partial \dot{m}}{\partial \dot{V}}\delta\dot{V}\right)^2 + \left(\frac{\partial \dot{m}}{\partial \rho}\delta\rho\right)^2\right]^{\frac{1}{2}}$$

$$\delta\dot{m} = \left[\left(\rho \cdot \delta\dot{V}\right)^2 + \left(\dot{V} \cdot \delta\rho\right)^2\right]^{\frac{1}{2}} \tag{B20}$$

This resulted in the uncertainty of approximately 0.01 kg/s.

B.6.4 Heat Flux

The heat flux uncertainty was calculated as follows:

$$\dot{q} = \frac{\dot{Q}}{A_s} \tag{B21}$$

$$\delta\dot{q} = \left[\left(\frac{\partial\dot{q}}{\partial\dot{Q}}\delta\dot{Q}\right)^2 + \left(\frac{\partial\dot{q}}{\partial A_s}\delta A_s\right)^2\right]^{1/2} \tag{B22}$$

$$\delta\dot{q} = \left[\left(\frac{1}{A_s}\delta\dot{Q}\right)^2 + \left(-\frac{\dot{Q}}{A_s^2}\delta A_s\right)^2\right]^{\frac{1}{2}} \tag{B23}$$

This resulted in the uncertainty of between 2 and 4.4 kW/m^2.

B.6.5 Test Section Outlet Temperature

The bulk coolant water temperature from the test section outlet was calculated as follows:

$$T_{out} = \frac{\dot{Q}}{\dot{m}\cdot C_p} + T_{in} \tag{B24}$$

$$\delta T_{out} = \left[\left(\frac{\partial T_{out}}{\partial\dot{Q}}\delta\dot{Q}\right)^2 + \left(\frac{\partial T_{out}}{\partial\dot{m}}\delta\dot{m}\right)^2 + \left(\frac{\partial T_{out}}{\partial C_p}\delta C_p\right)^2 + \left(\frac{\partial T_{out}}{\partial T_{in}}\delta T_{in}\right)^2\right]^{\frac{1}{2}}$$

$$\delta T_{out} = \left[\left(\frac{1}{\dot{m}\cdot C_p}\delta\dot{Q}\right)^2 + \left(-\frac{\dot{Q}}{\dot{m}^2\cdot C_p}\delta\dot{m}\right)^2 + \left(-\frac{\dot{Q}}{\dot{m}\cdot C_p^2}\delta C_p\right)^2 + (\delta T_{in})^2\right]^{\frac{1}{2}} \tag{B25}$$

This resulted in an outlet temperature uncertainty of between 0.02 and 0.06 ˚C. A value of 0.1 ˚C corresponding to the reference instrument uncertainty was used instead.

B.6.6 Mean Test Section Temperature

The mean test section water temperature was used for the determination of the water properties for the bulk coolant flowing through the test section. For the calculation of the heat transfer coefficient, the average of the inlet and outlet test section temperatures was computed as follows:

$$T_b = \frac{(T_{out} + T_{in})}{2} \tag{B26}$$

Following Eq. (B15), the uncertainty related to the surface temperature was computed as follows:

$$\delta T_b = \left[\left(\frac{\delta T_{out}}{2}\right)^2 + \left(\frac{\delta T_{in}}{2}\right)^2\right]^{\frac{1}{2}} \tag{B27}$$

This resulted in an outlet temperature uncertainty of 0.1 ˚C.

B.6.7 Heat Transfer Coefficient

The average wall temperature (T_w) was determined according to the Liu-Winterton method [B6]. The average heat transfer coefficient was computed using the Eq. (B28). The average heat transfer coefficient uncertainty was calculated as follows:

$$h = \frac{\dot{q}}{T_w - T_b} \tag{B28}$$

$$\delta h = \left[\left(\frac{\partial h}{\partial \dot{q}}\delta\dot{q}\right)^2 + \left(\frac{\partial h}{\partial T_w}\delta T_w\right)^2 + \left(\frac{\partial h}{\partial T_b}\delta T_b\right)^2\right]^{\frac{1}{2}}$$

$$\delta h = \left[\left(\frac{1}{T_w - T_b}\delta\dot{q}\right)^2 + \left(\frac{-\dot{q}}{(T_w - T_b)^2}\delta T_w\right)^2 + \left(\frac{-\dot{q}}{(T_w - T_b)^2}\delta T_b\right)^2\right]^{\frac{1}{2}} \tag{B29}$$

This resulted in the uncertainty of between 230 W/m^2.˚C (± 3.8 % at 6 kW/m^2.˚C) and about 574 W/m^2.˚C (± 4 % at 14 kW/m^2.˚C)

B.6.8 Reynolds Number

The equation for the Reynolds number and the uncertainty is given by:

$$Re = \frac{4 \cdot \dot{m}}{\mu \cdot L \cdot \pi} \tag{B30}$$

$$\delta Re = \left[\left(\frac{\partial Re}{\partial \dot{m}}\delta\dot{m}\right)^2 + \left(\frac{\partial Re}{\partial \mu}\delta\mu\right)^2 + \left(\frac{\partial Re}{\partial L}\delta L\right)^2\right]^{\frac{1}{2}}$$

$$\delta Re = \left[\left(\frac{4}{\mu \cdot L \cdot \pi}\delta\dot{m}\right)^2 + \left(-\frac{4\,\dot{m}}{\mu^2 \cdot L \cdot \pi}\delta\mu\right)^2 + \left(-\frac{4\,\dot{m}}{\mu \cdot L^2 \cdot \pi}\delta L\right)^2\right]^{\frac{1}{2}} \tag{B31}$$

This resulted in a Reynolds number uncertainty of between 180 and 786 for the lowest to highest flow rates.

B.7 Conclusion

The uncertainty analysis conducted for the various measurands in this study provided a measure to gauge the accuracy and precision levels of the experimental data. This also allowed the results to be analysed in comparison with other research works and/or correlations in order to determine the agreement of fit and hence verification and validation of the experimental method. The resulting

uncertainties from this analysis were found to be relatively consistent with previous research with respect to boiling heat transfer.

Nomenclature: Appendix B

A_s	Surface area	m^2
a	Best-fit intercept	
b	Bias or best-fit slope	m^2
C_p	Specific heat	J/kg.°C
D	Diameter	m
D_H	Hydraulic diameter	m
h	Heat transfer coefficient	$W/m^2.°C$
I	Current input	A
k	Thermal conductivity	W/m.°C
L	Length	m
m	The slope of the regression line	
$\dot{m}$	Mass flow rate, $\rho v A_c$	kg/s
M	Number of data sets	
N	Number of data points	
n	Total number of data points	
p	Precision	
Pr	Prandtl number	
$\dot{Q}$	Heat transfer rate	W
$\dot{q}$	Heat flux	W/m^2
R	Parametric result	
Re	Reynolds number, $(4\dot{m}) \ / \ (\mu L \pi)$	
S_{xx}	Sum of the squares of x	
S_{xy}	Sum of the squares of x and y	
S_{yx}	Standard error or best-fit	
T	Temperature	°C
t	Student's *t*-variable	
u	Root-sum-square (RSS) result	
V	Voltage input	V
$\dot{V}$	Volumetric flow rate	m^3/s
x	*x*-axis variable or single measurand	
y	*y*-axis variable	

Greek Symbols

ρ	Density	kg/m^3
μ	Dynamic viscosity	kg/m.s
δ	Uncertainty	

Subscripts

b	Bulk coolant
ci	Calculated value
i	Index or bias of measurand probe
in	Inlet
$meas$	Measured value

out	Outlet
p	Accuracies as stated by probe manufacturer
w	Wall or clad tube surface
x	Axial position relative to a datum point

Superscripts

$-$	The average or mean value

Abbreviations

AC	Alternating current
DAQ	Data acquisition unit
DPT	Differential pressure transducer
EMF	Electromagnetic force
FSO	Full-scale output
RF	Radio frequencies
RSS	Root-sum-square method
SiC	Silicon carbide
SSR	Solid state relay
Zr-4	Zircaloy-4®

References: Appendix B

[B1] R. Moffat, "Describing the Uncertainties in Experimental Results," Experimental Thermal and Fluid Science, vol. 1, no. 1, pp. 3-17, 1988.

[B2] P. Dunn, Measurement and Data Analysis for Engineering and Science, Boca Raton: CRC Press, 2010.

[B3] R. Johnson, Probability and Statistics for Engineers, Upper Saddle River, New Jersey: Pearson Prentice Hall, 2005.

[B4] C. Popiel and J. Wojtkowiak, "Simple Formulas for the Thermophysical Properties of Liquid Water for Heat Transfer Calculations (from 0 °C to 150 °C)," Heat Transfer Engineering, vol. 19, pp. 87-101, 1998.